Title

Signaling Mechanisms Involved in the Induction and Maintenance of Secondary Cartilage on the Coronoid Process of the Mandible

Permalink

Author

Woronowicz, Katherine C

Publication Date

2017

Peer reviewed|Thesis/dissertation

Signaling Mechanisms Involved in the Induction and Maintenance of
Secondary Cartilage on the Coronoid Process of the Mandible

by

Katherine C. Woronowicz

DISSERTATION

Submitted in partial satisfaction of the requirements for the degree of

DOCTOR OF PHILOSOPHY

in

DEVELOPMENTAL AND STEM CELL BIOLOGY

in the

GRADUATE DIVISION

of the

UNIVERSITY OF CALIFORNIA, SAN FRANCISCO

Approved:

Dedication and acknowledgements

This work is dedicated to those who helped me find my way through this project. I wish to thank my parents, for instilling me with an appreciation of learning; my siblings, for encouraging all my endeavors, no matter how odd; my mentor, Rich, who furnished my growth as a writer, a storyteller, and a scientist; the members of my committee, who helped strengthen my weaknesses; my reinforcing circle of friends, who push me to do better in all things; and, finally, my partner, who is my biggest cheerleader and a source of inspiration.

To these people, I give my sincerest thanks. I could not have accomplished this alone.

Abstract

How does form arise during development and change during evolution? How does form relate to function, and what enables structures of embryos to presage their later use in adults? To address these questions, we leverage the distinct functional morphology of the jaw in duck, chick, and quail. Duck develop secondary cartilage at the tendon insertion of their jaw adductor muscle on the mandible. An equivalent cartilage is absent in chick and quail. We hypothesize that species-specific jaw architecture and mechanical forces promote secondary cartilage in duck through differential regulation of FGF and TGFβ signaling. First, we examine the role of neural crest mesenchyme (NCM), which produces all jaw skeletal and connective tissues, in establishing species-specific pattern by transplanting NCM from chick to duck. Second, we investigate links between jaw architecture and mechanical forces by examining motility and by using finite element modeling. Third, we utilize loss-of-function approaches to determine whether candidate signaling mechanisms like voltage-gated ion channels and FGF or TGFβ signaling are required for secondary cartilage induction. Fourth, we perform gain-of-function experiments to determine whether FGF and TGFβ signaling are sufficient to induce chondrogenesis. Fifth, we quantified FGF and TGFβ pathway member expression in paralyzed and control samples to pinpoint potential mechanically regulated target genes. Our results provide insights on mechanisms linking musculoskeletal form and function during development, disease, and evolution.

Table of Contents

List of Tables

List of Figures

Chapter 1

Introduction

Introduction

Beginning with Aristotle, biologists endeavored to categorize species based on physical characteristics (Russell, 1916). This effort was largely motivated by the narcissistic conviction that all life on earth was inferior to "man." Each organism was studied and categorized under the erroneous belief that a hierarchy of forms could be constructed, culminating with "man" at the top. Ernst Haeckel, a major proponent of this philosophy, believed that all forms of the animal kingdom were "recapitulated" during human development. To Haeckel and the staunch recapitulationists, arresting the unfurling of human development, at any stage, whether as a single celled zygote, a blastocyst, a neurula, or a more advanced stage, would produce one of the "inferior" forms in the *Stammbaum des Menschen*, or family tree of man (Gould, 1977; Haeckel, 1891). Eventually, evidence accrued against recapitulation and the belief that "Ontogeny recapitulates phylogeny" until its stronghold on developmental and evolutionary thought was rightfully overturned (De Beer, 1958; Garstang, 1922; Hall, 1999).

The issue was that human hubris confined embryologists to labor after constructing an ascending ladder. Adaptations were not recognized as radiation to fill ecological niches. Recapitulationists had to acknowledge that the diversity of forms in the animal kingdom was not some byproduct of developmental arrest. They had to grapple with the realization that, biological forms may reflect their evolutionary roots in the tree of life, but they also reflect **the current pressures of survival and the physical demands of life.** This shift was precipitated by the publication of Charles Darwin's masterpiece, *On the Origin of Species* (1859).

Darwin was among the first to assert that form was shaped by opportunity. In his eyes, life was a struggle for survival. Function dovetailed with form, and over incredible lengths of time, generation after generation, healthy populations adapted with their environment. This iterative process whereby functionality is rewarded is responsible for the diversity of life. In Darwin's own words, "endless forms most beautiful, and most wonderful, have been, and are being, evolved" (1859).

D'Arcy Thompson expanded on the inseparable connection between form and function in his seminal work, *On Growth and Form* (1917). Thompson viewed form as simple geometry and sought to explain every length, angle, volume, and surface area as the product of physical phenomena, writing, "the mechanical phenomena…are profoundly associated with Life, and inseparable from our understanding of Growth and Form" (1917). Thompson encouraged biologists to embrace the physical and mathematical sciences. "Even now, the zoologist has scarce begun to dream of defining in mathematical language even the simplest organic forms" (1917).

In the light of his view that all forms are merely the products of physical forces acting on cells and tissues over a lifetime, his philosophy stood in stark contrast to the recapitulationists. By discarding the rigid mold of natural history and preformation theory, **like Darwin before him, Thompson's work asserted that all life forms are perfect.**

Even at the very beginning, and bathed in fluid, embryogenesis is itself the product of mechanical forces bending, pushing, and pulling tissues to construct an embryo. Thompson knew this well, writing, "the morphologist is *ipso facto* a student of physical science" (1917). "In short, the form of an object is a "diagram of forces," in this sense…we can judge of or deduce the forces that are acting or have acted upon it…" (1917).

The musculoskeleton is exquisitely adapted to detect and respond to the mechanical environment. In fact, musculoskeletal form and proper functional stimulation are entangled from the very beginning. From the first neuromuscular connection, muscles periodically contract, thereby flexing and extending nascent joints. Such rhythmic contractions encourage joint cavitation, and even alter the shapes of bones for optimum load bearing, in seeming anticipation of functions like locomotion following the embryo's exit from its watery enclosure.

The work contained in this dissertation sheds light on molecular mechanisms that allow form to respond and adapt to functional cues, ultimately reinforcing a form that is exquisitely suited to that function. In this way, form and function are inseperable from cause and effect, like the chicken, born of an egg, which, in turn, lays an egg of its own. This project provided an extended opportunity to reflect on the quandary, as posed by E. S. Russel, of whether "function arises from form or whether form arises from function" (1916).

These pages contain evidence supporting the notion that mechanical stimulation contributes to ontogeny and recounts genetic mechanisms that enable such responses. This thesis is divided into 3 chapters that detail my research into molecular and cellular mechanisms that couple form with function. In chapter 2, I outline fundamental developmental processes of musculoskeletal morphogenesis of craniofacial structures and describe likely mechanisms that mediate adaptation. In chapter 3, I describe experiments pertaining to the mechanical induction of secondary cartilage on the coronoid process of the mandible, a duck specific adaptation that provides robust osteointegration for the mandibular adductor insertion. We examined the role of neural crest mesenchyme (NCM) in establishing species-specific muscle patterning. I quantified jaw motility and used finite element modeling to determine mechanical contributions to jaw morphogenesis. Third, I determined that FGF and TGFβ signaling are each necessary and sufficient to induce secondary chondrogenesis on the coronoid process of both duck and quail, and that signaling activity in both pathways is likely mechanically mediated. In chapter 4, I describe results from ion channel inhibition experiments that suggest L-type calcium channel activity may contribute to induction and maintenance of secondary chondrogenesis. My results provide insight into the mechanisms that enable musculoskeletal adaptation to the mechanical environment in development, evolution, and disease states.

Chapter 2

Cellular Mechanisms Underlying the Evolution of Form and Function in the Vertebrate Jaw

(In collaboration with Richard A. Schneider and included as a book chapter in *The Cell's View of Animal Body Plan Evolution*. Lyons and Srivastava (editors))

Introduction

How does form arise during development and change during evolution? How does form relate to function, and in particular, what processes allow structures of embryos to presage their later use in adults? These are fundamental questions in biology and there is a long history of efforts to answer them. Early attempts to link form and function began at the gross anatomical level. Meticulous comparative studies conducted in a pre-evolutionary framework such as those of Goethe, Oken, Buffon, Daubenton, Lamarck, Geoffroy, Cuvier, and Owen, laid the foundation for comparative methods to study morphological variation and adaptation (Appel, 1987; Russell, 1916). Describing form and function among animals required special language, and Owen defined the words, "homology" and "analogy" with this goal in mind, especially in the context of his work on the vertebrate skull (Owen, 1848). Such precision in language opened the field up for discussions about whether structures being compared across taxa were indeed "the same organ in different animals under every variety of form and function" (Owen, 1843, p. 379).

In the latter half of the 19th Century, questions of form and function became rooted in embryology, especially around the laws of von Baer and Haeckel (de Beer, 1930; Gould, 1977). Haeckel attempted to explain how the forms of animals related to one another during development and evolution when he succinctly (and rather erroneously) stated that, "ontogeny recapitulates phylogeny." Even Darwin emphasized an important role for development when he advanced the notion that anatomical features became highly adapted to their environment through natural selection and descent with

7

modification (Darwin, 1859). His conclusions were based on methodical observations of species-specific form and function. Darwin mused about "the mysterious laws of the correlation of growth":

"Any change in the embryo or larva will almost certainly entail changes in the mature animal. In monstrosities, the correlations between quite distinct parts are very curious…Breeders believe long limbs are almost always accompanied by an elongated head." (Darwin, 1859, pg. 11-12).

These 18th and 19th Century workers practiced their craft and advanced their theories through anatomical and histological observations. The contributions from such early work were invaluable for building a vocabulary and an intellectual framework through which we can probe mechanisms of structural and functional integration in the jaw complex using modern experimental strategies. The goal of this chapter is to lay out the cellular and molecular events that underlie jaw form and function during development, disease, and evolution.

Development and Evolution of the Vertebrate Jaw Complex

The vertebrate jaw skeleton evolved as a composite structure made up of components from two distinct skeletal systems: the viscerocranium and dermatocranium (Noden and Schneider, 2006). The viscerocranium is the cartilaginous skeleton of the jaws, gill arches, and their derivatives while the dermatocranium consists of bones in the palate, cranial vault, and tooth-bearing elements around the mouth (Hall, 2005). The composite

nature of the jaw skeleton is especially evident during embryogenesis. Skeletal elements of the viscerocranium are pre-formed in cartilage and are typically replaced by bone through endochondral and perichondral ossification. In contrast, jaw elements from the dermatocranium form as mesenchymal condensations that differentiate directly into bone through intramembranous ossification (Helms and Schneider, 2003). These are termed dermal bones (Hall, 2005; Patterson, 1977).

During the intramembranous ossification of bone, mesenchymal cells condense and secrete a dense extracellular matrix, called osteoid, which is rich in collagen I and other fibers (Beresford, 1993; Hall and Miyake, 1992). Shortly afterwards, osteoid mineralizes by incorporating calcium phosphate crystals that are absorbed from the vasculature and which provide rigidity to the fibrous network. During cartilage formation, mesenchymal cells condense and secrete an extracellular matrix rich in collagen II and other fibers to produce an avascular tissue (Hall, 1983; Hall, 2005; Patterson, 1977; Thorogood, 1983). This process causes a tissue expansion such that chondrocytes become separated by vast amounts of extracellular matrix. Typically, as chondrocytes mature, they undergo apoptosis, vasculature invades the cartilage and brings in mineral, and the cartilage template is replaced by bone through endochondral ossification. However, chondrocyte death is not required for bone formation. Recent fracture-healing studies have revived the theory that chondrocytes may transform and contribute directly to bone (Almubarak et al., 2016; Bahney et al., 2014; Beresford, 1981; Jing et al., 2015; Park et al., 2015; Roach, 1992, 1997; Scammell and Roach, 1996; Yang et al., 2014a; Yang et al., 2014b; Zhou et al., 2014). Despite these differences in histogenesis, bones that

arise via endochondral and intramembranous ossification, and elements that transform from cartilage to bone become seamlessly integrated both structurally and functionally within the jaw skeleton.

The viscerocranium evolved as a series of arches in support of the gill apparatus along the pharynx. Each pharyngeal arch contains upper and lower skeletal portions, as well as muscular, nervous, and circulatory elements (Noden and Schneider, 2006). The first arch forms the jaws although there has been considerable debate as to whether the jaws are in fact serially homologous with the other arches (Cerny et al., 2004; Kuratani et al., 2013; Miyashita, 2016). Thus, some have suggested using the term "oropharyngeal" to encapsulate the differences in arch development and evolution (Noden and Schneider, 2006). The rostral expansion of cranial structures and ultimately the emergence of vertebrate jaws was likely tied to a shift from passive, sessile feeding to active modes of predation (Gans and Northcutt, 1983; Northcutt, 2005; Northcutt and Gans, 1983). Ancestrally, the upper portion of the viscerocranial jaw skeleton is the palatoquadrate cartilage whereas the lower is Meckel's cartilage, which is the condition still present in groups like sharks (Fig. 1A) (Eames et al., 2007). In many other vertebrate lineages, however, these two cartilages have been reduced and no longer become the main contributors to the functional adult jaws. In reptiles and birds, the palatoquadrate is divided into two distinct cartilages, the epipterygoid and the quadrate (Fig. 1B) (Romer, 1956). Generally, the epipterygoid contributes to the side of the braincase and the quadrate is where the upper jaw connects to the skull (Smith and Schneider, 1998). The functional upper jaw is made up of dermal bones, including the

premaxilla, maxilla, quadratojugal, palatine, and pterygoid (Moore, 1981). Ancestrally, the lower jaw is also made up of several separate elements, most of which are dermal bones including the dentary, surangular, angular, and splenial. Distinct from these dermal bones, the articular ossifies within the proximal portion of Meckel's cartilage (Eames et al., 2004) and contacts the quadrate to form the jaw joint. Therefore, while the jaws themselves arise primarily from dermal bones, the actual connection between the upper and lower jaw still comes from two ossified remnants (i.e., quadrate and articular) of the ancestral cartilaginous upper and lower portions of the first arch (Smith and Schneider, 1998). This characterizes the jaw joint for almost all non-mammalian jawed vertebrates.

In contrast, the mammalian first arch has substantially evolved from the ancestral condition. First, the homologue of the epipterygoid gives rise to a portion of the mammalian alisphenoid bone, which helps close off the braincase (Fig. 1C) (Maier, 1989; Presley, 1981; Presley and Steel, 1976; Schneider, 1999). Second, the quadrate, becomes reduced in size, no longer participates in the jaw joint, and transforms into the incus, which is one of the mammalian middle ear ossicles (Anthwal et al., 2013; Gaupp, 1913; Tucker, 2017). Third, the lower jaw goes from having six different bones to a single bone, the dentary (Moore, 1981). During this process, the articular, like the quadrate, forms another middle ear ossicle, the malleus (Amin and Tucker, 2006; Anthwal et al., 2013; Anthwal et al., 2017). In association with the ancestral jaw joint becoming ear ossicles, a new jaw joint evolves between the dentary and squamosal bones of the dermatocranium (i.e., the dentary-squamosal or temporal-mandibular joint)

in mammals. Such a transformation demonstrates how jaw bones have the remarkable ability to evolve new functions. In this case, bones that once functioned for mastication became bones for hearing (Anthwal et al., 2013; Anthwal et al., 2017). In reptiles and other animals with the ancestral condition, the bones that conduct sound to the inner ear remain closely associated with the jaw. In mammals, however, the sound-conducting middle ear ossicles are isolated from the jaw joint and encapsulated within the skull. Such an arrangement confers mammals with a keen sense of hearing even while chewing.

Form and Function of the Vertebrate Jaw

Vertebrate jaws display a marvelous array of sizes, shapes, and functions, and they have evolved to fill any conceivable dietary and predatory niche (Smith, 1993; Zusi, 1993). One purpose of the jaw apparatus is to obtain, manipulate, and ingest nutritional items. The teeth that often line the opposing surfaces of the upper and lower jaw can aid in grasping, tearing, mastication, or display. There are countless examples of how the form of the jaws has evolved in conjunction with specific functions (de Beer, 1937; Sánchez-Villagra and Smith, 1997; Schneider, 2015; Schultze, 1993; Smith, 1993; Tokita, 2003, 2004; Tokita et al., 2007; Tokita et al., 2013; Tokita and Schneider, 2009; Zusi, 1993). For instance, some deep-sea fish, dragonfish, are capable of ingesting prey rivaling their own size (Schnell and Johnson, 2017). To achieve this feat, they evolved a loose connection between the occiput and the first vertebra in which the space between the two bones is occupied by an anterior extension of the notochord. This flexible connection allows the head to elevate and achieve extremely wide gapes. They also

lack an intramandibular membrane which enables the jaws to shut with remarkable speed (Schnell and Johnson, 2017). Among reptiles, snakes often consume prey larger than their own skulls and accommodate extreme expansion with highly flexible upper and lower jaws. Large prey is incrementally forced down the esophagus by "snout shifting" or "pterygoid walking" in which tooth-bearing elements of the upper jaw alternately ratchet over the prey (Lee et al., 1999). Although jaws are typically symmetrical, crossbills, which are a type of finch, evolved asymmetrical beaks such that the distal tips cross. This unusual adaptation enables the birds to pry open conifer cone scales and extract seeds (Benkman and Lindholm, 1991). Within mammals, giant anteaters, which retrieve insects from tightly confined spaces like insect burrows, feature a specialized moving morphology in which the jaw "opens" by rotating the mandibles about their long axes rather than by depressing the jaws (Naples, 1999). Though myriad jaw morphologies exist and have existed, all vertebrate jaws share common developmental and evolutionary origins, and their functional units typically integrate with the same adjoining nervous, muscular, vascular, and connective tissue components (de Beer, 1930; Goodrich, 1930).

In general, jaw movement is enabled by pairs of adductor, abductor, and levator muscles that originate on the skull and insert onto various aspects of the mandible (Herring, 1993; Noden and Francis-West, 2006). The main jaw adductor muscles are innervated by the trigeminal nerve (n. V) whereas the abductors are innervated by the facial nerve (n. VII) (Fig. 2D) (Noden, 1991). For most species, lateral movement is fairly restricted and jaw abduction and adduction occurs in a motion that resembles

opening and closing a book. As a means to transmit force, muscles and bones are joined by tendons, which are continuations of the mysia that ensheath skeletal muscles. In contrast to muscle and bone, which are well-vascularized, tendons are avascular. The junction between tendon and bone, called an enthesis, is marked by a transition zone between the fibrous matrix of tendon and the mineralized matrix of bone (Apostolakos et al., 2014; Lu and Thomopoulos, 2013; Schwartz and Thomopoulos, 2015; Smith et al., 2012; Subramanian and Schilling, 2015; Zelzer et al., 2014). The bundles of densely packed, axially aligned fibers that comprise a tendon must smoothly transform into cortical bone for effective transmission of mechanical loads. Understanding molecular and cellular mechanisms that enable certain tendons to achieve robust osteointegration, has clinical implications for enhancing the capacity of torn muscle insertions to be re-attached to bone via molecular therapies (Bunker et al., 2014; Hashimoto et al., 2007; Li et al., 2006; Nakase et al., 2010; Rundle et al., 2014; Sasaki et al., 2008; Thomopoulos et al., 2010; Wang et al., 2010).

Tendons primarily distribute tension from muscle to bone, but in tendons that wrap around bones, like the insertions of the calcaneal tendon or the fibularis longus in humans, regions of compression may be created where the tendon is pressed against the surface of the bone (Benjamin and Ralphs, 1998; Carter and Beaupré, 2007). Fibrocartilage may develop within compressed regions of tendons (Benjamin and Ralphs, 1998; Carter and Beaupré, 2007). Hallmarks of fibrocartilaginous tendons include sparsely distributed chondrocytes and a cartilaginous matrix enriched with

molecules associated with resisting compression (Benjamin and Ralphs, 1998; Carter and Beaupré, 2007).

A specialized fibrocartilaginous joint, the temporal mandibular joint, (TMJ) is a critical component of normal mammalian jaw function. Temporomandibular disorders (TMD) are highly prevalent human clinical conditions that affect approximately 10% of the population (LeResche, 1997; Liu and Steinkeler, 2013) and cause acute pain and suffering for patients (Wadhwa and Kapila, 2008). Many TMD arise from genetic or environmental perturbations to the structural integrity of the jaw musculoskeletal system, which ultimately compromises the function of the TMJ. Strategies for molecular and cell-based therapies to restore normal temporomandibular joint (TMJ) function impaired by birth defects, injury, or disease can benefit from identifying mechanisms that control the development of a highly specialized tissue called secondary cartilage, which is present on certain regions of the jaw skeleton.

Secondary cartilage forms independent of, and subsequent to the primary cartilaginous skeleton, and is found within joints, sutures, ligaments, and tendons of birds and mammals (Bailleul et al., 2012, 2013; Beresford, 1981; Hall, 2005). Although, fossil evidence suggests that a non-avian dinosaur, *Hypacrosaurus stebingeri,* possessed secondary cartilage within a mandibular adductor insertion, raising the possibility that this tissue was also present in some reptiles (Bailleul et al., 2012, 2013). In the human jaw, secondary cartilage at the condylar and coronoid processes is required for proper kinetic movement of the TMJ (Kantomaa and Rönning, 1997; Merida-Velasco et al.,

2009; Merida-Velasco et al., 1999; Shibata et al., 2013; Yuodelis, 1966). Secondary cartilage degeneration and TMD often result from trauma, altered mechanical loading, genetic perturbations, and/or hormonal changes. The coronoid process plays an essential role during normal TMJ function by helping to maintain a proper condyle-fossa relationship and intercuspal position. Coronoid process anomalies such as hyper- and hypoplasias, osteochondromas, or those associated with hemifacial microsomia and DiGeorge syndrome may have, as part of their etiology, disruptions to molecular and biomechanical signals that affect secondary cartilage (Amorim et al., 2010; Amorim et al., 2008; Bernstein and Fernandez, 1984; Fernandez Ferro et al., 2008; Gatti et al., 1985; Hernandez-Alfaro et al., 2000; Huang et al., 2013b; Jerome and Papaioannou, 2001; Shibata et al., 2003; Vargervik and Miller, 1984; Villanueva et al., 2006). Also, some patients with restricted ability to open their mouths have an enlarged coronoid process due to either congenital defects or mandibular hypomobility following internal TMJ derangement (Isberg and Eliasson, 1990; Kantomaa and Rönning, 1997). Thus, focusing on determinants of secondary cartilage is crucial for treating and ultimately preventing a wide range of TMD. In particular, mechanisms through which chondrogenic and mechano-responsive factors are regulated, and how changes to the mechanical environment alter expression of these factors, remain obscure. Thus, elucidating how secondary cartilage is induced and maintained can help shed light on a major unmet clinical need.

Formation of secondary cartilage relies on mechanical stimulation and therefore, the evolutionary presence or absence of secondary cartilage reflects species-specific

variation in functional jaw anatomy (Beresford, 1981; Fang and Hall, 1997; Hall, 1979; Stutzmann and Petrovic, 1975). In humans, rats, cats, and duck, secondary cartilage forms at the tendon insertion (i.e., enthesis) of the jaw adductor muscles on the coronoid process (Fig. 2H) (Amorim et al., 2010; Amorim et al., 2008; Hall, 2005; Horowitz and Shapiro, 1951; Kantomaa and Rönning, 1997; Moore, 1973, 1981; Solem et al., 2011; Soni and Malloy, 1974; Vinkka, 1982; Washburn, 1947). An equivalent secondary cartilage is absent in mice, guinea pigs, chick, and quail (Boyd et al., 1967; Moss and Meehan, 1970; Rot-Nikcevic et al., 2007; Shibata et al., 2003; Solem et al., 2011). Why secondary cartilage arises at this location in some species and not others is unclear but presumably the underlying mechanisms are responsive to differential forces generated by muscle attachments and jaw movements (Carter and Beaupré, 2007; Hall, 1967, 1968, 1986; Solem et al., 2011). In humans and duck, secondary cartilage at the coronoid process provides a broad lateral insertion for the adductor muscles, which enhances leverage and facilitates the sliding motion needed for their specialized modes of feeding (Amorim et al., 2010; Amorim et al., 2008; Dawson et al., 2011; Hems and Tillmann, 2000; Radlanski et al., 2004; Spyropoulos, 1977; Yuodelis, 1966; Zweers, 1974; Zweers, 1976; Zweers et al., 1976; Zweers et al., 1977). Duck feed via levered straining of water and sediment. This involves rapid opening and closing of the mandible, which requires sudden acceleration and significant force (Zweers et al., 1977). Conversely, in quail and chick, which peck at their food, the adductor muscles insert dorsally and the coronoid process appears as a slight bony ridge (Fig. 2G) (Baumel, 1993; Chamberlain, 1943; Fitzgerald, 1969; Jollie, 1957; Lucas and Stettenheim, 1972; McLeod, 1964; Shufeldt, 1909; Van den Heuvel, 1992). Exploiting

such species-specific differences can potentially lead to the discovery of mechanisms through which mechanical forces and molecular signals become integrated and produce secondary cartilage (Solem et al., 2011).

Cellular Origins of Jaw Tissues

The form, function, and evolutionary origin of the jaws are well established, but how do individual components arise during development and become properly patterned? Derivatives of all three germ layers (i.e., ectoderm, mesoderm, endoderm) and especially a major contributor, neural crest mesenchyme (NCM), must communicate seamlessly to produce a musculoskeletal system that is functionally and structurally integrated (Fig. 2A-D). Achieving proper size and shape in the jaws is a dynamic multidimensional problem that vertebrate embryos have to solve. In particular, there must be precise control over cell cycle, cell size, cell number, cell fate, metabolism, and more (Linde-Medina et al., 2016). Teasing apart mechanisms underlying the migration, proliferation, and differentiation of jaw precursor populations is essential for understanding how the jaws become patterned and structurally integrated.

The bones of the face and jaws are derived from embryonic prominences flanking the stomodeum, or presumptive oral cavity (Fig. 2C). The first oropharyngeal arch contains two pairs of prominences, the maxillary processes, which lie lateral to the stomodeum and give rise to the secondary palate and portions of the upper jaws; and the mandibular processes, which lie inferior to the stomodeum and produce the lower jaws (Schneider, 2005; Schneider et al., 1999). The frontonasal process and the lateral and

medial nasal processes give rise to the mid and upper face and the primary palate (Hu and Marcucio, 2012; Hu et al., 2003; Szabo-Rogers et al., 2010). While these prominences allow diverse and complex morphologies to develop and evolve, fusion defects, particularly during palatal formation, are among the most common birth defects (Cordero et al., 2002; Eames and Schneider, 2005; Schneider et al., 1999; Shkoukani et al., 2013).

The oropharyngeal arches are populated by NCM, which arises at the boundary between the neural plate and the non-neural ectoderm followed by an epithelial to mesenchymal transformation (Baker and Bronner-Fraser, 1997; Bronner-Fraser, 1994; Hörstadius, 1950; Saint-Jeannet, 2006; Selleck and Bronner-Fraser, 1996; Selleck and Bronner-Fraser, 1995; Theveneau and Mayor, 2012; Tosney, 1982). NCM migrates extensively and gives rise to numerous derivatives in the jaw apparatus including cartilage, bone, tendon, and muscle connective tissues (Couly et al., 1993; Dupin et al., 2010; Jheon and Schneider, 2009; Jiang et al., 2002; Le Lièvre, 1978; Le Lievre and Le Douarin, 1975; McBratney-Owen et al., 2008; Morriss-Kay, 2001; Noden and Schneider, 2006; Noden, 1978, 1983a; Yoshida et al., 2008). Chemoattractant gradients appear to draw NCM to the oropharyngeal arches (McLennan et al., 2015a). Many molecules like fibroblast growth factors (FGFs), vascular endothelial growth factors (VEGFs), and other secreted molecules are thought to attract migrating NCM, but whether such gradients are sufficient to guide long-range NCM migration remains an open question (Creuzet et al., 2004; McLennan et al., 2015b; Olesnicky Killian et al., 2009; Shellard and Mayor, 2016). Other *in vivo* and *in silico* data predict that a chemoattractive gradient may not be

required for collective NCM migration. Instead, contact inhibition may drive the long-range, directional migration of NCM (Kulesa et al., 2004; Roycroft and Mayor, 2016; Shellard and Mayor, 2016; Theveneau and Mayor, 2012; Trainor et al., 2002b). Repulsive signals also direct streams of migrating NCM by way of Eph/ephrin and neuropilin/semaphorin signaling for example (Gammill et al., 2007; Golding et al., 2000; Minoux and Rijli, 2010; Yu and Moens, 2005). Likely a combination of contact inhibition along with attractive and repulsive signals regulate cranial NCM streaming and funnel the cells into their proper oropharyngeal destinations.

Among others, the NCM contributes to the peripheral nervous system, the endocrine system, and pigmentation, but only cranial neural crest normally form the skeletal system and associated muscle connective tissues (Baroffio et al., 1988; Couly et al., 1992; Dupin et al., 2010; Le Lievre and Le Douarin, 1975; Noden, 1978, 1983a, 1988; Noden and Trainor, 2005). Though NCM differentiates into many cell types, the extent of their potency has been disputed. Conflicting interpretations of clonal analyses and lineage tracing have obscured whether NCM is truly multipotent, or whether NCM is a diverse population of fate-restricted cells (Baroffio et al., 1988; Bronner-Fraser and Fraser, 1989; Bronner-Fraser and Fraser, 1988; Dupin et al., 2010; Henion and Weston, 1997; Krispin et al., 2010; Luo et al., 2003; Sieber-Blum, 1989; Stemple and Anderson, 1992). Recent lineage tracing experiments using a fluorescent "confetti" reporter indicate that individual migratory neural crest cells commonly contribute to many cell types and multiple tissues, suggesting that NCM is indeed multipotent (Baggiolini et al., 2015; Snippert et al., 2010). An understanding of the sophisticated gene regulatory

network governing NCM differentiation will shed light on the genetic underpinnings of neurocristopathies, which often have widespread and debilitating effects (Jones et al., 2008; Kissel et al., 1981; Sanchez-Villagra et al., 2016).

Once populated by NCM, the jaws rely on discrete and nested molecular programs to establish positional information in the dorsoventral, mediolateral, and proximodistal axes. Despite the wide variety of craniofacial forms in nature, the basic layout of the jaw complex and the underlying genetic modules are conserved (Depew and Compagnucci, 2008; Hanken and Hall, 1993). Jaws are oriented such that the most proximal components articulate at a hinge while the distal components may vary greatly in length and in form (Fig. 2E and F). This simplified view of jaw patterning is known as the "Hinge and Caps Model" (Depew and Compagnucci, 2008). Changes to protein coding sequences, ligand and receptor expression domains, duration of gene expression, and sensitivity to signaling may alter the proportions and relative positions of skeletal elements along the proximodistal axis while maintaining the basic "hinge and caps" organization of the vertebrate jaw (Abzhanov and Tabin, 2004; Ealba et al., 2015; Fish et al., 2014; Mallarino et al., 2011; Schoenebeck et al., 2012; Schoenebeck and Ostrander, 2013).

In contrast to the anteroposterior axis of the trunk or the proximodistal axes of the limbs, which are patterned by overlapping expression domains of Hox-family transcription factors, the frontonasal, maxillary, and mandibular prominences of the first oropharyngeal arch are Hox-free (Hunt et al., 1991; Trainor and Krumlauf, 2000, 2001;

Wilkinson et al., 1989). Instead, jaw patterning depends upon epithelial-mesenchymal signaling interactions and a suite of other homeobox family transcription factors, such as the Msx, Dlx, Prx, and Barx genes to confer identity to the mandibular and facial prominences (Alappat et al., 2003; Beverdam et al., 2002; Depew et al., 1999; Depew et al., 2002; Depew et al., 2005; Jeong et al., 2008; Kuraku et al., 2010; Liu et al., 1997; Minoux and Rijli, 2010; Qiu et al., 1997; Qiu et al., 1995; Richman and Lee, 2003; Sato et al., 2008; Shigetani et al., 2000; Shigetani et al., 2002; Talbot et al., 2010; Trainor et al., 2002a). For example, perturbing Dlx gene expression causes a transformation of maxillary versus mandibular identity in the jaw bones (Depew et al., 2002; Depew et al., 2005; Jeong et al., 2008). Homeotic transformations caused by disruptions to homeobox genes such as Dlx and others, demonstrate that this family of transcription factors are master regulators of craniofacial morphogenesis.

Dorsoventral polarity is conferred to the jaws by a series of epithelial-mesenchymal signaling interactions. Retinoic acid (RA) expression in the frontonasal process (FNP) triggers a sequence of reciprocal signaling events between the surface ectoderm, the NCM, and the neuroepithelium to establish a sonic hedgehog (Shh) expression domain in the forebrain (Lee et al., 2001; Schneider et al., 2001). NCM responds to the Shh domain in the forebrain and relays the signal to the surface ectoderm such that the shape of the forebrain and the shape of the face are tightly correlated (Hu and Marcucio, 2009, 2012; Parsons et al., 2011; Schneider et al., 2001). Epithelial-mesenchymal signaling between the NCM and the surface ectoderm establishes a signaling center called the Frontonasal Ectodermal Zone (FEZ) that consists of

complementary FGF8 and Shh signaling domains separated by a precise boundary (Hu and Marcucio, 2009, 2012). RA signaling maintains FGF8 and Shh expression domains in both the neuroepithelium and surface ectoderm (Schneider et al., 2001; Song et al., 2004). Rotating the FEZ 180 degrees induces numerous dorsoventral axes, and produces multiple upper aspects of the jaws (Hu and Marcucio, 2009; Hu et al., 2003). Likewise, Shh mediates interactions between NCM and the pharyngeal endoderm to induce cartilaginous elements and establish anteroposterior polarity in the jaw skeleton (Brito et al., 2006; Couly et al., 2002; Helms and Schneider, 2003). Ablating localized regions of pharyngeal endoderm prevents formation of the nasal capsule, elements of the upper jaw, Meckel's cartilage, the articular, and/or the quadrate. Rotating pharyngeal endoderm by 90°, 180°, or 270° leads to ectopic and correspondingly re-oriented cartilaginous elements. Furthermore, ectopic midline structures like egg teeth can be induced in the lateral nasal process by simultaneous local inhibition of BMP signaling and exogenous RA, which presumably mimics the local signaling environment of the frontonasal process (Lee et al., 2001; Richman and Lee, 2003). These experiments and many others underscore the role of epithelia in establishing the relative positions of cartilage, bone, and epithelial jaw structures (Abzhanov and Tabin, 2004; Ahlgren and Bronner-Fraser, 1999; Ahlgren et al., 2002; Chong et al., 2012; Hu et al., 2015; Schneider et al., 2001; Sheehan-Rooney et al., 2013).

Signaling Interactions Underlying Jaw Patterning

Along with participating in establishing the major axes of the head, NCM dictates the species-specific size and shape of jaws. Neural crest transplant experiments involving

salamanders, frogs, birds, and mice have shown that patterning the jaws is largely driven by cell-autonomous genetic-based responses (Andres, 1949; Mitsiadis et al., 2006; Mitsiadis et al., 2003; Schneider and Helms, 2003; Tucker and Lumsden, 2004; Wagner, 1959). Moreover, chimeric transplant systems have allowed the complex interactions between the NCM and surrounding mesenchymal, and epithelial tissues to be interrogated on the molecular level. For example, transplanting quail NCM into a duck host produces a smaller jaw skeleton with quail-like, species-specific morphology via changes in expression of genes known to be involved in craniofacial patterning (Ealba et al., 2015; Eames and Schneider, 2005, 2008; Hall et al., 2014; Merrill et al., 2008; Solem et al., 2011; Tokita and Schneider, 2009). Furthermore, NCM is remarkably plastic, taking cues from the cellular environment and, under experimental conditions, competent to respond to signals that pattern lateral cranial elements, like the pleurosphenoid, that are normally derived from mesoderm (Schneider, 1999). This is a testament to the evolutionary significance and developmental plasticity of the NCM (Fish and Schneider, 2014b; Gans and Northcutt, 1983; Jheon and Schneider, 2009; Noden and Schneider, 2006; Sanchez-Villagra et al., 2016; Trainor et al., 2003).

Additionally, jaw bone development requires numerous unidirectional and bidirectional, NCM-mediated, epithelial-mesenchymal signaling interactions (Fish and Schneider, 2014b; Griffin et al., 2013; Merrill et al., 2008; Tyler and Hall, 1977). For example, intramembranous ossification of the lower jaw depends upon precisely timed, reciprocal interactions with overlying epithelium (Merrill et al., 2008; Tyler and Hall, 1977). Surgically removing mandibular epithelium prevents mesenchyme from forming bone,

while Meckel's cartailge is unaffected (Merrill et al., 2008; Tyler and Hall, 1977). However, there is nothing intrinsically osteogenic about mandibular epithelium. Transplanting epithelium from the forelimb to the mandible, demonstrates that osteogenic mesenchyme is capable of interacting with non-osteogenic epithelium to form bone (Hall, 1981). These and other transplant experiments provide compelling evidence that NCM wields the power to drive the location of osteogenesis.

In addition, signaling interactions between osteogenic mandibular mesenchyme and overlying epithelium are precisely timed. Once the reciprocal signaling events between epithelium and mesenchyme have occurred, bone forms independent from the presence of the overlying epithelium (Merrill et al., 2008; Tyler and Hall, 1977). Quail-duck chimeric transplants exploit inherent differences in developmental rate, and show that a cell-autonomous, NCM mediated developmental program, dictates the timing of epithelial-mesenchymal signaling. Unilateral NCM transplants from quail, which hatch in 17 days, to duck, which hatch in 28 days, show that precocial bone forms in the mandibular mesenchyme on the quail-donor side a full three developmental stages earlier than on the contralateral duck-host side (Merrill et al., 2008). Such chimeric transplant systems shed light on the timing of bidirectional signaling events and underscore the dominant role of the NCM in dictating the timing of developmental processes like intramembranous ossification.

While craniofacial muscles derive from prechordal mesoderm and unsegmented cranial paraxial mesoderm,,aspects of their pattern are dictated by NCM (Diogo et al., 2015;

Evans and Noden, 2006; Lescroart et al., 2015; Noden, 1983a, b; Noden and Francis-West, 2006; Noden et al., 1999; Noden and Trainor, 2005; Rinon et al., 2007; Sambasivan et al., 2011; Solem et al., 2011; Tokita and Schneider, 2009; Trainor et al., 1994). Myogenic precursors migrate alongside NCM into to the first and second oropharyngeal arches (Trainor and Tam, 1995; Trainor et al., 1994) and provide musculature for the jaws and face, respectively, where their origins and insertions are patterned by NCM derived tendon and connective tissues (Diogo et al., 2015; Grenier et al., 2009; Noden, 1983a; Olsson et al., 2001; Sadaghiani and Thiebaud, 1987; Sambasivan et al., 2011; Solem et al., 2011; Tokita and Schneider, 2009; Tzahor, 2009). Embryological experiments that exploit the species-specific differences between quail and duck shed light on the effects of NCM on cranial muscle patterning. Quail and duck have distinct jaw morphologies in connection with their species-specific modes of feeding (Solem et al., 2011). Transplanting NCM from quail to duck embryos produces duck host derived muscles with quail-like shape and attachment sites (Tokita and Schneider, 2009). Thus, NCM generates species-specific jaw muscle pattern and promotes structural and functional integration of the musculoskeletal system during evolution.

Cranial muscles are distinct from trunk muscles in terms of both embryonic origin and the gene regulatory networks regulating differentiation (Bothe et al., 2007; Diogo et al., 2015; Lescroart et al., 2015; Mootoosamy and Dietrich, 2002; Noden, 1983b; Noden and Francis-West, 2006; Noden et al., 1999; Sambasivan et al., 2009; Shih et al., 2007; Tajbakhsh et al., 1997; Tzahor, 2009; Tzahor et al., 2003). While transcription factors

like Mrf4, Myf5, MyoD, and myogenin are required for myogenesis throughout the body, the specific subsets of genes and the genetic hierarchy regulating these factors varies between muscle groups. For example, the muscles of mastication require a different suite of genes than trunk muscles or even other cranial muscles (Diogo et al., 2015; Sambasivan et al., 2011; Tzahor, 2009). Furthermore, masticatory muscles derive from unsegmented cranial paraxial mesoderm while trunk muscles arise from somites. These differences in tissue origin and differentiation highlight the complex evolutionary history of the head and may explain how congenital muscle defects are often restricted to particular groups of muscles.

Muscles and their surrounding connective tissues are intimately linked both spatially and functionally, even during embryonic development (Kardon, 1998). In fact, reciprocal signaling events regulate muscle patterning and differentiation. Yet, as with myogenic transcription factors, the signaling events that govern cranial muscle differentiation have some important distinctions. Some molecules, like BMP4, repress muscle differentiation in both the head and trunk, while other essential signaling pathways like Shh and canonical Wnt signaling are context dependent. For instance, while Shh, Wnt3a, and Wnt13 promote muscle differentiation in the trunk, they inhibit muscle differentiation in the head (Tzahor et al., 2003). The connective tissues surrounding head muscles express antagonists like Gremlin and Frzb, which relieve repression of muscle development by BMPs and Wnts and allow cranial muscles to differentiate (Couly et al., 1992; Noden, 1983a, b; Tzahor et al., 2003). Connective tissue fibroblasts supply critical signals for both fast- and slow-twitch muscle differentiation and establish basic muscle

patterns prior to tendon differentiation (Kardon et al., 2003; Mathew et al., 2011). Because cranial muscle connective tissues are NCM derived, this provides another developmental mechanism by which NCM mediates species-specific differences in form and function of the head.

Signaling events in tendon development are similarly context-dependent. TGFβ signaling promotes mouse limb tendon development, while FGF signaling is inhibitory (Havis et al., 2014; Subramanian and Schilling, 2015). By contrast, FGF signaling is a well-documented pro-tendon signal in chick limbs while promoting axial tendon development in both mouse and chick (Brent et al., 2005; Brent et al., 2003; Smith et al., 2005). While the mechanisms of head and trunk myogenesis are slowly being teased apart, what has become clear is that the complex and distinct programs generating skeletal muscle is are a testament to the plasticity of coopted genetic networks. Such plasticity enables vertebrates to adapt and create jaw muscle arrangements suited for novel functions.

Establishing anatomical size and shape is another critical process underlying the structural and functional integration of the jaw complex. The modules of gene expression responsible for subtle evolutionary changes to the dimensions of chondrogenic and skeletogenic elements of the head have been interrogated using quail, chick, duck, Darwin's Finches, and other model systems (Attanasio et al., 2013; Fish et al., 2011; Mallarino et al., 2011; Schneider, 2007; Young et al., 2010). Studies of Darwin's Finches and other birds have uncovered modules that modify beak depth,

width, and length (Abzhanov et al., 2006; Abzhanov et al., 2004; Campas et al., 2010; Mallarino et al., 2011; Schneider, 2007; Wu et al., 2006; Wu et al., 2004). For example, BMP (depth and width), calcium (length), TGFβ, and Wnt signaling have been implicated in regulating the shape and size of the upper jaw. Sequence changes in transcription factors, like Alx1 for example, are also associated with alterations in jaw shape (Lamichhaney et al., 2015). Moreover, there are thousands of putative active enhancers during craniofacial morphogenesis indicating that many yet to be discovered mechanisms from paracrine signaling to transcriptional regulation likely govern jaw size and shape (Attanasio et al., 2013).

The Role of Mechanical Forces During Jaw Development

During embryogenesis, the formation and growth of jaw tissues are influenced by external factors, including the mechanical environment. Muscles, bones, and tendons are attuned to detect biomechanical forces. These tissues respond and adapt to mechanical stimulation, often undergoing hypertrophy in the presence of increased loading, and atrophy with disuse (Benjamin and Ralphs, 1998; Blitz et al., 2009; Carter and Beaupré, 2007; Giori et al., 1993; Kuo and Tuan, 2008; Maeda et al., 2011; Matyas et al., 1995; Schweitzer et al., 2010; Sharir et al., 2011; Thomopoulos et al., 2007).

Developmental plasticity in response to mechanical cues is key for creating robust muscle insertions. In sites where tendons transduce high magnitude forces from muscles, bony eminences may form. Pools of cells which express both cartilage (*Sox9*) and tendon (*Scx*) lineage markers contribute to bony eminence development throughout

the body such as the deltoid protuberance, the great trochanter of the femur, and the angular process of the mandible (Blitz et al., 2013; Sugimoto et al., 2013). An example of developmental plasticity comes from descriptions of a bipedal goat born without forelimbs (Slijper, 1942; West-Eberhard, 2005). In this case the gluteus muscle became elongated anteriorly and featured novel tendons (Slijper, 1942). Thus, proper musculoskeletal development depends upon the dynamic ability of tendons to detect and respond to biomechanical cues in the local environment.

During development, the formation of neuromuscular junctions facilitates muscle contractions leading to embryonic motility. Avians are well suited for characterizing and quantifying embryonic motility because their large embryos are easily observed (Bradley, 1999; Chambers et al., 1995; Hamburger, 1965; Hamburger and Oppenheim, 1967; Hamburger et al., 1966; Hammond et al., 2007; Muller, 2003; Oppenheim, 1966, 1968, 1970). In chick, the first neuromuscular junctions form in the trunk (Hosseini and Hogg, 1991). Random depolarizations strengthen neuromuscular junctions and mature into cyclic, stereotyped movements of the head, trunk, and limbs. Cyclic motility such as the stepping patterns observed late in chick development may enhance precocial behaviors like the chick's ability to walk shortly after hatching (Ryu and Bradley, 2009).

Embryonic motility is a fundamental mechanism by which embryonic form can presage adult function (Blitz et al., 2009; Carter and Beaupré, 2007; Hall, 1967, 1968, 1972, 1986; Hall and Herring, 1990; Schweitzer et al., 2010; Sharir et al., 2011; Solem et al., 2011; Wu et al., 2001). As Wolff's Law predicts, disruptions to embryonic motility cause

widespread, severe musculoskeletal defects. Early paralysis can cause severe defects in joint cavitation (Kahn et al., 2009; Lamb et al., 2003; Murray and Drachman, 1969; Osborne et al., 2002; Persson, 1983; Roddy et al., 2011). Later paralysis can lead to defects in the size, shape, extent of ossification, and relative proportions of skeletal elements (Blitz et al., 2009; Pitsillides, 2006; Pollard et al., 2014; Sharir et al., 2011; Shwartz et al., 2012). Embryos with muscle contractility defects tend to have cylindrical long bones. Wild-type littermate bones are irregularly shaped when axially cross-sectioned, which computer models predict makes bones better able to withstand loads from standing and walking. Paralysis also negatively affects bone ridges and large muscle attachment sites (Blitz et al., 2009). However, the mechanisms that facilitate the relationship between mechanical stimulation and musculoskeletal development and remodeling remain largely unknown.

Proper mechanical stimulation is also required for secondary cartilage induction and maintenance (Hall, 1967, 1968, 1986; Murray, 1963; Murray and Smiles, 1965; Murray and Hall, 1966). *Ex-vivo* culture of embryonic chick jaws shows that secondary chondrogenesis at the ball-and-socket joint between the quadrate and quadratojugal depends upon cyclic mechanical stimulation (Hall, 1967, 1968). But is embryonic motility sufficient to explain species-specific differences in secondary chondrogenesis such as the difference in the duck and quail coronoid process? Secondary cartilage fails to form on the duck coronoid process in the absence of proper mechanical stimulation, but, even though no such cartilage forms in quail, the jaws begin moving at the same developmental stage (Solem et al., 2011). This seeming contradiction may be explained

by species-specific jaw geometry. The lateral nature of the mandibular adductor insertion in duck is predicted to create a combination of axial tension as well as compression when the adductor contracts, similar to wrap-around tendons (Carter and Beaupré, 2007; Solem et al., 2011). By comparison, cells in the dorsal, quail mandibular adductor insertion are expected to experience primarily axial tension (Solem et al., 2011). Based on these observations, species-specific jaw geometry and the resulting differences in the mechanical environment may determine the presence or absence of secondary cartilage, indicating that secondary chondrogenesis on the coronoid process is induced by the quality rather than the quantity of mechanical stimulation. But which pathways are required for the cells to adapt and respond to the mechanical environment? Knowledge of the signaling events that depend upon biomechanical forces, and which signaling pathways in particular respond to the mechanical environment, is limited. Wnt signaling and the osteocyte-specific Wnt inhibitor, sclerostin, have been implicated in mechanosensitive bone remodeling (Robling et al., 2016; Robling et al., 2008; Tu et al., 2012). Other potential mechanisms may include ligands being freed from the extracellular matrix, ion channels, focal adhesions, cytoskeletal dynamics, and many others (del Rio et al., 2009; Dupont et al., 2011; Hamill and McBride, 1996; Maeda et al., 2011; Mammoto and Ingber, 2010; Matthews et al., 2006; McBeath et al., 2004; Pruitt et al., 2014; Quinn et al., 2002; Raizman et al., 2010; Ramage et al., 2009; Roberts et al., 2001; Shakibaei and Mobasheri, 2003; Solem et al., 2011; Vincent et al., 2002; Vincent et al., 2007; Wang et al., 2009).

Studies on mechanical aspects of form and function of the jaw tend to operate in a different realm than studies of jaw development and evolution. There is little overlap in the techniques utilized. Mechanical studies tend to shy away from cell-biological details, and vice-versa. Fostering collaboration and interdisciplinary approaches that blend the strengths of engineering and modeling with novel cell biological, genetic, and imaging tools *in vivo* will shed light on the intersection between evolution, developmental biology, and the mechanical environment.

Chapter 3

Developmental Mechanisms Linking Form and Function during Jaw Evolution

(In collaboration with Stephanie E. Gline, Safa T. Herfat, Aaron J. Fields, and Richard A.

Schneider and submitted to bioRxiv)

Introduction

One of the most remarkable aspects of being an embryo, and a phenomenon that has intrigued embryologists since Aristotle, is the ability to grow in a manner "rather prospective than retrospective" (Thompson, 1917). In theory, how the form of an embryo can presage later adult function is explained by Aristotle's notion that "the organism is the $τελος$, or final cause, of its own process of generation and development" (Thompson, 1917). But elucidating precise molecular mechanisms that link form and function, and specifically whether form arises from function or function follows form remains challenging, because, like the chicken and the egg, form and function are seamlessly intertwined during development and evolution

Some of the most illustrious instances of form and function appear in the craniofacial complex in birds, which are masters of adaptation. A highly specialized beak seems to exist for every avian diet: insectivore, granivore, nectarivore, frugivore, carnivore, omnivore, etc. (Schneider, 2007; Zusi, 1993). Each diet is supported by a range of structural adaptations to the jaw including size, shape, and sites of muscle attachments (Fish and Schneider, 2014b; Tokita and Schneider, 2009). For example, in *Anseriformes*, or waterfowl such as duck, which use their broad bills to dredge sediment for food, the mandibular adductor muscle attaches laterally to a large protruding coronoid process on the mandible. Such a configuration provides a robust insertion site for transmitting the high magnitude forces associated with suction pump and levered straining jaw movements (Dawson et al., 2011; Zweers, 1974; Zweers et al., 1977). In duck, as in humans, the coronoid process develops via a secondary cartilage

intermediate (Solem et al., 2011). Secondary cartilage requires proper mechanical stimulation for its induction and maintenance, and is a feature of many joints in neognathic avian skulls, as well as in select tendon and muscle insertions (Hall, 1967, 1968, 1972, 1986). In paralyzed duck, secondary cartilage fails to form at the coronoid process suggesting that the mechanical environment (i.e., function) during development promotes secondary chondrogenesis (Solem et al., 2011). By comparison, *Galliformes* like quail and chick, feed primarily by pecking seed and this is reflected in the relatively gracile construction of the jaw and adductor muscles, which insert dorsally on the mandible and lack secondary cartilage on the coronoid process. Exploiting such species-specific differences in quail and duck, as we have done previously (Ealba et al., 2015; Eames and Schneider, 2008; Fish et al., 2014; Hall et al., 2014; Schneider, 2005; Schneider and Helms, 2003; Tokita and Schneider, 2009) provides an opportunity to investigate molecular and cellular mechanisms that integrate form and function in the jaw apparatus during development and evolution.

The species-specific jaw morphology that distinguishes duck from quail is mediated by the neural crest mesenchyme (NCM), which gives rise to all of the associated cartilage, bone, and muscle connective tissues (Noden and Schneider, 2006). Transplanting NCM from quail into duck demonstrates that NCM controls the size and shape of the jaw skeleton, as well as the orientation and insertion of muscles (Ealba et al., 2015; Eames and Schneider, 2008; Fish et al., 2014; Hall et al., 2014; Schneider and Helms, 2003; Solem et al., 2011; Tokita and Schneider, 2009). Chimeric "quck" embryos develop a quail-like jaw musculoskeleton including a dorsal mandibular adductor insertion that

lacks secondary cartilage. Presumably, for such a transformation to occur, quail NCM alters the duck-host environment in a manner that changes not only the form of the jaw apparatus but also the function, since the presence or absence of secondary cartilage depends upon mechanical stimulation. In this context, the lateral versus dorsal insertion of the mandibular adductor muscle might produce distinct mechanical forces, but differences in the quantity and/or quality of such forces in quail versus duck are completely unknown. Furthermore, those signaling pathways that are mechanoresponsive and ultimately govern the species-specific adaptation to the mechanical environment remain unclear.

We hypothesized that the specialized form of the duck mandibular adductor complex creates a species-specific mechanical environment, which activates molecular programs for secondary chondrogenesis at the coronoid process. To test our hypothesis, we employed a range of strategies. First, we modulated the form of the duck mandibular adductor complex by titrating the amount of donor versus host NCM-derived connective tissues in chick-duck chimeras. Second, we quantified embryonic jaw motility in duck versus quail to determine if differences in the frequency of jaw movement underlie species-specific jaw morphology. Third, we used finite element analysis to model the mechanical environment of the mandibular adductor complex and to uncover the magnitude, direction, and distribution of mechanical forces present during development. Fourth, we disrupted the mechanical environment of the mandibular adductor complex by paralyzing duck embryos and then assayed for changes in molecular programs for secondary chondrogenesis at the coronoid process.

Fifth, we investigated potential signaling pathways through which mechanical forces induce secondary cartilage by utilizing biochemical inhibitors. Sixth, we rescued the paralysis with recombinant proteins to test if the pathways we identified are sufficient to induce secondary cartilage in the absence of normal mechanical loading (i.e., in paralyzed embryos). And seventh, we induced secondary cartilage in the quail mandibular adductor insertion where, ordinarily, there is none.

Our results reveal that the form of the mandibular adductor complex is patterned by NCM in a dose-dependent manner. We find that distinct mechanical forces are present at the presumptive coronoid process despite the fact that we observe little difference in the embryonic motility of the developing jaw in quail versus duck. Additionally, we discover that both FGF and TGFβ signaling are responsive to mechanical forces within the mandibular adductor complex, and are necessary and sufficient for secondary chondrogenesis at the coronoid process. Overall, this study draws a direct connection among species-specific morphology, mechanical forces, resultant changes in signaling activity, and musculoskeletal plasticity, demonstrating that form initially dictates function but that function is also a potent modulator of musculoskeletal form during development and evolution.

Methods

The use of avian embryos

Fertilized eggs of Japanese quail (*Coturnix coturnix japonica*) and white Pekin duck (*Anas platyrhynchos*) were purchased from AA Lab Eggs (Westminster, CA) and incubated at 37.5°C in a humidified chamber (GQF Hova-Bator, Savannah, GA) until they reached embryonic stages appropriate for manipulations, treatments, and analyses. For all procedures, we adhered to accepted practices for the humane treatment of avian embryos as described in S3.4.4 of the AVMA Guidelines for the Euthanasia of Animals: 2013 Edition (Leary et al., 2013). Embryos were matched at equivalent stages using an approach that is based on external morphological characters and that is independent of body size and incubation time (Hamilton, 1965; Ricklefs and Starck, 1998; Starck and Ricklefs, 1998). The Hamburger and Hamilton (HH) staging system, originally devised for chick, is a well-established standard (Hamburger and Hamilton, 1951). Separate staging systems do exist for duck (Koecke, 1958) and quail (Ainsworth et al., 2010; Nakane and Tsudzuki, 1999; Padgett and Ivey, 1960; Zacchei, 1961) but these embryos can also be staged via the HH scheme used for chicken (Ainsworth et al., 2010; Le Douarin et al., 1996; Lwigale and Schneider, 2008; Mitgutsch et al., 2011; Schneider and Helms, 2003; Smith et al., 2015; Starck, 1989; Yamashita and Sohal, 1987; Young et al., 2014). Criteria utilized to align quail and duck at a particular HH stage change over time depending on which structures become prominent. For early embryonic stages, we used the extent of neurulation, neural crest migration, and somitogenesis as markers (Fish et al., 2014; Lwigale and Schneider, 2008; Schneider and Helms, 2003); whereas later, we

relied on growth of the limbs, facial primordia, feather buds, and eyes since these become more diagnostic (Eames and Schneider, 2005; Merrill et al., 2008).

Histology

Embryos were fixed overnight in 10% neutral buffered formalin at 4°C, paraffin embedded, and sectioned at 10µm. Cartilage, bone, muscle, and tendon were visualized using Milligan's Trichrome or Safranin-O (Presnell and Schreibman, 1997).

Clearing and staining

Embryos were fixed overnight at 4°C in 10% neutral buffered formalin before clearing and staining with Alcian Blue and Alizarin Red to visualize cartilage and bone of the jaw complex including the coronoid process (Wassersug, 1976).

cDNA preparation

RNA was isolated from microdissected duck samples using the ARCTURUS PicoPure RNA Isolation Kit (ThermoFisher, Waltham, MA). Reaction specifications and reverse transcription programs were followed as previously published (Ealba and Schneider, 2013).

In situ hybridization

Spatial and temporal patters of gene expression were analyzed by in situ hybridization as previously described (Albrecht et al., 1997; Schneider et al., 2001). Species-specific probes against duck FGF and TGFβ ligands (*Fgf4, Fgf8, Tgfβ2, Tgfβ3*), receptors

(*Fgfr2, Fgfr3, Tgfβr2*), and downstream effectors (*Pea3, Erm, and Smad3*), were cloned

from duck HH33 cDNA libraries isolated from whole heads (Table S1). Probes were

designed to recognize all isoforms. High fidelity Pfu DNA polymerase (Strategene, La

Jolla, CA) was used to amplify target genes. The protocol was: step 1, 2 minutes at

94°C; step 2, 30 seconds at 94°C; step 3, 30 seconds at 37.5°C; step 4, 2 minutes at

72°C; step 5, repeat steps 2 to 4 39 times; step 6, 5 minutes at 72°C; step 7, hold at

4°C. PCR products were run on a 1% agarose gel. Bands of the appropriate molecular

weight were gel extracted using QIAEX II Gel Extraction Kit (Qiagen, Hilden, Germany).

PCR products were ligated into pGEM-T Easy Vector System I (Promega, Madison, WI)

or CloneJET PCR Cloning Kit (ThermoFisher, Waltham, MA) and used to transform

NEB 5α E. coli cells (New England Biolabs, Ipswitch, MA). Clones were sequenced

(McLab, South San Francisco, CA) using a T7 promoter primer. Sequencing results

were analyzed using Geneious (Biomatters, Auckland, New Zealand). Once probe

sequences were confirmed, DIG-labeled RNA probes were synthesized using DIG RNA

labeling mix (Roche, Basel, Switzerland). Cloned species-specific duck probes were

used to identify gene expression patterns in embedded and sectioned HH33 and HH36

paralyzed and stage matched control duck.

TUNEL staining

10µm tissue sections of duck embryos 24 hours after treatment with SU5402,

SB431542, or DMSO soaked beads were processed using a fluorescent TUNEL

staining kit (Roche, Basel, Switzerland). As a positive control, DNase was added to a

subset of DMSO-treated tissue sections. The percentage of cell death was quantified

using 3D microscopy processing software Imaris (Bitplane, Belfast, United Kingdom). Image intensity was rendered in 3D and Hoescht (Sigma-Aldrich, St. Louis, MO) and TUNEL-stained nuclei within 100μm of the implanted bead were counted using software-enabled volumetric criteria (surface detail=5μm, background subtraction=12μm, seed point diameter=30μm). Statistical significance was determined by ordinary one-way ANOVA (Prism 7, GraphPad Software, Inc., La Jolla, CA).

Surgical bead implantation

10mM of SU5402 (Sigma-Aldrich, St. Louis, MO), a small molecule that prevents autophosphorylation of receptor tyrosine kinases and is most specific to FGFRs (Sun et al., 1999; Sun et al., 1998), and 100mM of SB431542 (Santa Cruz Biotechnology, Santa Cruz, CA), a small molecule that inhibits autophosphorylation of TGFβRs (Callahan et al., 2002; Inman et al., 2002), were diluted in DMSO. Formate bound AG1-X2 (50-100 mesh, 250-850μm, Bio-Rad, Hercules, CA) beads of about 250-350μm were washed in DMSO at room temperature for about ten minutes before binding small molecule inhibitors. 1mg/ml recombinant human FGF4 (R&D Systems, Minneapolis, MN) was re-suspended in 0.1% filter sterilized BSA in 1x PBS. Heparin acrylic beads about 250-350 μm (Sigma-Aldrich, St. Louis, MO) were used to deliver FGF4 to duck embryos. A 160μg/ml solution containing equal parts recombinant human TGFβ2 and TGFβ3 (R&D Systems, Minneapolis, MN) was prepared using filter sterilized 4mM HCl in PBS containing 0.1% BSA. Affigel Blue beads about 250-300μm (50-100 mesh, 150-300μm, BioRad, Hercules, CA) were used to deliver TGFβ ligands to quail and duck embryos. Both FGF4 bound heparin acrylic beads and TGFβ2 and TGFβ3 bound Affigel Blue

beads were implanted into duck embryos to deliver a combination of all three ligands. Beads were soaked in small molecule inhibitors or ligands for one hour at room temperature before implantation. All concentrations were based on those used previously (Eames and Schneider, 2008; Hayamizu et al., 1991; Niswander et al., 1993; Schneider et al., 2001). Stage HH32 and HH33 embryos were housed in room temperature incubators for one hour before surgeries to minimize embryonic motility. For each bead type used, control surgeries were conducted using beads to deliver carrier. All surgically implanted embryos were collected at HH38. Cleared and stained cases with extensive cartilage and/or bone defects were excluded from analysis under the assumption that a malformation in the jaw skeleton would adversely affect the native mechanical environment. Two-tailed Fisher's exact test was used to determine statistical significance (Prism 7, GraphPad).

Endoscopy and jaw motility quantification

In ovo video footage of quail and duck from HH32 to HH38 was recorded while eggs incubated at 37.5°C. Video recordings were captured using a 1088 HD High Definition Camera (Stryker, Kalamazoo, MI) with a 4mm, 30° arthroscope (Stryker, Kalamazoo, MI). A universal, dual-quartz, halogen, fiber-optic light source (CUDA Surgical, Jacksonville, FL) was threaded onto the endoscope to provide illumination. The arthroscope was inserted through a small opening in the incubation chamber until it was submerged in albumin. Embryos were acclimated to the light source for 15 minutes prior to recording. Three 10-minute videos were collected from each embryo. The interval of time from the first jaw movement to 5 seconds after the last jaw movement was defined

as an activity period, similar to a published quantification method (Hamburger et al., 1965). Average percent active time was calculated along with 95% confidence intervals. Significance was determined using an unpaired, two-tailed Holm-Sidak test adjusted for multiple comparisons (Prism 7, GraphPad).

3D reconstruction and finite element analysis

To characterize species-specific differences in the biomechanical environment of the jaw adductor complex, linear finite element analysis (FEA) was used to predict the magnitude and distribution of the von Mises stress on the coronoid process at the adductor insertion. HH33 mandibles from duck and quail were serially sectioned (10μm thickness), stained with Milligan's trichrome, and imaged at 2.5X magnification. Images were aligned using the orbit and Meckel's cartilage as landmarks. Meckel's cartilage, the quadrate, surangular, and the mandibular adductor were manually segmented and reconstructed in 3D (Amira 6; FEI, Hillsboro, OR). The resulting 3D reconstructions of the jaw complexes were imported into commercial FEA software (ANSYS 17; Canonsburg, PA), which was used for meshing and analysis. Tissues were meshed using tetrahedral elements, which were sized based on convergence results from an iterative mesh refinement procedure. Final models utilized 178,378 (duck) and 54,954 elements (quail). The material properties calculated by Tanck et al. (2000) for mineralized embryonic mouse metatarsals (Young's Modulus (E) = 117MPa; Poisson's Ratio (v) = 0.3) were used for the surangular and Meckel's. The other structures were suppressed prior to performing FEA. Boundary conditions were prescribed to mimic those arising during jaw gaping, and included: 1) a fixed support at the contact surface

between Meckel's and the quadrate; and 2) tensile force (duck 3.28E-04 N; quail 1.05E-04 N) aligned with the longitudinal axis of the mandibular adductor. The magnitudes of the adductor forces were determined using cross-sectional area measurements performed at the longitudinal midpoints and an assumed tensile stress of 1.11kPa (Landmesser and Morris, 1975). Statistical significance was determined using an unpaired, two-tailed, t-test (Prism 7, GraphPad).

Embryo paralysis

HH32 or HH33 duck were paralyzed using 10mg/ml decamethonium bromide (DMBr) (Sigma-Aldrich, St. Louis, MO) in Hank's Buffered Sterile Saline (HBSS) and filter sterilized using a 0.22μm filter. Each embryo was treated with a 0.5ml dose of the DMBr solution administered as previously described (Hall, 1986; Solem et al., 2011).

Microdissections, RNA extraction, RT-qPCR, and analysis

Mandibular adductor insertions were dissected from paralyzed and control duck embryos at HH33 and HH36 and snap frozen in 70% EtOH mixed with dry ice. Microdissected samples were homogenized using a bead-mill (Omni International, Kennesaw, Kentucky) and RNA was isolated using the ARCTURUS PicoPure RNA Isolation Kit (ThermoFisher, Waltham, MA). 200ng cDNA libraries were generated from RNA samples using iScript reverse transcriptase (BioRad, Hercules, CA). Each cDNA library was subsequently diluted to 2ng/μl. Duck *MYOD1*, *SOX9*, *TN-C*, and *UCHL-1* primer pairs were used to determine the relative enrichment of muscle, cartilage, tendon, and nerve tissues, respectively, relative to cDNA libraries from duck jaw

complexes (Table S1). For quality control, HH33 cDNA libraries were excluded from analysis if the sample was enriched for muscle (>1 fold enrichment of *MYOD1* over control cDNA libraries), nerve (>1.5 fold enrichment of *UCHL-1* over control cDNA libraries), or tendon (>2.5 fold enrichment of *SOX9* over control cDNA libraries). At HH36, the top six tendon enriched samples with less than 4-fold *MYOD1* enrichment were included in the analyses. *Fgf2, Fgf4, Fgf8, Fgfr1, Fgfr2, Fgfr3, Pea3, Erm, Tgfß2, Tgfß3, Tgfßr1, Tgfßr2, Tgfßr3, Smad3, Smad7b, and Pai1* expression was determined by quantitative reverse transcription PCR (RT-qPCR) using duck-specific primer pairs (Table S1). For all genes, expression was normalized to *β-Actin* and analysis was done following the ΔΔC(t) method (Ealba and Schneider, 2013; Livak and Schmittgen, 2001). P-values for - ΔΔC(t) values were calculated using an unpaired, two-tailed, Holm-Sidak test adjusted for multiple comparisons (Prism 7, GraphPad).

Generation of chimeras

GFP-chick (Crystal Bioscience, Emeryville, CA) and white Pekin duck eggs were incubated to HH9. Tungsten needles and Spemann pipettes were used to graft two differently sized populations of NCM from chick donors into stage-matched duck hosts, producing chimeric "chuck" (Fish and Schneider, 2014a; Fish et al., 2014; Merrill et al., 2008; Schneider, 1999; Schneider and Helms, 2003; Tucker and Lumsden, 2004). Small grafts extended from the middle of the midbrain to the rostral hindbrain at rhombomere 2, whereas large grafts extended from the forebrain–midbrain boundary to rhombomere 2. Comparable-sized regions were excised from duck hosts. Orthotopic

grafts and sham operations were performed as controls. Controls and chimeras were incubated side-by-side to ensure accurate staging during collections.

Results

Adult jaw morphology is presaged during embryonic development

There are many species-specific differences between Japanese quail and white Pekin duck mandibles. Quail mandibles are slender with a smooth coronoid process and diminutive retroarticular process (Fig. 1A). Duck mandibles feature a robust, laterally protruding coronoid process. Furthermore, duck mandibles are larger than quail, both absolutely and in relative proportion, and have a sizeable retroarticular process (Fig. 1B). Clearing and staining reveals that species-specific jaw morphology is established during embryonic development (Fig. 1C,D). At HH38, an elongate Meckel's cartilage is surrounded by dermal lower jawbones, and the retroarticular processes are still largely comprised of cartilage, yet quail and duck jaw morphologies are already distinguishable. The most obvious difference is the presence of a secondary cartilage intermediate within the mandibular adductor insertion along the surangular bone in duck. Such cartilage is visible in cleared and stained duck embryos as early as HH36. A secondary cartilage never forms on the quail or chick coronoid process.

NCM patterns the mandibular adductor complex in a dose-dependent manner

NCM transplanted from HH9 GFP-positive chick into stage-matched duck hosts transforms the morphology of the jaw and coronoid process (Fig. 1E,F,I,J). The extent of transformation and the distribution of GFP-positive NCM-derived connective tissues depends upon donor graft size. Small NCM transplants result in a limited distribution of GFP-positive skeletal and connective tissues, and produce minor changes to the size and shape of the jaw skeleton, but not enough to affect the coronoid process (Fig.

1G,H). In contrast, large transplants result in extensively distributed GFP-positive skeletal and connective tissues, which transforms the duck jaw skeleton to become more chick-like, including the absence of a secondary cartilage on the donor side (Fig. 1K,L).

The progression of embryonic jaw motility is similar in quail and duck

In ovo videos of embryonic jaw motility captured periodic jaw gaping in quail and duck embryos (Fig. 2A,B,C,D)(Movie S1,S2). The first quantifiable jaw movements occur at HH33 in both quail and duck. HH33 quail are active 10.46% of the time (95% CI ±3.07%, n=9) while stage matched duck are active 5.2% of the time (95% CI ±1.06%, n=10). Both the frequency and duration of jaw movements increase with developmental time in quail and duck (Fig. 2E,F). Quail and duck jaw motility track very closely at HH34 (18.82%±8.32%, n=12 for quail and 15.72%±3.28%, n=18 for duck) and at HH35 (28.58%±16.63%, n=6 for quail and 29.35%±6.57%, n=2 for duck). No statistically significant differences in motility are observed in the developmental stages preceding the appearance of secondary cartilage. A significant difference is observed at HH36 (26.66%±8.36%, n=22 for quail, and 43.97%±5.06, n=26 for duck, $p < 0.0005$), however, by this stage, a secondary cartilage has already formed on the coronoid process. Peak quail jaw motility is observed at HH37 (67.39%±5.7%, n=6 in quail, versus 51.72%±8.69%, n=13 in duck) while duck motility peaks at HH38, but does not exceed quail motility (60.76%±5.79%, n=7 in duck versus 61.67%±5.49%, n=7 in quail).

Finite element analysis predicts distinct mechanical environments at the quail and duck coronoid process

3D reconstructions of HH33 quail and duck jaws including Meckel's, the quadrate, postorbital, surangular, and mandibular adductor were created by manually segmenting histological images (Fig. 3A,B). Reconstructions reveal the species-specific, geometrical differences in the cross-sectional area of the muscle, the direction of contractile force, and the area of the surangular over which force is applied. In duck, the mandibular adductor inserts on the lateral aspect of the surangular, while in quail, the insertion is dorsal. In duck, the insertion is also more proximal to the jaw joint. At its widest, the cross-sectional area of the duck mandibular adductor is $321,000\mu m^2$, while the slender quail muscle is only $114,192\mu m^2$ indicating that the maximum contractile force of the duck muscle is roughly 2.8 times greater than quail.

Finite element models of the insertion between the mandibular adductor and the surangular predict that duck experience a maximum shear stress concentration roughly 60 times greater than quail (0.96MPa in duck versus 0.016MPa in quail)(Fig. 3C,D). Furthermore, the mean von Mises stress experienced in duck (0.053MPa) is significantly higher than in quail (0.0045MPa; p<0.0001). Histograms also reveal the state of shear stress at the insertion is more homogeneous in quail than in duck (Fig. 3E).

FGF pathway member expression changes during development and is affected by paralysis

RT-qPCR analyses on microdissected duck mandibular adductor insertions reveal significant increases in expression of FGF ligands *Fgf2* (5.34±1.50 fold change, p<0.0005), *Fgf4* (449.89±237.59 fold change, p<0.0005), and *Fgf8* (56.22±44.55 fold change, p<0.0005) from HH33 to HH36 (n=13 for HH33 controls, n=10 for HH36 controls)(Fig. 4A). FGF receptors *Fgfr1* (0.76±0.21 fold change, p<0.05), *Fgfr2* (0.19±0.18 fold change, p<0.0005), and *Fgfr3* (0.68±0.30 fold change, p<0.05) significantly diminish in expression over this time. Transcriptional effectors of FGF signaling such as *Pea3* (5.61±1.09 fold change, p<0.0005) and *Erm* (2.44±0.54 fold change, p<0.0005) are both significantly more abundant at HH36 than at HH33.

Paralysis at HH32 does not result in significant changes to expression of FGF signaling pathway members or effectors at HH33 relative to stage-matched controls. In HH36 paralyzed embryos, the only FGF ligand with a significant increase in expression is *Fgf2* relative to HH33 controls (3.67±1.30 fold change, p<0.0005)(n=12 for HH33 paralyzed, n=11 for HH36 paralyzed). However, *Fgf2* expression at HH36 is still significantly less in paralyzed embryos than in stage-matched controls (p<0.05)(asterisk, Fig. 4A). In paralyzed HH36 embryos, *Fgf4* expression is 21.49±33.68 fold more abundant than in HH33 controls and *Fgf8* is 4.79±5.06 fold more abundant, but both genes are still significantly less expressed than in stage-matched controls (p<0.005 for both)(asterisks, Fig. 4A). At HH36, *Fgfr1* (0.55±0.22 fold change, p<0.0005) and *Fgfr2* (0.35±0.29 fold change, p<0.0005) expression are significantly down in paralyzed samples, similar to gene expression dynamics seen in controls over the same period. Unlike control samples, expression of *Pea3* (2.58±2.75 fold change) and *Erm* (1.49±0.67 fold change)

remains relatively flat in paralyzed embryos and, by HH36, are significantly less expressed than in HH36 controls (p<0.05 for both)(asterisks, Fig. 4A).

Analysis of the spatial and temporal patterns of gene expression was conducted in control and paralyzed duck at HH33 and HH36 (Table 1). At HH33, in sagittal section, the mandibular adductor is visible as two muscle bundles divided proximodistally by the mandibular branch of the trigeminal nerve (Fig. 4B). Proximal to the mandibular nerve, the mandibular adductor appears fan-like and inserts broadly. Distal to the mandibular nerve, unipinnate muscle fibers are joined by a fibrous aponeurosis. The musculature and aponeurosis appear relatively disorganized following 24 hours of paralysis (Fig. 4F).

At HH33, *Fgf4* is expressed throughout primary cartilages like the quadrate, and Meckel's, as well as in skeletal muscles like the mandibular adductor, the mandibular adductor insertion, and the mesenchymal condensation that will give rise to secondary cartilage (n=5 for each gene)(Fig. 4C). After 24 hours of paralysis, *Fgf4* expression is maintained in the quadrate and Meckel's, but diminished in the mandibular adductor and its insertion (Fig. 4G). *Fgf8* is expressed in the mandibular adductor, the mandibular adductor insertion, the secondary cartilage insertion, and the surangular condensation (Fig. S1). There is also *Fgf8* expression in primary cartilages like Meckel's cartilage and the quadrate. The secondary cartilage condensation and its *Fgf8* expression domain are not present in embryos 24 hours after paralysis (Fig. S1). *Fgfr2* is expressed in cartilages like the quadrate and Meckel's, particularly in the perichondrium, as well as in the secondary cartilage condensation and the nascent surangular (Fig. 4D). Following

24 hours of paralysis, expression in primary cartilage is maintained, while expression in the secondary cartilage condensation and surangular condensation are diminished (Fig. 4H). *Fgfr3* is expressed in cartilages like the quadrate and Meckel's, but not perichondria, and in the surangular condensation with greater expression around the periphery (Fig. 4E). Paralysis leads to decreased expression in the surangular condensation while expression in primary cartilages is maintained (Fig. 4I). *Pea3* is expressed in the mandibular adductor, the mandibular adductor insertion and the secondary cartilage condensation (Fig. S1). There is also expression in the surangular condensation, primary cartilages and perichondria. 24 hours after paralysis, the secondary cartilage condensation fails to form and the corresponding region of *Pea3* expression is absent (Fig. S1).

By HH36, secondary cartilage is present within the mandibular adductor insertion and is encapsulated in a dense fibrous sheath (Fig. 4J). By this time, the mandibular adductor muscles have begun to separate into distinct superficial sheet-like, proximal fan-like, and distal groups of fibers. HH36 paralyzed embryos have poor muscle and tendon organization and lack a secondary cartilage condensation (Fig. 4N). *Fgf4* (n=5 for each gene), is strongly expressed in HH36 skeletal muscles like the mandibular adductor, the mandibular adductor insertion, and bones like the surangular and periostea (Fig. 4K). The quadrate and Meckel's also express *Fgf4* throughout the cartilage and the perichondrium. *Fgf4* expression is also seen within the secondary cartilage condensation. Paralysis prevents secondary chondrogenesis, however, *Fgf4* expression is maintained in muscle, bone, and primary cartilages (Fig. 4O). *Fgf8* is expressed in

the mandibular adductor, tendon, and throughout the secondary cartilage (Fig. S1). *Fgf8* is also expressed in the surangular bone, the periosteum, and primary cartilage. Paralysis prevents secondary cartilage from forming, but *Fgf8* is still expressed in the muscle and its connective tissues (Fig. S1). *Fgfr2* is expressed in muscle, tendon, bone, periostea, cartilage, perichondria, and within the secondary cartilage (Fig. 4L). Following paralysis, the only change to *Fgfr2* expression is the absence of a secondary cartilage domain (Fig. 4P). *Fgfr3* is expressed by cartilages like the quadrate and Meckel's as well as in the periosteum of bones like the surangular. *Fgfr3* is also expressed by muscle, tendon, bone, periostea, cartilage, perichondria, and secondary cartilage (Fig. 4M). Expression in the secondary cartilage is highest at the center and grows lower towards the periphery. In paralyzed embryos, only the *Fgfr3* expression domain in secondary cartilage is absent (Fig. 4Q). *Pea3* is expressed in the mandibular adductor muscle, tendon, and the secondary cartilage condensation (Fig. S1). *Pea3* is also expressed in primary cartilage, perichondria, bone, and periostea. Due to the absence of secondary cartilage in paralyzed embryos, that *Pea3* expression domain is absent in HH36 embryos (Fig. S1).

TGFβ pathway member expression changes during development and is affected by paralysis

RT-qPCR shows that *Tgfβ2* (4.28±1.29 fold change, p<0.0005) and *Tgfβ3* (7.19±2.11 fold change, p<0.0005) expression increases significantly from HH33 to HH36 (n=10 for HH33 controls, n=10 for HH36 controls)(Fig. 5A). Paralyzed embryos mirror the increases in *Tgfβ2* (2.87±1.36 fold change, p<0.05) and *Tgfβ3* (5.50±2.30 fold change,

p<0.0005) over the same period. Transcriptional activity of receptors *Tgfβr1*, *Tgfβr2*, *Tgfβr3*, and transcriptional effectors *Smad3*, *Smad7b*, and *Pai1* remain flat in controls. In contrast, HH36 paralyzed samples express more *Pai1* (2.53±1.89 fold change) than HH33 controls (p<0.05), and achieve significantly greater expression than HH36 control samples (p<0.05)(asterisk, Fig. 5A).

Our qualitative analyses show that at HH33, *Tgfβ2* is expressed in the mandibular adductor muscle, the mandibular adductor insertion, and the secondary cartilage condensation (Fig. 5B,C). At HH33, following 24 hours of paralysis, expression in muscle and tendon persists while the secondary cartilage condensation and its *Tgfβ2* expression domain does not (Fig. 5F,G). *Tgfβ2* is also expressed in the mandibular adductor muscle, the mandibular adductor insertion, primary cartilage like Meckel's and the quadrate, and the secondary cartilage condensation (Fig. 5D). At this stage, the only *Tgfβ3* expression domain affected by paralysis is the secondary cartilage condensation and its expression domain (Fig. 5H). *Tgfβr2* is expressed in muscles like the mandibular adductor, the mandibular adductor insertion, and in the secondary cartilage condensation (Fig. 5E). *Tgfβr2* is also expressed in primary cartilages like Meckel's and the quadrate. Following paralysis, the only expression domain affected is the secondary cartilage condensation and its expression domain (Fig. 5I). *Smad3* is expressed in the mandibular adductor, the insertion, and the secondary cartilage condensation (Fig. S1). *Smad3* is also expressed in the quadrate, Meckel's cartilage, and other primary cartilages. The secondary cartilage expression domain does not appear in stage-matched, paralyzed embryos (Fig. S1).

In HH36 duck, *Tgfß2* is expressed in muscles like the mandibular adductor, tendons like the mandibular adductor insertion, bones like the surangular and their periostea, and cartilages like Meckel's, the quadrate, and their perichondria (Fig. 5K). *Tgfß2* is also expressed throughout the secondary cartilage on the coronoid process. Following paralysis, the only change in expression at HH36 is the absence of the secondary cartilage on the coronoid process and its *Tgfß2* expression domain (Fig. 5O). *Tgfß3* is expressed in all the same tissues as *Tgfß2* in HH36 control and paralyzed embryos, including the secondary cartilage (Fig. 5L,P). By HH36, *Tgfßr2* is expressed in dermal bones like the surangular, as well as the secondary cartilage on the coronoid process (Fig. 5M). Following paralysis, the secondary cartilage and its *Tgfßr2* expression domain are absent while *Tgfßr2* expression in bone is unaffected (Fig. 5Q). *Smad3* is expressed in the mandibular adductor, the insertion, and the secondary cartilage. There is also *Smad3* expression in primary cartilages, perichondria, bone, and periostea (Fig. S1). Paralyzed HH36 embryos do not form secondary cartilage so the corresponding *Smad3* expression is absent (Fig. S1).

Inhibiting FGF or TGFβ signaling affects the condensation of secondary cartilage

Unilateral delivery of FGF signaling inhibitor SU5402 blocks the formation of, or reduces the size of the secondary cartilage on the coronoid process (n=18 at HH32, n=29 at HH33)(Fig. 6A,C). No change in secondary cartilage is observed following delivery of DMSO control beads (n=6). The efficacy of secondary cartilage inhibition at HH38 depends upon the embryonic stage of treatment, with HH32 embryos being more

sensitive to FGF inhibition than HH33 embryos (Fisher's exact test, p=0.0047). In 88.9%

of embryos treated with SU5402 at HH32, secondary cartilage is either lost or reduced

in size (n=16/18). Of those secondary cartilage phenotypes, 50% are reduced in size

(n=8/16), and 50% have a complete absence (n=8/16) of secondary cartilage. FGF

inhibition at HH33 reduces the size of the secondary cartilage in 31.01% of cases

(n=9/29) and prevents secondary cartilage induction in 13.79% of cases (n=4/29).

Inhibition of TGFβ signaling by delivering SB431542 also frequently causes loss or

reduction in the size of the secondary cartilage on the coronoid process (n=37 at HH32,

n=66 at HH33)(Fig. 6 B,D). Although the statistical distribution of outcomes does not

depend on whether embryos are treated at HH32 (40.54% absent or reduced secondary

cartilage, n=15/37) or HH33 (39.39% absent or reduced secondary cartilage, n=26/66),

treatment at HH32 tends to be more efficacious at completely preventing secondary

chondrogenesis (13.51%, n=5/37) than delivery at HH33 (3.03%, n=2/66).

Inhibiting FGF or TGFβ signaling does not lead to increased cell death

TUNEL staining shows that implanting AG1-X2 chromatography beads soaked in

DMSO (n=3 embryos) or small molecule inhibitors of FGF signaling (n=6 embryos) or

TGFβ signaling (n=7 embryos) by bead at HH32 increases cell death. 24 hours after

implantation, 0.69% of cells surrounding DMSO soaked beads are undergoing

apoptosis (n=5 sections)(Fig. 6E,F). There is no significant increase in cell death over

control beads with SU5402 (1.42%, n=19 sections) or SB431542 (0.22%, n=29

sections)(Fig. 6H,I) treatments. For comparison, DNase-treated positive control slides

show significantly more cell death (52.60%, n=3 sections, unpaired t-test p<0.0001)(Fig. 6G).

Exogenous FGF4, TGFβ2, and TGFβ3 treatments can restore cartilage in embryos

HH38 duck paralyzed and treated with FGF4 beads at HH32 form cartilage adjacent to or surrounding the bead in 27.27% of cases (n=3/11)(white arrow, Fig. 7B). No cartilage is induced in any embryos treated with BSA beads alone (n=4 heparin acrylic, n=12 Affigel blue)(asterisk, Fig. 7A), or in cases where recombinant protein soaked beads are located far from the mandibular adductor insertion (n=4 for FGF4, n=2 for TGFβ2/TGFβ3, and n=4 for FGF4/TGFβ2/TGFβ3 combined treatments). Paralysis and implantation of beads soaked in a combination of TGFβ2 and TGFβ3 induce cartilage in 75% of cleared and stained HH38 duck (n=15/20)(black arrow, Fig. 7C). Implanting both FGF4 and TGFβ2/TGFβ3 soaked beads in paralyzed HH32 duck embryos induces cartilage in 85.71% of cases (n=12/14)(black arrow, Fig. 7D). Treating HH32 quail with exogenous TGFβ2 and TGFβ3 induces a chondrogenic response in 11.11% of embryos (n=1/9)(black arrow, Fig. 7E). Safranin-O staining confirms the analyses of cleared and stained embryos and shows a glycosaminoglycan-rich cartilaginous extracellular-matrix surrounding the beads (n=2/3)(black arrow, Fig. 7F). Although spherical beads were implanted, the axial orientation of Safranin-O positive tissue surrounding the beads is not radially symmetrical and tends to align with the orientation of the mandibular adductor insertion. Analysis of paralyzed duck rescue experiments reveal that the distribution of phenotypes depends upon the ligand or ligands received (Fisher's Exact Test, p=0.005)(Fig. 7G).

Discussion

Neural crest mesenchyme controls the species-specific pattern of jaw muscle insertions

We showed previously that NCM establishes the species-specific size and shape of the jaw skeleton and associated musculature via cell-autonomous morphogenetic programs (Solem et al., 2011; Tokita and Schneider, 2009). Here we demonstrate that this effect is dose-dependent. First-arch muscles, which arise from cranial paraxial mesoderm (Noden, 1983a), are directed by NCM derived tendon and connective tissues to adopt chick-like organization and attachments on the surangular (Solem et al., 2011; Tokita and Schneider, 2009). Because the extent of transformation in chimeras is directly related to the degree of chimerism (Ealba and Schneider, 2013), we were able to modulate the presence or absence of secondary cartilage on the coronoid process by titrating the size of donor NCM transplants and thus the distribution of NCM-derived connective tissues. Small transplants did not alter the development of secondary cartilage whereas larger transplants did. Based on our prior analyses of muscle and connective tissue patterning (Solem et al., 2011; Tokita and Schneider, 2009) and the critical role for interactions between NCM and muscle precursors (Bothe et al., 2007; Evans and Noden, 2006; Grenier et al., 2009; Noden, 1983a, 1988; Noden and Trainor, 2005; Rinon et al., 2007), we expect that this results from donor NCM moving the mandibular adductor insertion from a duck-like lateral position to one that is more dorsal and chick-like. Based on these species-specific differences in the adductor muscle insertion, we predicted that quail (and chick) would experience primarily tension in the local mechanical environment whereas cells at the lateral, duck-like insertion would

experience a combination of tension and compression (Solem et al., 2011). In this way and concomitant with its patterning abilities, NCM would be acting not only as a major determinant of cranial muscle architecture, but also as a regulator of the mechanical environment whereby certain loading conditions would induce secondary cartilage.

Quality not quantity of mechanical stimulation drives secondary chondrogenesis

Proper musculoskeletal development depends upon the ability of muscle, tendon, cartilage, and bone to sense and adapt to biomechanical cues. An essential source of biomechanical stimulation is embryonic motility. Early paralysis may prevent joint cavitation (Kahn et al., 2009; Lamb et al., 2003; Murray and Drachman, 1969; Osborne et al., 2002; Persson, 1983; Roddy et al., 2011) while later paralysis may alter the size, shape, proportionality, and extent of ossification (Blitz et al., 2009; Brunt et al., 2017; Hall and Herring, 1990; Pitsillides, 2006; Pollard et al., 2014; Sharir et al., 2011; Shwartz et al., 2012). For example, the radial asymmetry observed in cross-sections of wild-type, embryonic mouse bones is predicted to be optimized for load bearing during standing and walking (Blitz et al., 2009). Mice with muscle contractility defects develop cylindrical long bones. Such developmental plasticity and the ability to respond to biomechanical loading are mechanisms by which embryonic form comes to presage adult function (Anthwal et al., 2015; Blitz et al., 2009; Carter and Beaupré, 2007; Hall, 1967, 1968, 1972, 1986; Hall and Herring, 1990; Havis et al., 2016; Huang et al., 2013a; Kardon, 1998; Schweitzer et al., 2010; Sharir et al., 2011; Solem et al., 2011; Wu et al., 2001).

Secondary cartilage development can be divided into two phases: induction and maintenance. Both phases require proper biomechanical stimulation. Embryonic motility is an essential source of biomechanical stimulation and the developmentally plastic response to biomechanical loading is a potent mechanism through which embryonic form comes to presage adult function(Anthwal et al., 2015; Blitz et al., 2009; Brunt et al., 2017; Carter and Beaupré, 2007; Hall, 1967, 1968, 1972, 1986; Hall and Herring, 1990; Havis et al., 2016; Huang et al., 2013a; Kardon, 1998; Pitsillides, 2006; Pollard et al., 2014; Schweitzer et al., 2010; Sharir et al., 2011; Shwartz et al., 2012; Solem et al., 2011; Wu et al., 2001). For induction of secondary cartilage to occur, the frequency of mechanical stimulation must cross a threshold (Hall, 1967, 1968). The size of a secondary cartilage can also be decreased by inducing paralysis after secondary chondrogenesis has begun (Solem et al., 2011). The early similarity in quail and duck motility indicates that frequency of jaw activity is an unlikely determinant of species-specific secondary chondrogenesis. A significant difference in motility manifests at HH36, though a secondary cartilage is already formed in duck by that time. Thus, we conclude that the frequency of mechanical stimulation is not, itself, sufficient to induce secondary cartilage in quail versus duck, which points to the role of biomechanical stress resulting from a combination of species-specific muscle pattern and resultant differences in the quality or type of functional loading on the muscle insertion.

Mechanical cues result from and contribute to species-specific morphology

Prior work has highlighted the contribution of the mechanical environment in wrap-around tendons (Benjamin and Ralphs, 1998; Blitz et al., 2013; Carter and Beaupré,

2007; Murchison et al., 2007; Schweitzer et al., 2010; Shwartz et al., 2013). Such a configuration, in which a tendon experiences not only axial tension when the muscle contracts, but also compression in which the tendon is held taught against the bone, is conducive to the fibrocartilage development. Other examples of wrap-around tendons are the deltoid, which inserts onto a robust deltoid protuberance on the mouse humerus, and the *peroneus longus* in humans, which, in addition to harboring fibrocartilage occasionally forms an *os peroneus* (Blitz et al., 2009; Koo et al., 2017). Thus, the evolutionary presence or absence of secondary cartilage on the CP reflects species-specific variation in functional anatomy (Beresford, 1981; Fang and Hall, 1997; Hall, 1979; Stutzmann and Petrovic, 1975). In taxa such as humans, rats, cats, and duck, secondary cartilage forms at the jaw adductor muscle insertion (Amorim et al., 2010; Amorim et al., 2008; Hall, 2005; Horowitz and Shapiro, 1951; Kantomaa and Rönning, 1997; Moore, 1973, 1981; Solem et al., 2011; Soni and Malloy, 1974; Vinkka, 1982; Washburn, 1947) whereas an equivalent cartilage is absent in mice, guinea pigs, chick, and quail (Anthwal et al., 2008; Anthwal et al., 2015; Boyd et al., 1967; Moss and Meehan, 1970; Rot-Nikcevic et al., 2007; Shibata et al., 2003; Solem et al., 2011). Our work suggests the reason secondary cartilage forms at this location in some species and not others is due to the way NCM-mediated muscle pattern leads to differential forces during embryonic motility.

In our study, finite element modeling illuminates the difference in both the predicted magnitude and spatial distribution of von Mises stress experienced by cells in the mandibular adductor insertion of embryonic quail and duck prior to secondary

chondrogenesis. Perhaps the wide range of shear stresses distributed across the surface of the duck surangular mediates the precise biomechanical cues required to elicit a spatially restricted domain of secondary cartilage. The secondary cartilage is the future site of an ossification center that fuses to the surangular, enables robust osteointegration, and further distinguishes both the form and the functional mechanics of the duck versus quail jaw apparatus. In adult quail and duck, which occupy different trophic niches, the mechanical environments experienced at the coronoid process would likely be even more disparate due to the way these birds feed. However, the mechanisms that facilitate the relationship between mechanical stimulation and musculoskeletal adaptation have remained largely unknown. While previous studies have implicated FGF and TGFβ signaling in both early, muscle-independent, and late, muscle-dependent, phases of tendon development (Havis et al., 2016; Havis et al., 2014), our findings suggest that mechanical cues drive differential activation of FGF and TGFβ signaling to induce species-specific secondary cartilage within a tendon insertion. Moreover, we do not observe any evidence for crosstalk between these pathways, given that paralysis downregulates FGF signaling while TGFβ expression remains unchanged. Conversely, despite the maintenance of TGFβ, FGF is downregulated. Such findings are consistent with the independent functions of these pathways during chick limb tendon morphogenesis (Havis et al., 2016).

FGF and TGFβ signaling are necessary and sufficient for secondary chondrogenesis

Molecular programs of tendon development are context-dependent. In mouse limbs, TGFβ signaling promotes tendon development while FGF signaling is inhibitory (Blitz et al., 2013; Havis et al., 2014; Pryce et al., 2009; Subramanian and Schilling, 2015). However, FGF signaling is a definitively pro-tendon signal in chick limbs and promotes axial mouse and chick tendon development (Brent et al., 2005; Brent et al., 2003; Edom-Vovard et al., 2001a; Edom-Vovard et al., 2002; Havis et al., 2016; Havis et al., 2014; Smith et al., 2005). Our quantitative and qualitative analyses demonstrate that FGF and TGFβ ligands, receptors, and effectors are expressed in musculoskeletal tissues throughout stages important for secondary cartilage induction and maintenance, and paralysis has a significant but differential effect on transcription of some of these genes. We find that *Fgf4* and *Fgf8* are dramatically affected by paralysis, indicating that their expression may be mediated by mechanical stimulation. Furthermore, FGF signaling activity is decreased following paralysis as demonstrated by the relative down regulation of *Pea3* and *Erm* transcription. While the role of FGF signaling in the context of muscle, tendon, bone, and cartilage development is well described (Brent et al., 2005; Edom-Vovard et al., 2001b; Eloy-Trinquet et al., 2009; Murakami et al., 2000; Ornitz and Marie, 2015), the influence of the mechanical environment on FGF signaling has remained unclear. While we do not observe an effect of paralysis on the transcription of TGFβ ligands or receptors, the downstream effector *Pai1* was significantly increased by paralysis, suggesting tissue atrophy and fibrosis in response to disuse (Naderi et al., 2009). There is a relationship between the mechanical environment and TGFβ signaling (Kleinnulend et al., 1995; Nguyen et al., 2013; Robbins et al., 1997; Shi et al., 2011), but how mechanical cues exert control over

TGFβ signaling is not as well understood. Our results suggest that, in this context, TGFβ signaling activity is primarily regulated by post-transcriptional modifications like phosphorylation of SMADs (Anthwal et al., 2008; Berthet et al., 2013; Maeda et al., 2011; Wipff et al., 2007) and regulation of free-active TGFβ ligands, something we plan to pursue in future studies.

Inhibiting FGF signaling had a greater effect on secondary chondrogenesis at an earlier stage (i.e., HH32) indicating that the pathway members may play dual roles during both induction and maintenance of secondary chondrogenesis, and that their activities may be temporally separated. TGFβ signaling inhibition also interfered with the induction of secondary cartilage and disrupted maintenance, however, unlike FGF inhibition, our data from the two treatment periods did not yield a clear distinction between the timing of TGFβ signaling in secondary cartilage induction versus maintenance. TGFβ signaling may quickly respond to the mechanical environment and act upstream of FGF signaling during secondary chondrogenesis induction, and TGFβ may exert its regulatory effects using post-transcriptional mechanisms.

Our results also point to a role for FGF signaling during mandibular osteogenesis. Treatment with an FGF inhibitor sometimes elicited ossification defects wherein less bone formed adjacent the implanted bead, likely due to altered mesenchymal differentiation rather than apoptosis as indicated by the TUNEL data. Cleared and stained samples with extensive bone defects were excluded from further analyses. When embryos were treated with FGF inhibitor at HH32, bone defects were sometimes

accompanied by malformations in which Meckel's cartilage was kinked upward at the site of bead implantation, as if unable to withstand mandibular adductor muscle contractions. Because any bending in Meckel's cartilage would adversely affect the native mechanical environment, any embryo with a malformation in Meckel's cartilage was excluded from analysis.

Knockouts of *Tgfβ2* and *Tgfβr2* in mice produce malformations of the dentary and its coronoid, condylar, and angular processes (Oka et al., 2008; Oka et al., 2007; Sanford et al., 1997). Despite a reduction in the size of condylar and angular processes in *Tgfβ2* nulls, the secondary cartilages on these processes persist. However, formation of secondary cartilage was prevented by *Tgfβr2* knockout. Published culture experiments confirm the TGFβ signaling requirement and demonstrate that condylar and angular secondary cartilage induction in mice does not require stimulation from muscle contractions (Anthwal et al., 2008). In the context of our experiments, TGFβ inhibition does not produce bone defects, and we do not observe abnormalities in Meckel's cartilage. This is consistent with TGFβ knockout data in which tendon formation is severely inhibited in the absence of *Tgfβ2*, *Tgfβ3*, or *Tgfβr2*, while primary cartilage is largely unperturbed (Pryce et al., 2009).

Our efforts to rescue paralyzed embryos by treating them exogenously with recombinant FGF4 or a combination of TGFβ2 and TGFβ3, led to the formation of a dense fibrous capsule and in many cases, a discrete cartilage around the bead. Although ligands were delivered using spherical beads and presumably diffused

uniformly (Eichele et al., 1984), the axis of Alcian blue or Safranin-O positive tissue surrounding the beads is not radially symmetrical. Directional three-dimensional distribution of induced cartilage in quail and duck suggests that the mesenchyme and surrounding connective tissues overlying the surangular are not all equivalent in their capacity to generate secondary cartilage. Furthermore, the locations where cartilage is induced are spatially restricted to the general region where secondary cartilage normally forms in controls. Such a spatial constraint is in keeping with published explant data in which the murine coronoid process, which does not ordinarily form a secondary cartilage, can be induced to do so by fetal bovine serum (FBS)(Anthwal et al., 2015). Though the FBS bathed the entire mandible, ectopic cartilage was only observed on the coronoid process. In duck and quail, beads implanted too distal from the jaw joint, or too superficial, superior or, inferior to the surangular did not elicit a chondrogenic response.

Other experiments on developing limb tendons demonstrate the ability of exogenous FGF and TGFβ ligands to maintain *Scx* expression even in the absence of mechanical stimulation from embryonic muscle contractions, but to our knowledge, no instances of induced cartilage have been reported in those contexts (Edom-Vovard et al., 2002; Havis et al., 2016). The FGF and TGFβ signaling-dependent chondrogenic response we observed may be localized to tendon and connective tissues surrounding the mandibular adductor insertion and is conserved between quail and duck. Though quail do not normally form secondary cartilage on their coronoid process, the surrounding connective tissues are able to do so given the proper signaling environment.

Induced cartilage appears to be encapsulated and distinct from the surangular bone, mirroring native secondary cartilage development on the duck coronoid process. Thus, the secondary cartilage on the coronoid process is likely derived from cells in the tendon and adjacent connective tissue, not the periosteum as in articular secondary cartilage (Buxton et al., 2003). Experiments in other contexts demonstrated the existence of cell populations expressing both tendon (e.g., *Scx*) and cartilage (e.g., *Sox9*) tissue markers that contribute functionally to establishing certain sites where tendons or ligaments insert onto primary cartilage and that such markers are involved in the patterning of these insertions (Blitz et al., 2013; Kardon, 1998; Kardon et al., 2003; Mathew et al., 2011; Schweitzer et al., 2001; Sugimoto et al., 2013). Cells that give rise to secondary cartilage on the coronoid process may express a similar complement of lineage markers, which is supported by our previous expression analyses (Solem et al., 2011; Tokita and Schneider, 2009).

Mechanical cues differentially regulate members of the FGF and TGFβ pathways

Clearly, musculoskeletal development and homeostasis depend upon proper biomechanical cues, however, the cell-biology that mediates this mechanosensation is not well understood. A variety of mechanisms including the primary cilium, Wnt signaling, and especially sclerostin, which is an osteocyte-specific Wnt inhibitor, have been implicated in mechanosensitive bone remodeling (Robling et al., 2016; Robling et al., 2008; Rolfe et al., 2014; Tu et al., 2012). Other potential mechanisms may include ligands being freed from the extracellular matrix, ion channels, focal adhesions, cytoskeletal dynamics, and many others (del Rio et al., 2009; Dupont et al., 2011;

Hamill and McBride, 1996; Maeda et al., 2011; Mammoto and Ingber, 2010; Matthews et al., 2006; McBeath et al., 2004; Pruitt et al., 2014; Quinn et al., 2002; Raizman et al., 2010; Ramage et al., 2009; Roberts et al., 2001; Shakibaei and Mobasheri, 2003; Solem et al., 2011; Vincent et al., 2002; Vincent et al., 2007; Wang et al., 2009; Wen et al., 2017).

From our qualitative and quantitative analyses, a subset of genes stands out as likely mediating development of the mandibular adductor complex (*Tgfß2, Tgfß3, Fgfr1,* and *Fgfr2*) as their abundance changes significantly and in the same direction regardless of whether the embryo was paralyzed or not (Fig. 8A). This group of genes includes *Tgfß2* and *Tgfß3*, which can also induce chondrogenesis when delivered as ligands to paralyzed duck embryos or normal developing quail, suggesting that TGFβ signaling activity may primarily be modulated post-transcriptionally and depend upon the availability of free-active TGFβ ligands. Also, we observe no change in *Tgfßr1*, *Tgfßr2*, *Tgfßr3*, *Smad3,* or *Smad7b* expression. Our analyses did find that one component of the TGFβ pathway was significantly more abundant in paralyzed samples. *Pai1*, a common transcriptional readout of TGFβ signaling (Kawarada et al., 2016), became significantly more abundant following paralysis. Our data support the hypothesis that TGFβ pathway-mediated responses to mechanical stimulation utilize post-transcriptional mechanisms. Quantifying free-active TGFβ ligands, or assaying phospho-SMAD abundance or nuclear localization would shed light on this phenomenon, something that we are working towards for future studies.

Our analyses also indicate that a second set of five FGF signaling pathway components (*Fgf2* , *Fgf4, Fgf8, Pea3*, and *Erm*), likely mediates normal development of secondary cartilage and depends upon embryonic muscle contractions to maintain their activation. Similarly, FGF signaling has been implicated in a number of other mechanosensitive processes (Vincent et al., 2002; Vincent et al., 2007; Wen et al., 2017), but there is still a lot to learn about how FGF ligands, receptors, and transcriptional effectors interact with the mechanical environment.

Our data suggest a model (Fig. 8) whereby species-specific secondary chondrogenesis on the coronoid process arises as a consequence of functional motility acting upon NCM-derived form. In our model, the resulting stress within the insertion of the mandibular adductor muscle onto the surangular bone differentially activates FGF and TGFβ signaling, which are each necessary and sufficient to induce chondrogenesis. Thus, by balancing cell-autonomous developmental programs and adapting to environmental cues, NCM generates species-specific jaw geometry and promotes structural and functional integration of the musculoskeletal system during development.

During normal function of the temporomandibular joint (TMJ), the CP plays an essential role in maintaining proper condyle-fossa and intercuspal positioning, and CP anomalies such as hyper- and hypoplasias, osteochondromas, or those associated with hemifacial microsomia and DiGeorge syndrome may have disruptions to molecular and biomechanical signals that affect secondary cartilage (Amorim et al., 2010; Amorim et al., 2008; Bernstein and Fernandez, 1984; Fernandez Ferro et al., 2008; Gatti et al.,

1985; Hernandez-Alfaro et al., 2000; Huang et al., 2013b; Jerome and Papaioannou, 2001; Shibata et al., 2003; Vargervik and Miller, 1984; Villanueva et al., 2006). Also, some patients with restricted ability to open their mouths have an enlarged CP due to either congenital defects or mandibular hypomobility following internal TMJ derangement (Isberg and Eliasson, 1990; Kantomaa and Rönning, 1997). In this context, we are hopeful that investigating mechanisms through which chondrogenic and mechano-responsive factors are regulated, and how changes to the mechanical environment alter expression of these factors will shed light on novel strategies for treatment and prevention of a range of TMJ disorders. Moreover, understanding how certain tendons achieve robust osteointegration has clinical implications for enhancing re-attachment of muscle to bone via molecular therapies (Bunker et al., 2014; Hashimoto et al., 2007; Li et al., 2006; Nakase et al., 2010; Rundle et al., 2014; Sasaki et al., 2008; Thomopoulos et al., 2010; Wang et al., 2010).

E. S. Russell in his classic book, *Form and Function* (1916) poses the question, "Is function the mechanical result of form, or is form merely the manifestation of function or activity? What is the essence of life, organisation or activity? (p. v)" Our findings indicate that form initially dictates function but then function modulates form. Cranial NCM establishes species-specific "organisation" prior to the onset of muscle "activity." However, the musculoskeleton is developmentally plastic. As jaw activity begins, form adapts to meet and support functional demands. In the case of a duck, species-specific form, coupled with jaw activity, creates stresses within the mandibular adductor insertion, differentially activates FGF and TGFβ signaling, and induces secondary

cartilage on the coronoid process. Appreciating the inextricable connection between form and function allows for a new perspective on the role of NCM in establishing form but also shows how the organism can modify that form to accommodate functional demands throughout development, under selective pressure, or in disease states.

Chapter 4

The Role of Ion Channels in Secondary Chondrogenesis Induction and

Maintenance

(In collaboration with Molly Bodendorfer and Richard A. Schneider)

Introduction

As discussed in the previous chapters, a major source of the coupling between form and function is the cell's ability to detect and respond to biomechanical stimulation. The previous chapter delved into the possibility of mechanically mediated transcriptional and post-transcriptional regulation of FGF and TGFβ signaling, respectively, but there are a host of other avenues for mechanical cues to elicit cellular responses and to induce and maintain secondary cartilage.

Chondrogenic cells isolated from chick limb buds express a complex suite of voltage-gated sodium and potassium ion channels (Varga et al., 2011). *In vitro* inhibition of voltage-gated potassium ion channel function decreases proliferation and differentiation of chondrogenic cells along with decreased calcium signaling. Even in non-excitable cells, plasma membrane potentials and cytosolic calcium levels have been implicated in basic cellular functions such as gene expression changes and proliferation (Blackiston et al., 2009; Mobasheri et al., 2010; Muramatsu et al., 2007; Nesti et al., 2007; Nesti et al., 2002).

Ion channels are attractive pharmacological targets for manipulating secondary chodrognesis because they are known mediators of cartilage development and homeostasis (Barrett-Jolley et al., 2010; Mancilla et al., 2007; Mouw et al., 2007; Shakibaei and Mobasheri, 2003; Uchiyama et al., 2008; Wu and Chen, 2000). While work on cartilage ion channels is primarily conducted in primary cartilages like articular chondrocytes, work from our lab has demonstrated that secondary chondrogenesis in

the quadrate-quadratojugal joint requires stretch-activated cation channel (SACC) activity, while secondary chondrogenesis in the mandibular adductor insertion on the coronoid process does not (Solem et al., 2011). This differential requirement for SACCs suggests that distinct developmental processes may be taking place in articular versus enthesis secondary chondrogenesis.

This study determined the extent to which voltage-gated sodium, potassium, and calcium ion channels mediate mechanical induction of secondary chondrogenesis within muscle insertions. A deeper understanding of secondary chondrogenesis may lead to novel treatments to repair or regenerate secondary cartilage defects arising from congenital malformation, injury or degeneration. The results suggest that L-type, voltage-gated calcium ion channels contribute to secondary cartilage induction and maintenance.

Methods

The use of avian embryos

Fertilized Japanese quail (*Coturnix coturnix japonica*) and white Pekin duck (*Anas platyrhynchos*) eggs were purchased from AA Lab Eggs (Westminster, CA) and incubated at 37.5°C in a humidified chamber (GQF Hova-Bator, Savannah, GA) until collection and analysis. For all procedures, we adhered to accepted practices for the humane treatment of avian embryos as described in S3.4.4 of the AVMA Guidelines for the Euthanasia of Animals: 2013 Edition (Leary et al., 2013).

Chemical treatments

Negative-control HH33 duck (n=6) were treated with 0.5mL doses of Hank's Balanced Salt Solution (HBSS)(Corning Inc. Corning, NY). In positive-control duck (n=6), paralysis was induced at HH33 by using a syringe to drip a 0.5mL dose of 10mg/mL Decamethonium Bromide (DMBr)(Sigma Aldrich, St. Louis, MO, D1260-5G) in HBSS into the egg. For each of the ion channel inhibitors, a dose-response curve was established to determine the appropriate treatment concentration for widespread inhibition. The HH33 dosage that most closely yielded 50% embryo survival by HH38 was identified as the ideal treatment concentration. Based on published literature and our prior experiments (Solem et al., 2011), embryos were treated with 0.5mL doses of ion channel inhibitors at a wide range of concentrations. Dosages were adjusted relative to embryo survival. HH33 duck were treated with tetrodotoxin (Abcam, Cambridge, United Kingdom, ab120054) in HBSS to block voltage-gated sodium channels, 4-aminopyridine (4-AP)(MP Biomedicals, Burlingame, CA, 0215036605) in HBSS to block

voltage-gated potassium channels, and nifedipine (Alfa Aesar, Haverhill, MA, J62811) in

HBSS to block L-type, voltage-gated calcium channels. All solutions were 0.22µm sterile

filtered and dripped directly onto the intact vitelline membrane.

Whole-mount embryo staining

Embryos were collected at HH38, fixed in 4% paraformaldehyde (PFA) overnight,

stained with Alcian blue and Alizarin red, and cleared in glycerol as previously described

(Wassersug, 1976). Each group of 4 images from Fig. 9 are taken from the same,

representative embryo at collection, and following clearing and staining.

Results

Dose response treatments (n=36) revealed a 50% survival rate between 0.5mL dosages of 4µg/mL (100% survival, 2µg/egg, n=3) and 6.5µg/mL (33% survival, 3.25µg/egg, n=3) for tetrodotoxin (Table 3, Fig. 9A). At HH33, a 0.5mL dose of 9µg/mL tetrodotoxin did not yield any gross disfiguration to surface structures (Fig. 9B,D) or to the cartilage and bone tissues revealed by skeletal preparation (Fig. 9C,E). Lateral and ventral views of a representative, cleared-and-stained embryo show that voltage-gated sodium channel inhibition does not affect the size or shape of the secondary cartilage condensation (white arrows) by HH38 (Table 4, n=9).

Voltage-gated potassium channel blockade at HH33 using 4-AP (n=64) crossed the 50% survival threshold between 1092µg/mL (73% survival, 546µg/egg, n=15), and 2000µg/mL (0% survival, 1000µg/egg, n=3) (Fig. 9F). Lateral (Fig. 9G,H) and ventral (Fig. 9I,J) views of freshly collected and cleared-and-stained HH38 specimens reveal neither any gross anatomical defects, nor chondrogenic or osteogenic effects resulting from voltage-gated potassium channel blockade (Table 4, n=5). The appearance of the secondary cartilage was unaffected as well (white arrows).

For 0.5mL treatments of Nifedipine (n=159), an inhibitor of L-type, voltage-gated calcium channels, 50% survival occurs between 9.8µg/mL (75% survival, 4.9µg/egg, n=4) and 12µg/mL (44.44% survival, 6µg/egg, n=27) concentrations, although, 26µg/mL (25.23% survival, 13µg/egg, n=107) induces death at roughly the same frequency as the next lowest dose (Fig. 9K). When 0.5mL doses of 26µg/mL nifedipine were

administered at HH33, pooled blood could be seen beneath the epithelium of a representative HH38 embryo (Fig. 9L,N). The size of the eyes was also unequal. The right eye appeared to develop normally, while the eye on the left side was demonstrably smaller. Despite outward asymmetry, clearing and staining revealed a bilateral absence of secondary cartilage on the coronoid process (Table 4, n=1 of 39). The effect of nifedipine treatment appears to be restricted to secondary cartilage as primary cartilages like Meckel's and the surangular and other bones appear normal.

Discussion

To understand molecular mechanisms through which cells in the enthesis sense mechanical force, we attempted to disrupt the ability of mechanical forces to be transduced across the cell membrane via ion channel activity. The results of our experiments reveal that, even though we determined the concentrations most likely to induce widespread voltage-gated sodium and potassium ion channel inhibition, all of the cleared and stained tetrodotoxin and 4-AP treated embryos form a normal looking secondary cartilage (Table 4). The treatment window from administration (HH33) to collection (HH38) encompassed periods of both secondary cartilage induction and maintenance on the coronoid process. This suggests that neither secondary cartilage induction nor maintenance depends upon voltage-gated sodium or potassium ion channel function.

Though the embryo is housed in an egg and the volume of albumin is not expected to change, it is possible that the molecules we administered were metabolized. One approach that would circumvent this would be to administer repeated doses over the period spanning from HH33 to HH38 rather than a single bolus. A foreseeable complication stemming from this approach is that the systemic concentration of drug may become quite elevated, requiring lower doses than our experimental groups received.

Another phenomenon that may be at play is compensation. We expect that the voltage gated ion channels we manipulated in these experiments modulate cellular response by

altering membrane voltage potential and or participating in calcium signaling (Barrett-Jolley et al., 2010; Mobasheri et al., 2010; Poiraudeau et al., 1997; Shakibaei and Mobasheri, 2003; Sugimoto et al., 1996). Inhibiting any one of these ion channels may be insufficient to interfere with secondary cartilage induction and maintenance due to compensation by other ion channels. Because we never administered any ion channel inhibitors in combination, we cannot exclude the possibility of compensation. Combinatorial ion channel inhibitor treatments at 50% survival concentrations may produce more penetrant secondary cartilage inhibition.

We did observe instances of either reduced size (5.13%, n=2 of 39) or absent (2.56%, n=1 of 39) secondary cartilage resulting from L-type, voltage-gated calcium ion channel inhibition (Table 4). Even at 26μg/mL, we never observed any paralysis resulting from nifedipine treatments, further suggesting that calcium channel activity may mediate mechanosensation in the mandibular adductor insertion on the coronoid process.

Calcium signaling has been implicated in maintaining healthy chondrocytes (Han et al., 2012). Additionally, intracellular calcium has been observed to regulate cytoskeletal and gene expression responses to mechanical loading (O'Conor et al., 2014). As such, calcium influx is often quantified as an indicator of mechanotransduction. Examples of other mechanically gated cation channels like PIEZO1 and PIEZO2 promote healthy articular cartilage, and have been shown to sustain injurious levels of calcium signaling following mechanical trauma to articular cartilage (Coste et al., 2010; Lee et al., 2014).

Although we only observed effects on the secondary cartilage when embryos were treated with an L-type, voltage-gated calcium channel inhibitor, this does not mean that voltage-gated sodium and potassium channels do not play a role during induction and maintenance of secondary cartilage in joints. It is likely that secondary cartilages arising in muscle insertions and joints utilize different mechanisms to adapt and respond to mechanical stimulation. Previous work with gadolinium, which blocks SACCs, had no effect on secondary cartilage on the coronoid process, while secondary chondrogenesis on the quadrate/quadratojugal joint was inhibited (Solem et al., 2011).

Taken together, our results suggest that intracellular calcium signaling may mediate the mechanical induction of secondary cartilage on the duck coronoid process. Promoting osteointegration following tendon or ligament avulsion is notoriously difficult. Orthopaedic repairs in which a tendon is directly affixed to bone by a surgically implanted fixture, create abrupt changes in material properties and do not mimic healthy tendon-bone interfaces (Galatz et al., 2004; Schwartz et al., 2012). Consequently, such procedures are prone to failure. In the future, robust repairs might make attempts to mimic the gradual transition from unmineralized tendon or ligament to mineralized bone. Being able to mimic the mechanical environment during development, or more likely, manipulating the activity of the proteins that transduce loading, like L-type, voltage-gated calcium ion channels, may prove beneficial to orthopaedic applications and achieving robust osteointegration in the clinic.

Chapter 5

Concluding Remarks

Concluding Remarks

While I find it hard to write in a manner "rather prospective than retrospective," I will put aside the feeling that predictions, coming from someone with less than a decade of research experience are presumptuous. In this final portion of text, I will point to trends that I think hold promise for teasing apart the relationship between form and function, particularly, during development and evolution.

Development and evolution are necessarily intertwined because they, both, are records of gene expression. Consequently, matters of genetics and transcriptional regulation are equally deserving of attention. Explanations for the array of adaptations in the natural world will ultimately be found in the regulatory mechanisms that determine the location, timing, and strength of gene expression.

Genomic regions that were once considered "junk DNA," because they did not encode proteins, are being recognized for mediating the essential function of spatiotemporally regulated gene expression. Particular importance should be placed on unraveling the genetic variations between and among species. As I see it, evolutionary and developmental biology is essentially the pursuit of correlating genotype with phenotype.

One strategy for unraveling the connection between genotype and phenotype is exploiting the existing differences between closely related species. Comparative models, like the quail-duck system, exploit species-specific differences to tease apart the myriad ways gene expression, particularly in the NCM, makes a duck a duck and a

quail a quail. To take an example from this dissertation, quail and duck both have the potential to develop a secondary cartilage within the mandibular adductor insertion but these secondary chondrogenic programs are differentially regulated such that duck develop a secondary cartilage intermediate on their coronoid process while no such cartilage forms in quail. However, it is possible to force the quail's hand, so to speak.

We found that exogenous TGFβ2 and TGFβ3 are sufficient to activate the quail secondary chondrogenic program. This combination of proteins also elicited a chondrogenic response from paralyzed duck. Remarkably, the TGFβ2 and TGFβ3 proteins we used were derived from human genes! Despite the great evolutionary divide between quail, duck, and human, and the obvious differences in the form of their jaws, the ability to respond and adapt to the presence of these proteins is conserved. This example demonstrates the immense power selection wields over preserving protein function, while permitting species-specific patterns of gene expression to diverge.

Spatiotemporal regulation of gene expression is a multifaceted and compelling phenomenon. Combinations of epigenetic mechanisms, signaling cues, the mechanical environment, and other mechanisms, likely underlie adaptations throughout biology. Investigating the multitude of mechanisms governing expression of the genome will deepen our understanding of the relationship between transcriptional expression, form, and function.

We now have at our disposal the tools to uncover enhancer and gene activity in real time, through the use of fluorescent reporters. New genome editing technologies make genetic manipulation faster and easier than ever before. Deep sequencing has become so affordable that seemingly every lab analyzes single cell transcriptomes. Cheap sequencing technologies also lower the barrier to entry for adopting new model organisms. My experience at the Woods Hole embryology course opened my eyes to the breadth of evolutionary and developmental insights that can be unlocked by embracing novel model systems. These are the tools that will allow biologists to access the cellular processes that underlie evolution and development.

The role of the mechanical environment in mediating gene expression and cell behavior is another avenue of interrogation that has only recently been paved. Unlike Thompson, who 100 years ago published his extensive observations on the geometry of life, we have technologies to visualize, to quantify, and to manipulate the physical world of cells and tissues in ways Thompson could have only dreamed. Biologists have long acknowledged the value in understanding the processes that mold the embryo. In the nineteenth century, Wilhelm His recognized the physical nature of morphogenesis and took to kinking, slitting, and otherwise distorting rubber tubing to model the cylindrical shapes he observed forming in the chick embryo (Gould, 1977; His, 1874). Yet, only recently have techniques emerged that enable us to manipulate and observe these processes on the cellular and subcellular levels.

Advanced culturing systems facilitate studies on self-formation, the processes by which homogenous clusters of stem cells are coaxed to undergo morphogenesis and form incredibly complex organoids comprised of heterogeneous cell populations, demonstrating that organogenesis can occur without external forces generated by adjacent tissues. *In vitro* live imaging techniques enable real-time visualization of cell contractility, cell migration, cytoskeletal rearrangements, calcium influx, and more. Widespread adoption of these techniques in embryos, will shed light on the intrinsic and extrinsic forces that propel basic morphogenetic processes like gastrulation, the folding of the neural tube, epithelial to mesenchymal transitions and more.

Structure and function cannot be considered in isolation. Considerable insights will spring from systems where the mechanical environment and the gene regulatory landscape can be integrated into a single story. Genetic techniques, biomechanical manipulations, and live imaging are indispensible to the study of form and function during development and evolution, and may ultimately be applied to address disease states.

Tables

Table 1

Catalog of primers utilized to clone in situ probes and to quantify gene expression

Duck In Situ Primer Pairs

Forward Primer	Reverse Primer
Erm F: *5'*-CTACTGCATCGACTCAGAAG-*3'*	*Erm* R: *5'*-GCCACCTTCTGCATGATG-*3'*
Fgf4 F: *5'*-GCAAACTCTATGGATCTACCCA-*3'*	*Fgf4* R: *5'*-GTGGGAGATACTTTATTGCC-*3'*
Fgf8 F: *5'*-GTGCACGCCAAGCTCAT-*3'*	*Fgf8* R: *5'*-GGTTGAAGGGGTAGTTGAG-*3'*
Fgfr2 F: *5'*-GCTGAAAGATGATGCTACAG-*3'*	*Fgfr2* R: *5'*-CTGAGGTCCAGATACTCCTCGTT-*3'*
Fgfr3 F: *5'*-AAGATGATGCCACAGACAAG-*3'*	*Fgfr3* R: *5'*-ACCCTCCCAAAGTGAAGATC-*3'*
Pea3 F: *5'*-ACATCAAGCAGGAGGTCG-*3'*	*Pea3* R: *5'*-GCCACCTTCTGCATGATGCC-*3'*
Smad3 F: *5'*-CCAGAGAACACTAACTTCC-*3'*	*Smad3* R: *5'*-GGTTCACAGACTGAGCCA-*3'*
Tgfβ2 F: *5'*-AATGCACTGCTATCTCCTG-*3'*	*Tgfβ2* R: *5'*-CAAATCTTGCTTCAGGCTCC-*3'*
Tgfβ3 F: *5'*-CACCGAGTCCGAGTACTATG-*3'*	*Tgfβ3* R: *5'*-CCATAGTCATCCTCACTGTC-*3'*
Tgfβr2 F: *5'*-CTCACAAGAAGAGGAAGCTC-*3'*	*Tgfβr2* R: *5'*-AGCCATGGAGTACACATCTG-*3'*

Duck RT-qPCR Primer Pairs

Forward Primer	Reverse Primer
Erm F: *5'*-GAGACTGGAGGGTAAGGTGAAGC-*3'*	*Erm* R: *5'*-GTCCAGGCGATGAAGTGAGC-*3'*
Fgf2 F: *5'*-GACGGCGTCCGCGAGAAG-*3'*	*Fgf2* R: *5'*-ATTTCAGTGCCAGCAATCTGCC-*3'*
Fgf4 F: *5'*-GCAAACTCTATGGATCTACCCA-*3'*	*Fgf4* R: *5'*-GCATTGTAGTTGTTTGGCAGG-*3'*
Fgf8 F: *5'*-GTGCACGCCAAGCTCAT-*3'*	*Fgf8* R: *5'*-CCTTCTTGTTCATGCAGATGTAGAA-*3'*
Fgfr1 F: *5'*-CTGAAGGAAGGCCACAGGATG-*3'*	*Fgfr1* R: *5'*-TCATGTACAGCTCGTTGGTGCA-*3'*
Fgfr2 F: *5'*-ACCTGCCAACTGCACCAATG-*3'*	*Fgfr2* R: *5'*-CTGAGGTCCAGATACTCCTCGTT-*3'*
Fgfr3 F: *5'*-TGGCCTTGCTAGAGACGTTCAC-*3'*	*Fgfr3* R: *5'*-CACAGGCAGCCGACCATTG-*3'*
MYOD1 F: *5'*-CAACGCCATCCGCTACATCG-*3'*	*MYOD1* R: *5'*-CTGTACTCCATCATGCCGTCG-*3'*
Pai1 F: 5'-AAGAGCGTGGACTTTGAGGA-*3'*	*Pai1 R: 5'*-GATTTCCACAAGCCCTTGAA-*3'*
Pea3 F: *5'*-CTGGACTGGAAGAGGGATGGAG-*3'*	*Pea3* R: *5'*-GCCACCTTCTGCATGATGCC-*3'*
Smad3 F: 5'-CATCCCAGAGACACCTCCTC-*3'*	*Smad3 R: 5'*-GTGTGCCGGAGACATAGGAT-*3'*
Smad7b F: 5'-CCCCCTCCGCCCTACTCCAG-*3'*	*Smad7b R: 5'*-GCCACCACGCACCAGTGTGA-*3'*
SOX9 F: *5'*-AGGGCTCCGAGCAGACCCAC-*3'*	*SOX9* R: *5'*-GCGACTGCCCTGAGTGCTCC-*3'*
Tgfβ2 F: *5'*-TGGCTCCATCACAGAGACAG-*3'*	*Tgfβ2* R: *5'*-CAAATCTTGCTTCAGGCTCC-*3'*
Tgfβ3 F: *5'*-CATCGAGCTCTTCCAGATCC-*3'*	*Tgfβ3* R: *5'*-AAAGTATGGCAAGGGCAGTG-*3'*
Tgfβr1 F: 5'-TGTAGCCACACAAGGCAAAC-*3'*	*Tgfβr1 R: 5'*-TTCCTACTCTGTGGTTGGGG-*3'*
Tgfβr2 F: 5'-GCGAGAGCATCCCTGCGTGG-*3'*	*Tgfβr2 R: 5'*-GCACACCATCTGGATGCCCTGA-*3'*
Tgfβr3 F: 5'-CCGTACAGTGCTTTCCAGGT-*3'*	*Tgfβr3 R: 5'*-TCATGCGACTTGATAACCCA-*3'*
TN-C F: *5'*-CACAGCAGGTGACTCCATGAC-*3'*	*TN-C* R: *5'*-AACACCCTGACTGTGGTTGTTG-*3'*
UCHL-1 F: *5'*-ATTGGTCTGATACACGCAGTTGC-*3'*	*UCHL-1* R: *5'*-TCAACCCGACACTGTCCTTCC-*3'*
β-Actin F: *5'*-ACAGCTTCACCACCACAGCCG-*3'*	*β-Actin* R: *5'*-GCCTCGGGGCACCTGAACCT-*3'*

Table 2

Spatial Localization of Gene Expression in HH33 Control Duck

Structure	Tissue Type		FGF Signaling Pathway					TGFβ Signaling Pathway			
			Fgf4	*Fgf8*	*Fgfr2*	*Fgfr3*	*Pea3*	*Tgfβ2*	*Tgfβ3*	*Tgfβr2*	*Smad3*
Meckel's Cartilage	Primary Cartilage	Perichondrium			X		X				X
		Cartilage	X	X	X	X	X		X	X	X
Coronoid Process	Secondary Cartilage	Condensation	X	X	X	X	X	X	X	X	X
Surangular	Bone	Condensation	X	X	X	X	X	X			
Mandibular Adductor	Muscle		X	X			X	X	X	X	X
Muscle Insertion	Tendon		X	X			X	X	X	X	X

Spatial Localization of Gene Expression in HH36 Control Duck

Structure	Tissue Type		FGF Signaling Pathway					TGFβ Signaling Pathway			
			Fgf4	*Fgf8*	*Fgfr2*	*Fgfr3*	*Pea3*	*Tgfβ2*	*Tgfβ3*	*Tgfβr2*	*Smad3*
Meckel's Cartilage	Primary Cartilage	Perichondrium	X		X	X	X	X	X		X
		Cartilage	X	X	X	X	X	X	X		X
Coronoid Process	Secondary Cartilage	Perichondrium		X		X	X	X	X		X
		Cartilage	X	X	X	X	X	X	X	X	X
Surangular	Bone	Periosteum	X	X	X	X	X	X	X		X
		Bone	X	X	X	X	X	X	X	X	X
Mandibular Adductor	Muscle		X	X	X	X	X	X	X	X	X
Muscle Insertion	Tendon		X	X	X	X	X	X	X	X	X

1. Strong *Fgfr2* expression throughout the perichondrium with isolated cells expressing *Pea3*
2. Strong *Fgfr3* expression throughout with isolated cells expressing *Fgf8* and *Pea3*
3. Strong *Fgfr2* expression throughout the surangular condensation with isolated *Pea3* expressing cells
4. *Fgf4* and *Pea3* expression appear strongest near muscle tips while *Tgfβ2* is strongly expressed throughout the muscle
5. Strong *Fgfr2* expression throughout while *Fgfr3* expression is spatially restricted to the center
6. *Fgfr2* and *Fgfr3* are expressed throughout bone, but periosteal expression is quite strong
7. *Smad3* expression strongest near muscle insertions

Table 3. Effect of ion channel inhibitors on embryonic survival

Tetrodotoxin

Dosage µg/mL	Survival (%)	Survival (n)
0.038	100	4 of 4
0.38	100	4 of 4
0.9	87	7 of 8
4	100	3 of 3
6.5	33	1 of 3
9	25	2 of 8
15	0	0 of 3
90	0	0 of 3

4-Aminopyridine

Dosage µg/mL	Survival (%)	Survival (n)
1.092	80	4 of 5
10.92	60	12 of 20
109.2	66	14 of 21
1092	73	11 of 15
2000	0	0 of 3

Nifedipine

Dosage µg/mL	Survival (%)	Survival (n)
2.6	100	4 of 4
7.6	100	6 of 6
9.8	75	3 of 4
12	44.44	12 of 27
26	25.23	27 of 107
110	0	0 of 4
260	0	0 of 7

Table 4. Summary of coronoid process phenotypes

Tetrodotoxin

unaffected	9
reduced	0
absent	0
Total	9

4-Aminopyridine

unaffected	5
reduced	0
absent	0
Total	5

Nifedipine

unaffected	36
reduced	2
absent	1
Total	39

Figures

Figure 1. Evolution of skeletal jaw anatomy. Development of upper and lower first-arch elements in (**A**) ancestral tetrapods, (**B**) birds and reptiles, and (**C**) mammals. In the ancestral condition, the epipterygoid, palatoquadrate, and quadrate form from a single cartilage, but in reptiles, birds, and mammals these jaw elements are constructed from two cartilages joined by mesenchymal condensations (dashed lines).

A ancestral jaw condition

epipterygoid

stapes

palatoquadrate

quadrate

articular

Meckel's cartilage

B birds and reptiles

epipterygoid

stapes

quadrate

articular

angular

Meckel's cartilage

C mammals

alisphenoid (epipterygoid)

stapes

incus (quadrate)

malleus (articular)

tympanic (angular)

Meckel's cartilage
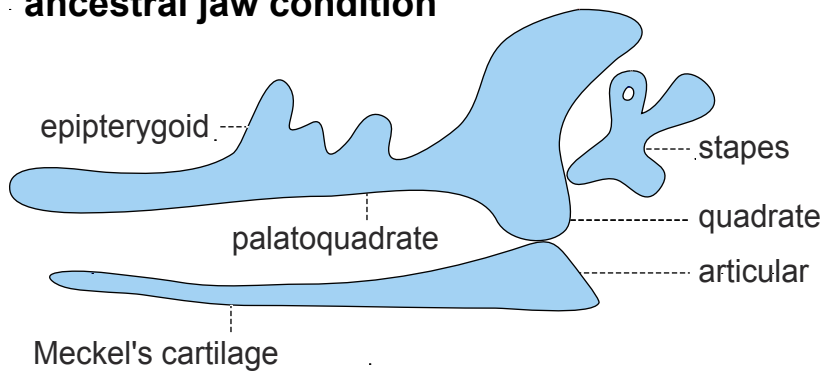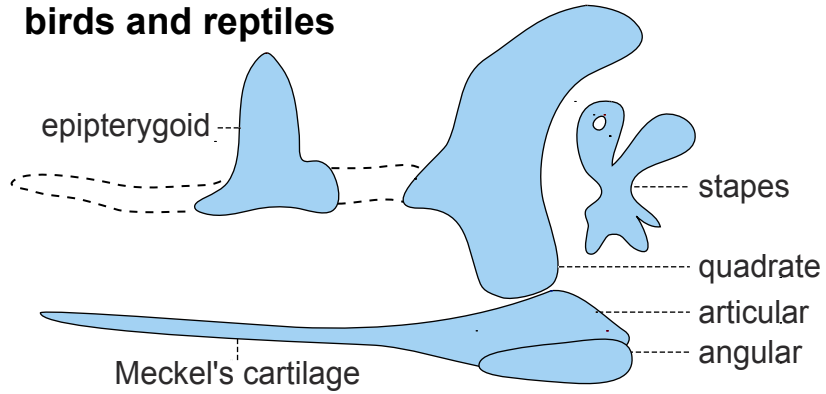
Figure 2. Developmental origins of the jaw are highly conserved despite species-specific morphological differences. (**A**) Schematic hemi-transverse section through the midbrain-hindbrain boundary of a stage 10 quail showing germ layers and migrating neural crest, cell types, cell-cell interactions, and tissue contributions to the jaw. (**B**) Prior to migration, at stage 9.5 (dorsal view) cranial NCC (light blue) delaminate from the forebrain (fb), midbrain (mb), and hindbrain rhombomeres (r; dark blue). Cranial NCC migrate alongside paraxial mesoderm (m; orange). (**C**) Frontal view of stage 25 quail. The frontonasal 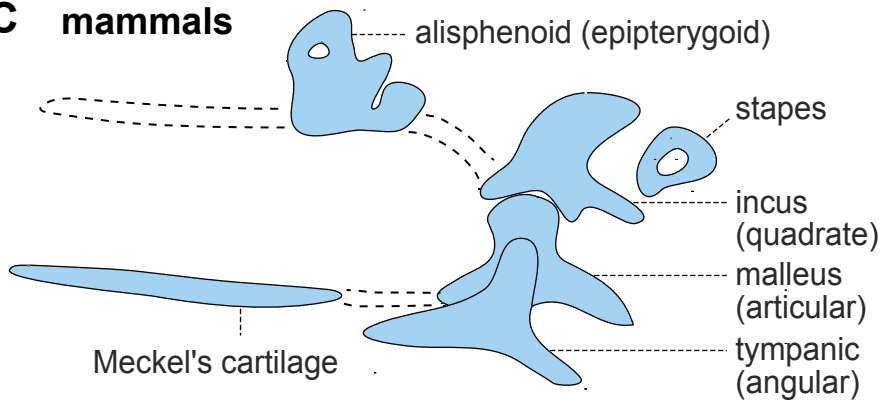(fn), maxillary (mx), and mandibular (ma) primordial are visible. Dotted line indicates the sagittal section plane for Fig. 2D. (**D**) By stage 25, the frontonasal (fn), maxillary (mx), mandibular (ma), and hyoid (hy) primordia (sagittal view) are populated by NCC surrounded by surface ectoderm (se; tan), pharyngeal endoderm (pe; yellow), and forebrain neuroepithelium (fb) and contain contributions from neural crest, nasal placode (np), and cranial ganglia (V, VII, IX). Mesoderm (m) that produces skeletal tissues is distributed caudally. (**E**) By stage 40, NCC produce the facial and jaw skeletons (light blue) whereas mesoderm forms the caudal cranial vault and skull base (orange). (**F**) Though their numbers are different, the boundary between neural crest (light blue) versus mesoderm (orange) derived skull bones and cartilages is highly conserved as shown in the newborn mouse. (**G**) By stage 38 in quail, the narrow mandibular adductor inserts dorsally onto the coronoid process of the surangular. (**H**) By stage 38 in duck, the broad mandibular adductor inserts laterally onto the coronoid process and contains a secondary cartilage (asterisk).
Source: Panels A-E modified from Fish and Schneider 2014 and F modified from Noden and Schneider 2006.

A *jaw progenitors*

quail

stage 10

cranial neural crest → chondrocytes → cartilage (*sox9*, *col2*)
osteoblasts → bone (*runx2*, *sp7*, *col1*)
tenocytes

neural ectoderm

paraxial mesoderm → angioblasts → vasculature (*tie2*)
osteoclasts
myocytes → muscle (*myoD*, *myf5*, *myo*)

surface ectoderm → mandibular epithelium

pharyngeal endoderm → mandibular epithelium → tendon (*tcf4*, *scx*, *tn-c*)

BMP, SHH, Wnt, FGF, TGFβ

B stage 9.5

fb
mb
r1
r2
r3
r4
r5
r6
r7
m

C quail — stage 25

fn
mx
ma
1mm

D stage 25

fb
se
fn
np
m
mx
V
se
ma
hy
VII
pe
3rd
IX

E quail

mesoderm
NCM

sq
mx
pa
pm
qd
sp
su
dentary
Meckel's cartilage
angular
stapes
articular
stage 40

F mouse

pm
mx
sq
palatine
dentary
in
Meckel's cartilage
tympanic
stapes
malleus
newborn

G quail

postorbital
mandibular adductor
quadrate
muscle
cartilage & bone
squamosal
Meckel's
surangular
retroarticular
mandibular depressor
stage 38

H duck

postorbital
mandibular adductor
squamosal
quadrate
*
Meckel's
surangular
retroarticular
mandibular depressor
stage 38

Figure 3. Species-specific form of the jaw and role of NCM. (**A,B**) Ventral views of isolated adult left mandibles reveal the smooth appearance of the quail jaw and the laterally protruding coronoid process in duck. (**C,D**) Left lateral views of cleared and stained HH38 quail and duck skulls. Cartilage is stained blue, and bone is stained red. In duck, a secondary cartilage intermediate forms on the lateral surface of the surangular bone, no such cartilage forms in quail. (**E**) Schematic of stage-matched HH9 GFP-chick donor, and wild type duck host embryos used to generate chimeras. Chimeric "chuck" were produced by unilaterally transplanting NCM from the midbrain and hindbrain of a GFP-chick-donor into the comparable axial position in a WT duck-host. In unilateral transplants, the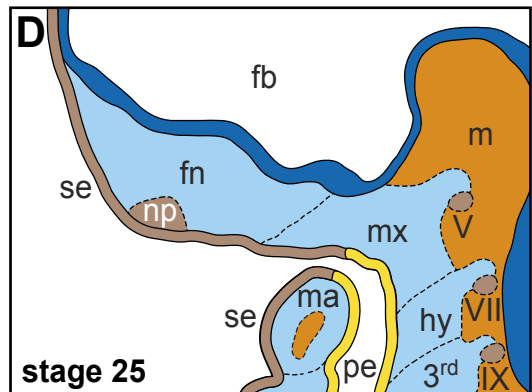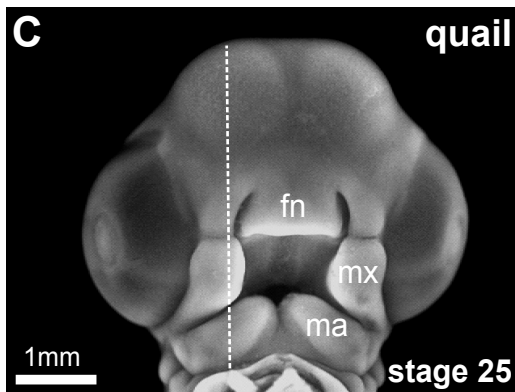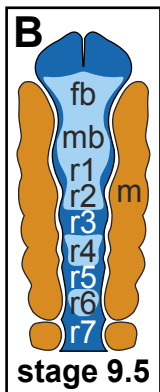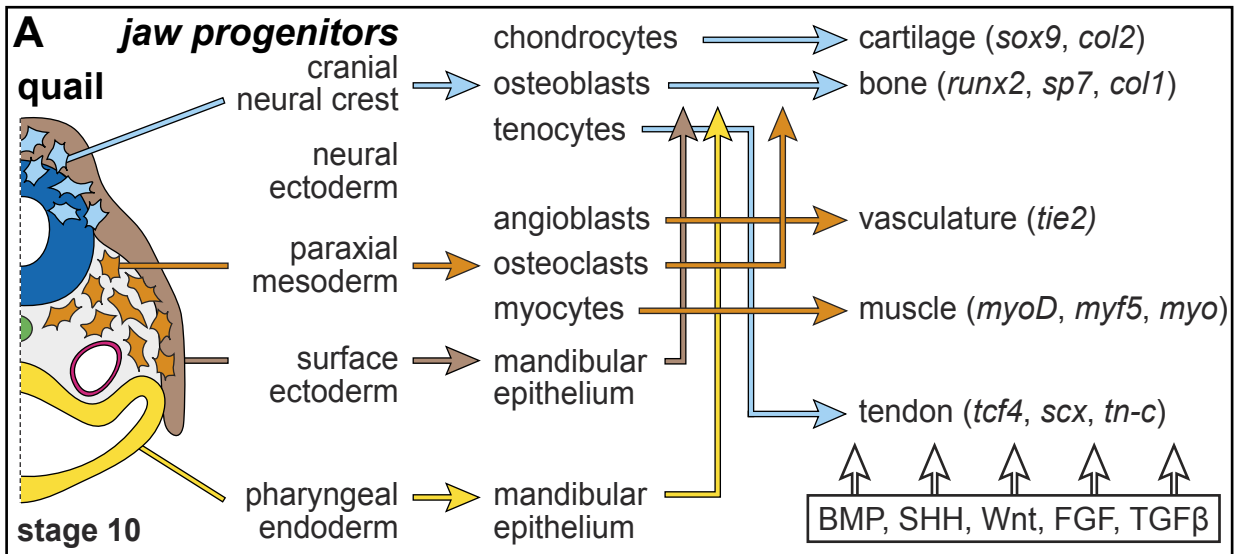 duck-host side develops normally and serves as an internal control. Here a small transplant region is depicted. (**F**) Epifluorescent image of an HH38 chimera. GFP-positive regions are derived from a small-sized NCM transplant. (**G,H**) Small GFP-chick transplants yield HH38 chimeras with a limited distribution of chick connective tissues, such that the chick-donor side of the jaw is minimally transformed and still resembles the morphology of the contralateral control duck side, complete with secondary cartilage on the surangular bone. (**I,J,K,L**) Transplanting large populations of chick NCM results in broader regions of GFP-positive cells throughout the HH38 jaw and the GFP-chick-donor side lacks secondary cartilage. In contrast, the contralateral, duck-host control side develops normally.

quail

A adult jaw

1 cm

duck

B coronoid process adult jaw

C HH38

eye

quadrate

2 mm

surangular

retroarticular

D HH38

eye

quadrate

surangular

retroarticular

GFP–NCM

E fb

mb

hb

NCM

HH9

fb

mb

hb

donor side

F HH38 *GFP⁺*

donor side

G HH38 *present*

host side

H HH38 *present*

I fb

hb

NCM

HH9

fb

hb

J HH38 *GFP⁺*

K HH38 *absent*

L HH38 *present*
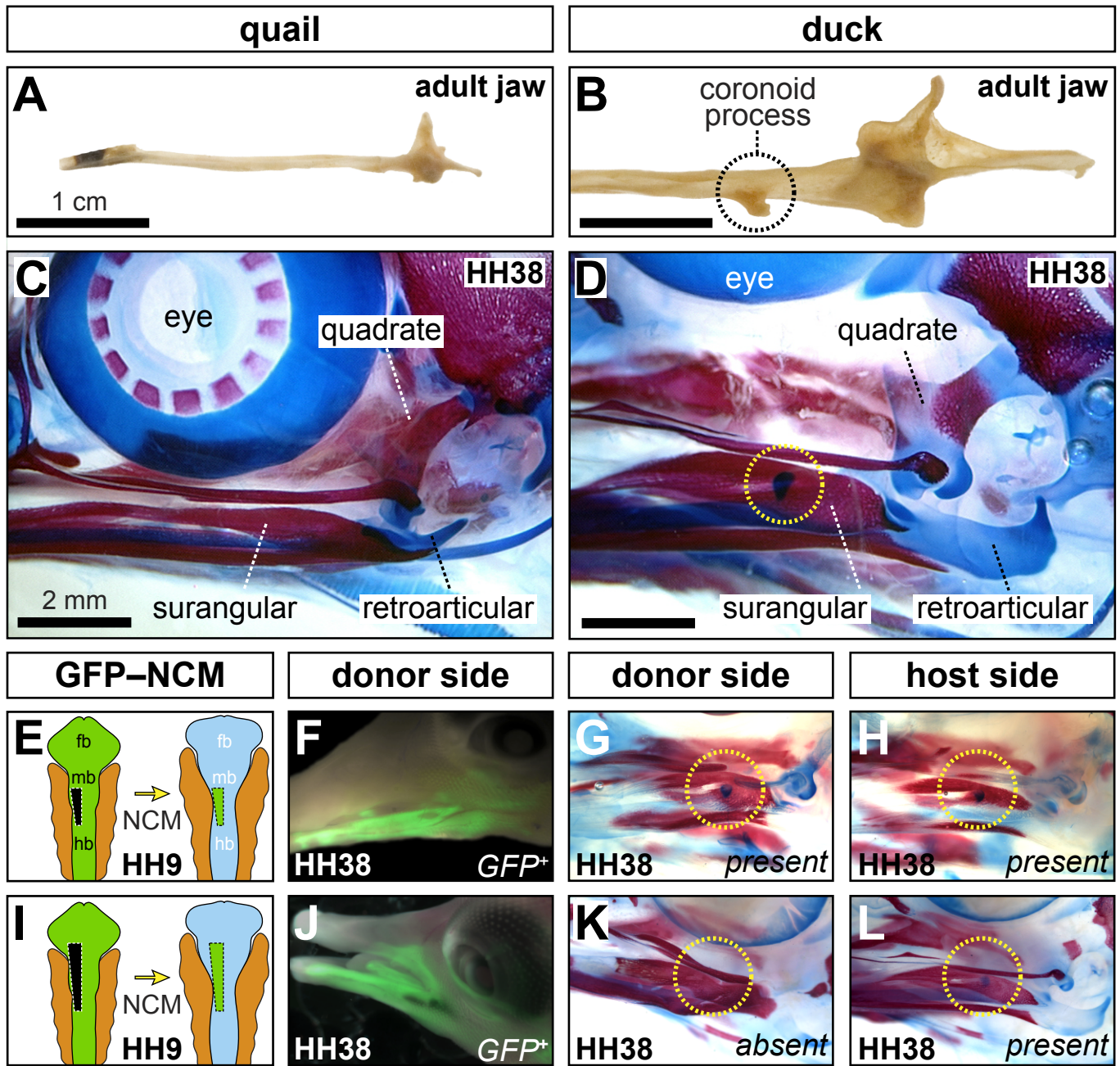
Figure 4. Comparison of embryonic quail and duck jaw motility *in ovo*. (**A**,**B**,**C**,**D**) Images depicting representative open and closed jaw gaping positions during *in ovo* motility in HH38 quail and duck. (**E**) Actogram depicting representative 30-minute observation periods of quail and duck motility *in ovo*. Observations were made during six consecutive developmental stages from HH33 to HH38. From HH33 to HH38, quail and duck activity periods steadily increase in frequency and duration. (**F**) During HH33, a key stage of secondary cartilage induction, the differences in jaw motility are minimal with quail being slightly more active, though the difference is not significant. Duck are significantly more active at HH36 (p<0.0005).

quail jaw gaping

A HH38 upper jaw / lower jaw 2 mm *closed*

B HH38 *open*

duck jaw gaping

C HH38 upper jaw / lower jaw *closed*

D HH38 *open*
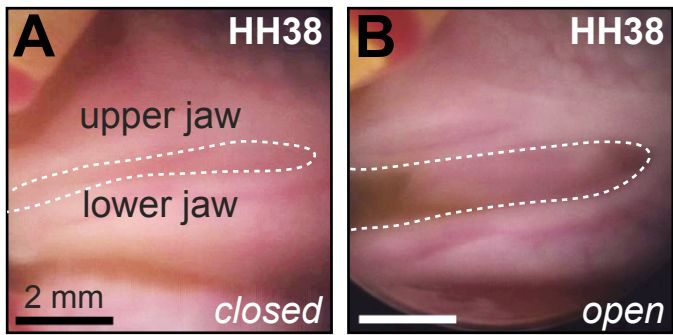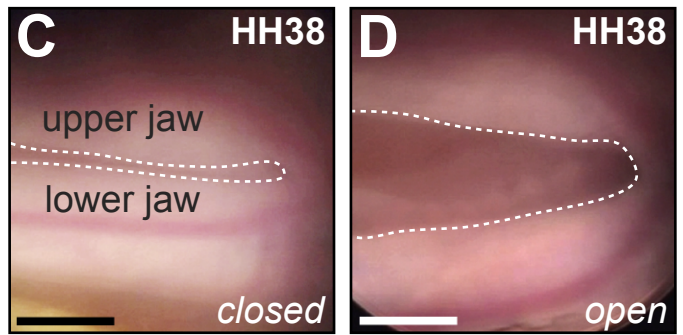
embryonic motility actogram

E ■ quail ■ duck

stage (HH): 33, 34, 35, 36, 37, 38

time (minutes): 0 10 20 30
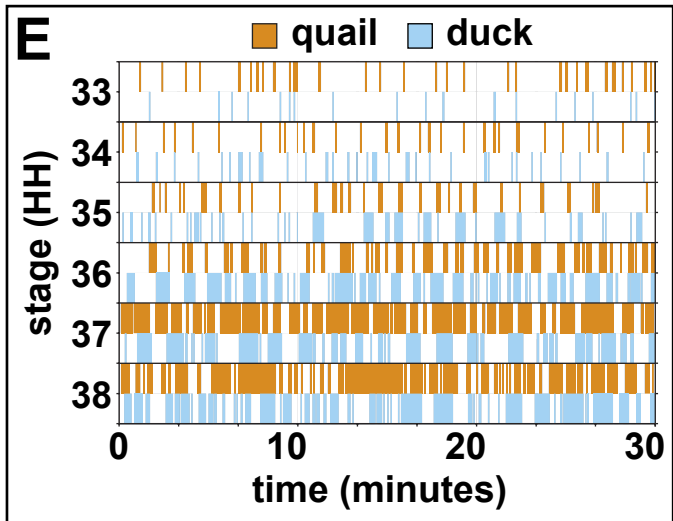
quail versus duck motility

F ■ quail ■ duck

motility (%): 90 70 50 30 10

stage (HH): 31 33 35 37

*
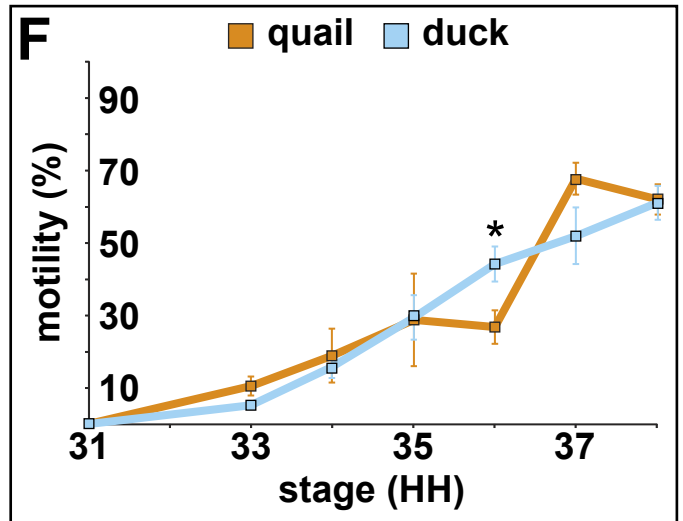
Figure 5. 3D reconstructions and finite element analysis of quail and duck adductor complexes. (**A**) Three-dimensional wireframe of left HH33 quail jaw anatomy showing the presumptive surangular (light-green), quadrate (red), mandibular adductor muscle (purple), post-orbital cartilage (dark-green), and Meckel's cartilage (blue). Note the slender mandibular adductor and its dorsal insertion on the surangular condensation. (**B**) Three-dimensional wireframe of left HH33 duck jaw anatomy. Note the bulky appearance of the mandibular adductor and its lateral insertion on the surangular condensation. (**C**) Finite element modeling predicts a maximum von Mises stress concentration of 0.0156 MPa within the medial portion of the contact area between the mandibular adductor and the surangular in quail. Color scales indicate predicted von Mises stress. (**D**) A maximum von Mises stress concentration of 0.9560 MPa is predicted within a dorsolateral region of the contact area between the mandibular adductor and the surangular in duck. (**E**) Histogram of the range of von Mises stresses in duck versus quail. The contact area between the mandibular adductor and the surangular is predicted to experience a wider range of stresses in duck versus quail, and maximum von Mises stress in quail is substantially less than in duck.

three-dimensional wireframe

A quail

surangular
mandibular adductor

Meckel's

1 mm

HH33

B duck

surangular
mandibular adductor

Meckel's

HH33

finite element analysis

C surangular

0.014

0.007

max = .0156 MPa

0.000

Meckel's

quail

D 0.900

max = .9560 MPa

0.045

0.000

surangular
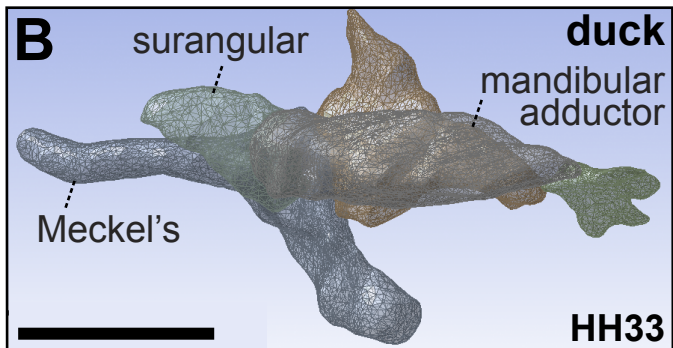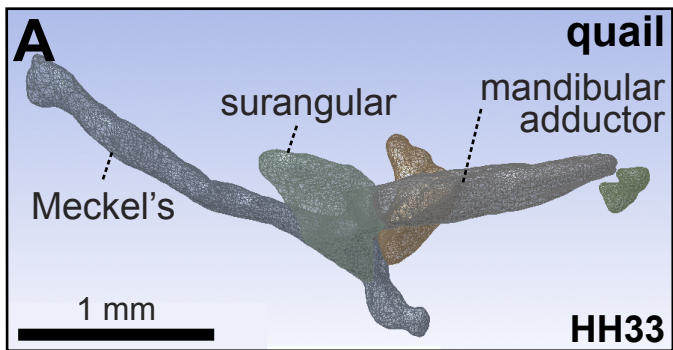
duck Meckel's
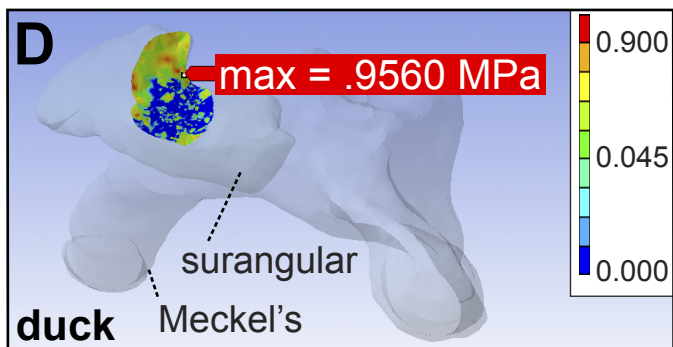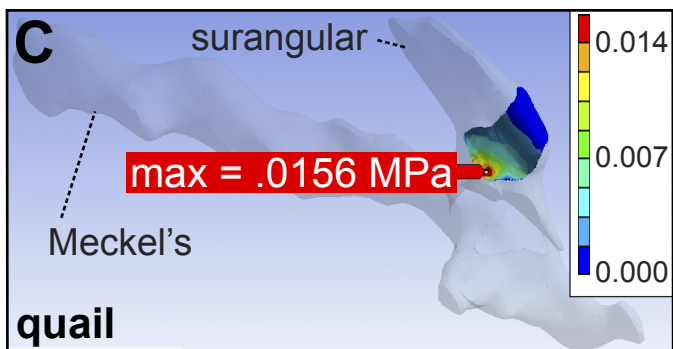
von Mises stress distribution

E HH33

30

10

tissue (%)

quail
duck

1×10^{-6} 3×10^{-4} 5×10^{-2}

von Mises stress (MPa)

Figure 6. FGF signaling pathway member expression in paralyzed and control duck. (**A**) RT-qPCR on microdissected HH33 and HH36 paralyzed and stage-matched control insertion samples. Paralysis at HH32 leads to differential expression of FGF signaling pathway 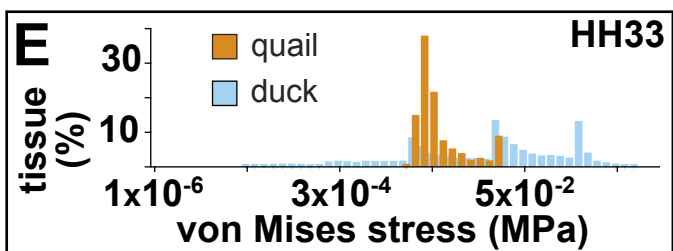members in subsequent developmental stages. Values for each gene were normalized to *β-Actin* and are displayed relative to HH33 control sample expression. Error bars represent standard deviation. Asterisks denote significant differences in gene expression between control HH36 samples and paralyzed HH36 samples. *p<0.05; **p<0.005. (**B**) Trichrome staining on a sagittal section through the HH33 mandibular adductor muscle insertion along the surangular condensation. The mandibular adductor muscle surrounding the proximal portion of the mandibular branch of the trigeminal nerve is visible. The mandibular adductor inserts along the surangular condensation. The dense mesenchymal condensation that gives rise to secondary cartilage can be seen in the distal portion of the mandibular adductor insertion on the coronoid process. (**C**) *Fgf4* (in purple) is expressed in the mandibular adductor, tendon, secondary cartilage condensation, and surangular condensation. (**D**) *Fgfr2* is expressed in the secondary cartilage condensation and the surangular condensation. (**E**) *Fgfr3* is expressed around the margins of the surangular condensation. (**F**) After 24 hours of paralysis, HH33 embryos show disrupted muscle and tendon morphology, and the mesenchymal condensation that yields secondary cartilage is absent. The mandibular branch of the trigeminal nerve appears unaffected. (**G**) *Fgf4* is expressed in the mandibular adductor and tendon, but the secondary cartilage expression domain is absent. (**H**) *Fgfr2* is expressed in the surangular condensation, but the secondary cartilage condensation domain is absent. (**I**) *Fgfr3* is expressed around the margins of the surangular condensation, similar to control embryos. (**J**) Trichrome stained sagittal section through the HH36 mandibular adductor muscle insertion on the coronoid process lateral to the surangular. The secondary cartilage condensation is well formed in control embryos. (**K**) *Fgf4* is expressed in the mandibular adductor muscle, tendon, and secondary cartilage. (**L**) *Fgfr2* is expressed in the mandibular adductor muscle, tendon, and secondary cartilage. (**M**) *Fgfr3* is expressed in the mandibular adductor muscle, tendon, and secondary cartilage. (**N**) Following paralysis at HH32, secondary cartilage fails to form and the mandibular adductor muscle interfaces directly with the surangular bone (asterisk). (**O**) *Fgf4* is expressed in the mandibular adductor muscle, tendon, and surangular bone. (**P**) *Fgfr2* is expressed in the mandibular adductor muscle, tendon, and surangular bone. (**Q**) *Fgfr3* is expressed in the mandibular adductor muscle, tendon, and surangular bone, especially in the periosteum. 2°, secondary cartilage; ma, mandibular adductor muscle; sa, HH33 surangular condensation or HH36 surangular bone.

Changes in FGF pathway members in duck from HH33 to HH36

A — -ΔΔ Ct value plotted for *Fgf2*, *Fgf4*, *Fgf8*, *Fgfr1*, *Fgfr2*, *Fgfr3*, *Pea3*, and *Erm* at stages 33 and 36. control (orange circle), paralyzed (blue square). Significance markers: *Fgf2* *, *Fgf4* **, *Fgf8* **, *Pea3* *, *Erm* *.

trichrome | *Fgf4* | *Fgfr2* | *Fgfr3*

B HH33 control — ma, sa, 400 μm
C HH33 control
D HH33 control
E HH33 control

F HH33 paralyzed — ma, sa
G HH33 paralyzed
H HH33 paralyzed
I HH33 paralyzed

J HH36 control — 2°, 200 μm
K HH36 control
L HH36 control
M HH36 control

N HH36 paralyzed — sa, *
O HH36 paralyzed
P HH36 paralyzed
Q HH36 paralyzed

Figure 7. TGFβ signaling pathway member expression in paralyzed and control duck. (**A**) RT-qPCR on microdissected HH33 and HH36 paralyzed and stage-matched control insertion samples. Paralysis at HH32 leads to differential expression of TGFβ signaling pathway members in subsequent developmental stages. Values for each gene were normalized to *β-Actin* and are displayed relative to HH33 control sample expression. Error bars represent standard deviation. Asterisk denotes a significant difference in *Pai1* gene expression between control HH36 samples and paralyzed HH36 samples. *$p < 0.05$. (**B**) Trichrome staining on a sagittally-sectioned, HH33 mandibular adductor muscle insertion along the surangular condensation. The mandibular adductor muscle, the mandibular branch of the trigeminal nerve, and the surangular condensation are all visible. The dense, distal mesenchymal condensation in the distal portion of the mandibular adductor insertion will give rise to secondary cartilage. (**C**) *Tgfβ2* is expressed in the mandibular adductor muscle, tendon, and secondary cartilage condensation. (**D**) *Tgfβ3* is expressed in the mandibular adductor muscle, tendon, and secondary cartilage condensation. (**E**) *Tgfβr2* is expressed in the mandibular adductor muscle, tendon, and secondary cartilage condensation. (**F**) After paralysis at HH32, HH33 embryos show disrupted muscle and tendon morphology, and the mesenchymal condensation that yields secondary cartilage is absent. The mandibular branch of the trigeminal nerve appears unaffected by paralysis. (**G**) *Tgfβ2* is expressed in the mandibular adductor muscle and tendon. (**H**) *Tgfβ3* is expressed in the mandibular adductor muscle and tendon. (**I**) *Tgfβr2* is expressed in the mandibular adductor muscle and tendon. (**J**) A well-developed secondary cartilage is visible in the trichrome stained, sagittally sectioned HH36 control mandibular adductor muscle insertion on the coronoid process lateral to the surangular. (**K**) *Tgfβ2* is expressed in the mandibular adductor muscle, tendon, and secondary cartilage. (**L**) *Tgfβ3* is expressed in the mandibular adductor muscle, tendon, and secondary cartilage. (**M**) *Tgfβr2* is expressed in the secondary cartilage condensation and the surangular bone. (**N**) Secondary cartilage fails to form by HH36 when embryos are paralyzed at HH32. The mandibular adductor muscle inserts directly onto the surangular bone (asterisk). (**O**) *Tgfβ2* is expressed in the mandibular adductor muscle, tendon, and the surangular bone. (**P**) *Tgfβ3* is expressed in the mandibular adductor muscle, tendon, and the surangular bone. (**Q**) *Tgfβr2* is expressed in the surangular bone. 2°, secondary cartilage; ma, mandibular adductor muscle; sa, HH33 surangular condensation or HH36 surangular bone.

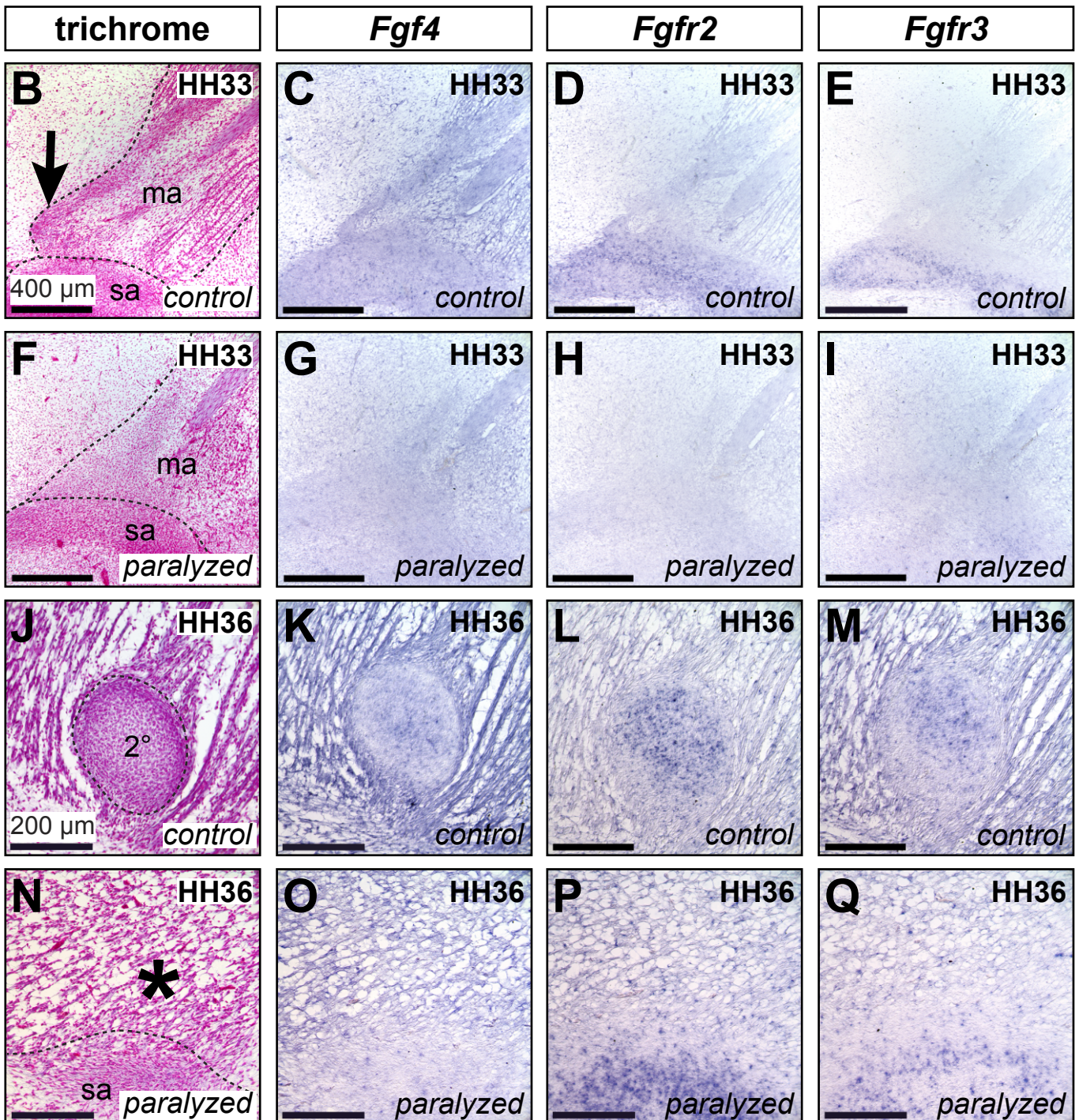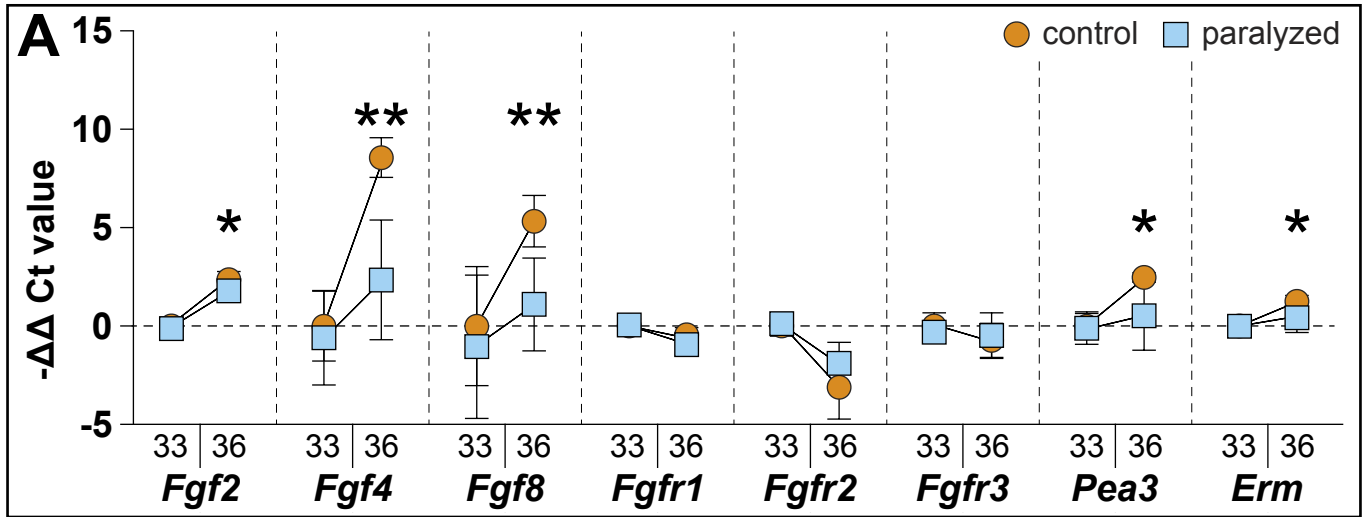**Changes in TGFβ pathway members in duck from HH33 to HH36**

A

-ΔΔ Ct value

Tgfβ2 *Tgfβ3* *Tgfβr1* *Tgfβr2* *Tgfβr3* *Smad3* *Smad7b* *Pai1*

control — paralyzed

| | trichrome | *Tgfβ2* | *Tgfβ3* | *Tgfβr2* |

B HH33 — ma, sa, *control*, 400 μm
C HH33 *control*
D HH33 *control*
E HH33 *control*

F HH33 ma *paralyzed*
G HH33 *paralyzed*
H HH33 *paralyzed*
I HH33 *paralyzed*

J HH36 2° *control* 200 μm
K HH36 *control*
L HH36 *control*
M HH36 *control*

N HH36 ma * *paralyzed*
O HH36 *paralyzed*
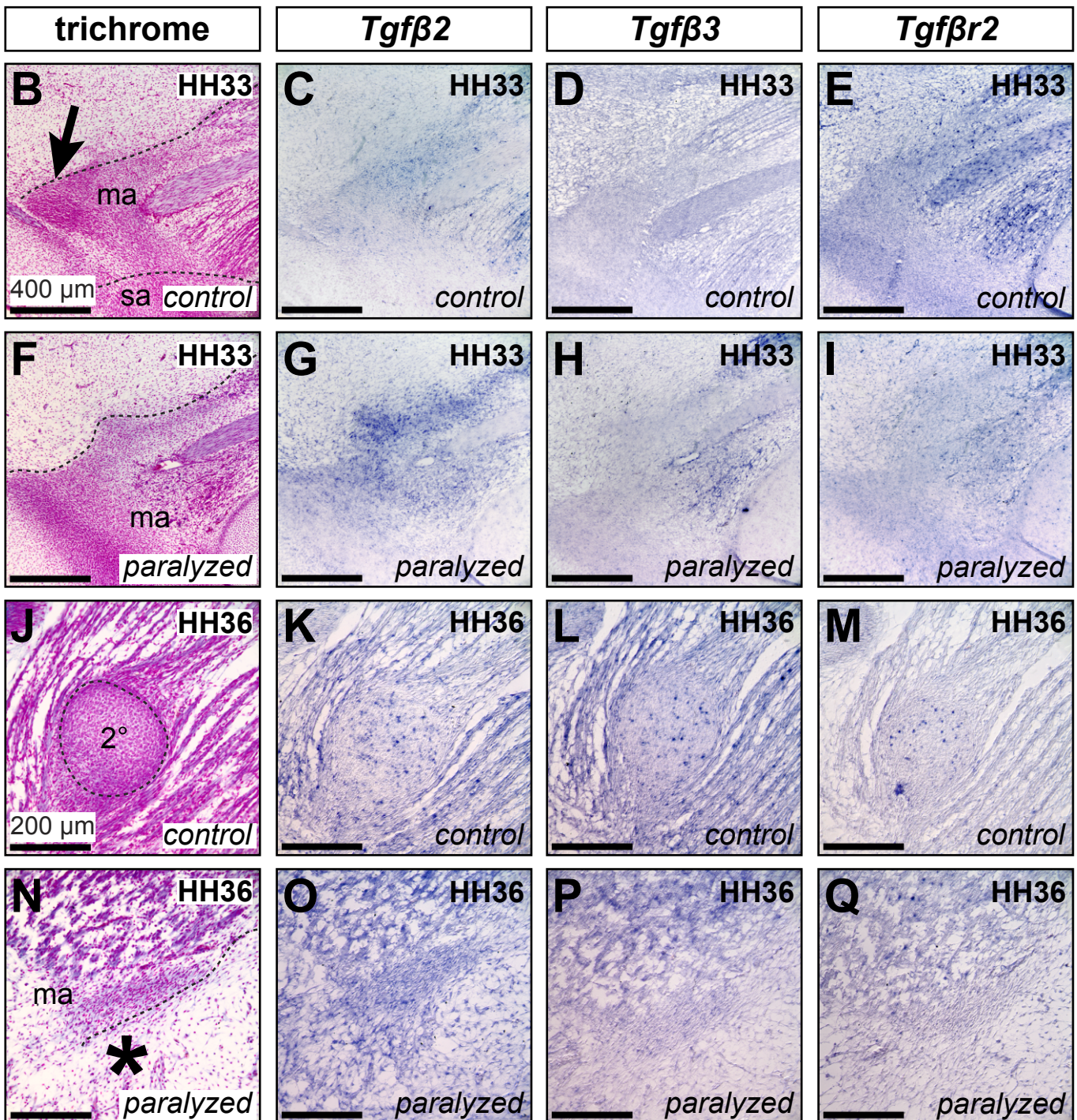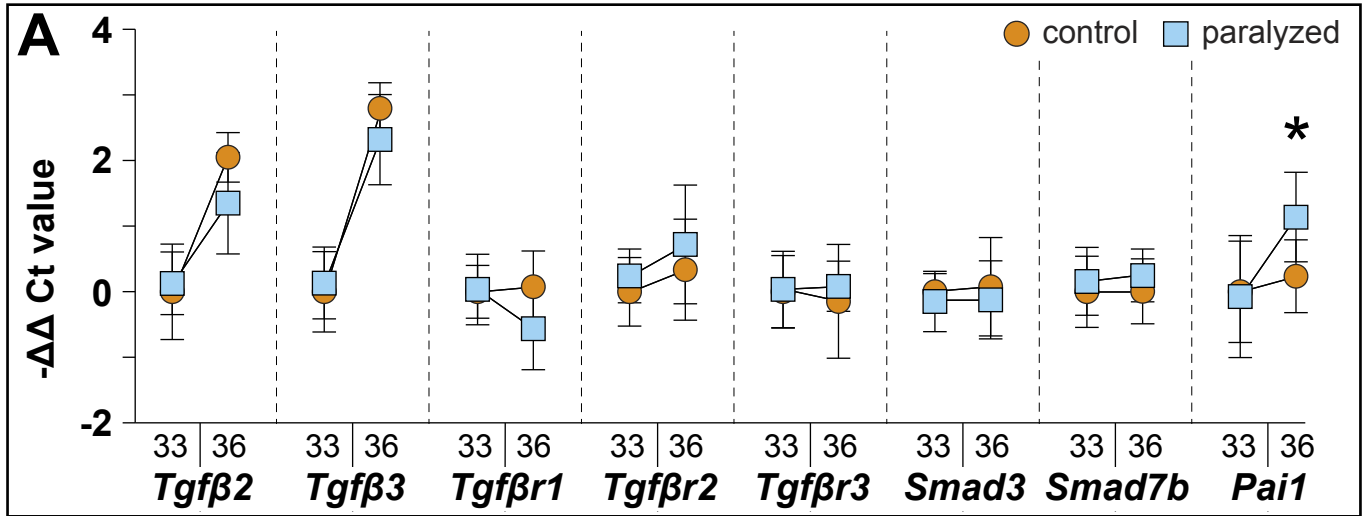**P** HH36 *paralyzed*
Q HH36 *paralyzed*

Figure 8. *Fgf8*, *Pea3*, and *Smad3* expression in paralyzed and control embryos (**A**) In stage HH33 embryos, *Fgf8* (in purple) is expressed in the mandibular adductor muscle, tendon, secondary cartilage condensation, and surangular condensation. (**B**) *Pea3* is expressed in the mandibular adductor muscle, tendon, secondary cartilage condensation, and surangular condensation. (**C**) *Smad3* is expressed in the mandibular adductor muscle, tendon, and secondary cartilage condensation. (**D**) In paralyzed HH33 embryos, *Fgf8* is expressed in the mandibular adductor, tendon, and surangular condensation. The secondary cartilage expression domain is absent. (**E**) *Pea3* is expressed in the mandibular adductor muscle, tendon, and the surangular condensation. The secondary cartilage expression domain is absent. (**F**) Smad3 is expressed in the mandibular adductor muscle and tendon. The secondary cartilage expression domain is disrupted. (**G**) In stage HH36 embryos, *Fgf8* is expressed in the mandibular adductor muscle, tendon, and secondary cartilage. (**H**) *Pea3* is expressed in the mandibular adductor muscle, tendon, and secondary cartilage. (**I**) *Smad3* is expressed in the mandibular adductor muscle, tendon, and secondary cartilage. (**J**) *Fgf8* is expressed in the mandibular adductor muscle, and tendon. The secondary cartilage expression domain is absent. (**K**) *Pea3* is expressed in the mandibular adductor muscle and tendon. The secondary cartilage expression domain is absent. (**L**) *Smad3* is expressed in the mandibular adductor muscle and tendon. The secondary cartilage expression domain is absent.

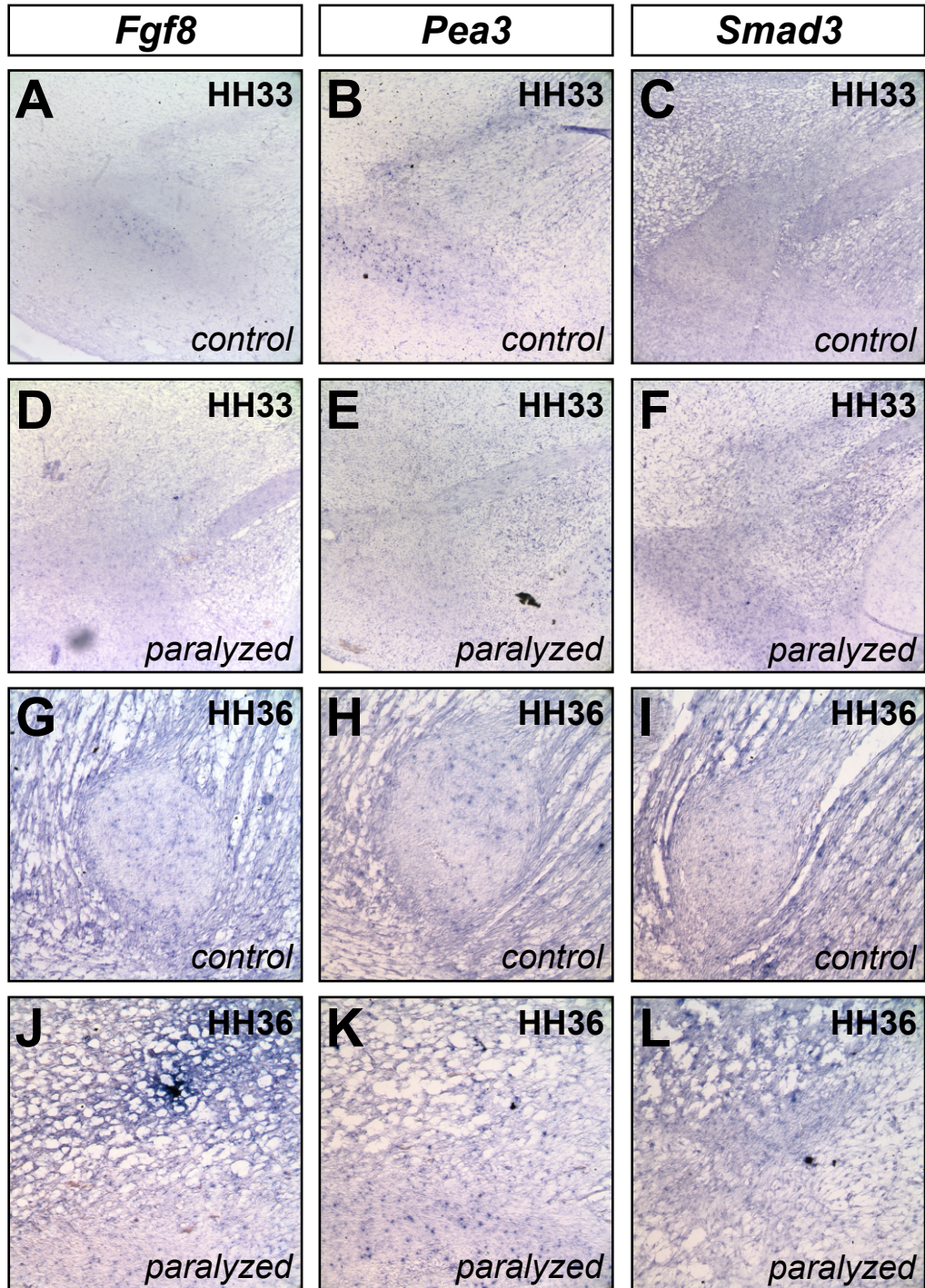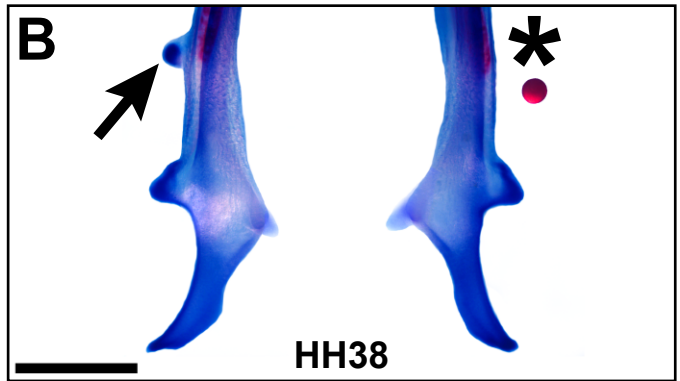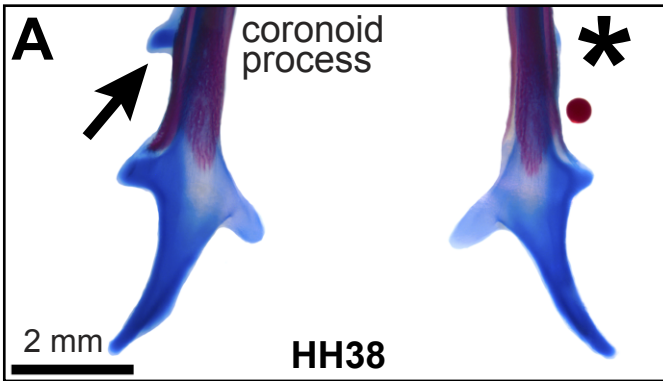|	*Fgf8*	*Pea3*	*Smad3*
	A HH33 *control*	**B** HH33 *control*	**C** HH33 *control*
	D HH33 *paralyzed*	**E** HH33 *paralyzed*	**F** HH33 *paralyzed*
	G HH36 *control*	**H** HH36 *control*	**I** HH36 *control*
	J HH36 *paralyzed*	**K** HH36 *paralyzed*	**L** HH36 *paralyzed*

Figure 9. Effects of inhibiting FGF and TGFβ signaling during secondary chondrogenesis. (**A**) Ventral view of an isolated cleared and stained HH38 duck mandible that was treated with a bead soaked in a small molecule inhibitor of FGF signaling (SU5402). Note that FGF inhibition results in loss of the secondary cartilage (asterisk) while the untreated side develops normally (black arrow). (**B**) Ventral view of HH38 duck mandible treated with a bead soaked in a small molecule inhibitor of TGFβ signaling (SB431542). Note that TGFβ inhibition results in loss of secondary cartilage (asterisk) while the control side develops normally (black arrow). (**C**) FGF signaling inhibition produces HH38 embryos with an absent or reduced-sized secondary cartilage on the treated side relative to control. FGF inhibition has a greater effect on secondary chondrogenesis when embryos are treated at HH32 than at HH33 (Fisher's Exact Test p<0.005). (**D**) TGFβ signaling inhibition results in HH38 embryos with absent or reduced-size secondary cartilage on the treated side relative to the control side. Treatment outcomes are not significantly affected by the stage of TGFβ inhibition, however, the frequency of secondary cartilage loss was greater with TGFβ inhibition at HH32. (**E**) Quantifying cell death 24 hours after FGF or TGFβ signaling inhibition reveals no significant increase over treatments with DMSO. As a positive control cell death was quantified in DNase treated slides from DMSO treated embryos (unpaired t-test p<0.0001) (**F,G,H,I**) Fluorescence microscopy of sectioned tissue implanted with SU5402, or SB431542 carrying beads (appear as a green circle when present) reveals no significant increase in cell death over DMSO control beads. Significant cell death only observed in positive control (i.e., DNase digested) sections from DMSO-treated embryos.

SU5402-treated duck at HH33

A coronoid process   *   2 mm   HH38

SB431542-treated duck at HH33

B   *   HH38

effects of SU5402

C

treated embryos (%)

HH32: 2 (unaffected), 16 (8) (reduced), absent
HH33: 16 (unaffected), 13 (9) (reduced), absent

□ unaffected   □ reduced   □ absent

effects of SB431542

D

treated embryos (%)

HH32: 22 (unaffected), 15 (10) (reduced)
HH33: 40 (unaffected), 26 (24) (reduced)

□ unaffected   □ reduced   □ absent

TUNEL analysis

E

TUNEL positive (%)

bead treatments at HH32: DMSO, DNase, SU5402, SB431542

TUNEL analysis

F HH32+24h   50 μm   *DMSO*

G HH32+24h   *DNase*

H HH32+24h   *SU5402*

I HH32+24h   *SB431542*
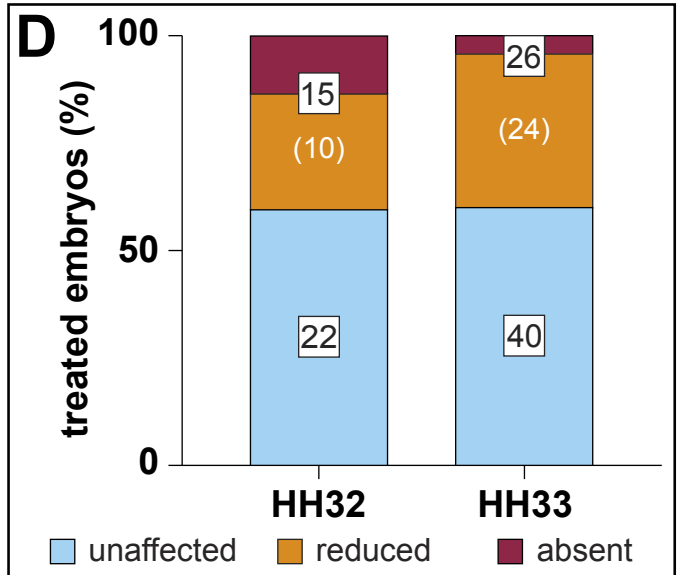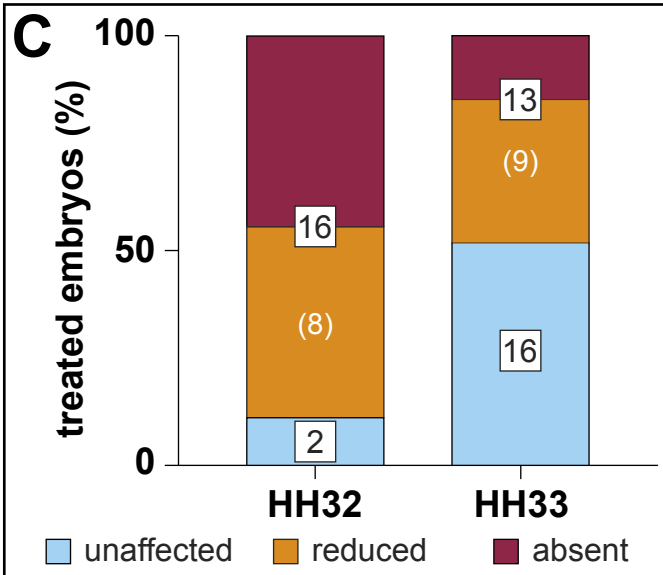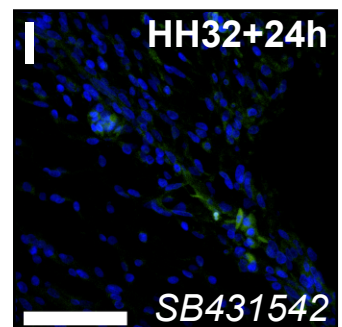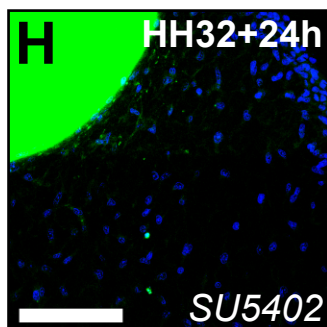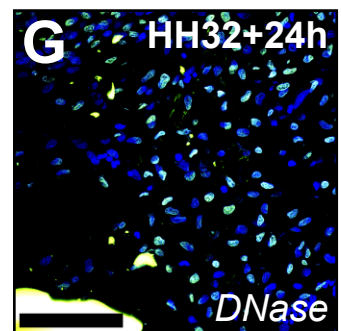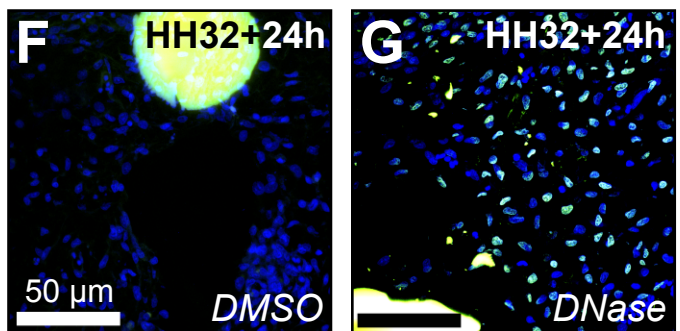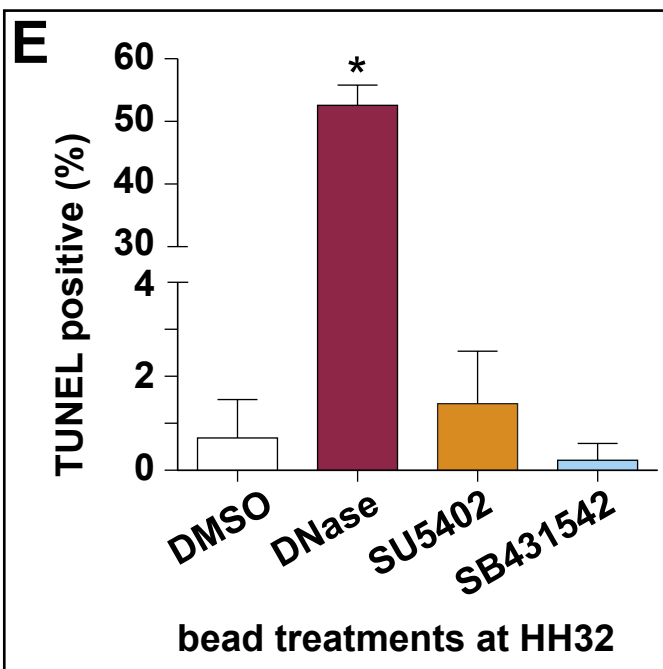
Figure 10. FGF4 and TGFβ2/TGFβ3 induce chondrogenesis. (**A**) Using beads to deliver BSA to control embryos at HH32 has no effect on secondary chondrogenesis (asterisk). (**B**) Embryos paralyzed at HH32 and treated exogenously with beads carrying recombinant FGF4 form cartilage around the bead (white arrow). (**C**) Embryos paralyzed at HH32 and implanted with beads carrying TGFβ2/TGFβ3 form cartilage around the bead (black arrow). (**D**) Cartilage forms around beads carrying FGF4 and TGFβ2/TGFβ3 in an embryo paralyzed at HH32 (black arrow). (**E**) Safranin-O stained sagittal section through an embryo treated with FGF4 and TGFβ2/TGFβ3 on separate beads. A dense layer of positively stained mesenchyme surrounds the beads (asterisk). (**F**) Quail treated with TGFβ2/TGFβ3 at HH32 form cartilage around the bead (black arrow). (**G**) Summary of treatment outcomes at HH38 when paralyzed embryos are treated with exogenous FGF4, TGFβ2/TGFβ3, or all three ligands delivered on two separate beads at HH32. The distribution of treatment outcomes depends upon the ligand or ligands embryos receive (Fisher's Exact Test p=0.005).

control

A HH38

duck

1 mm

FGF4

B HH38

paralyzed

TGFβ2/3

C HH38

paralyzed

FGF4/TGFβ2/3

D HH38

paralyzed

FGF4/TGFβ2/3

E

200μm

paralyzed

TGFβ2/3

F HH38

1 mm

quail
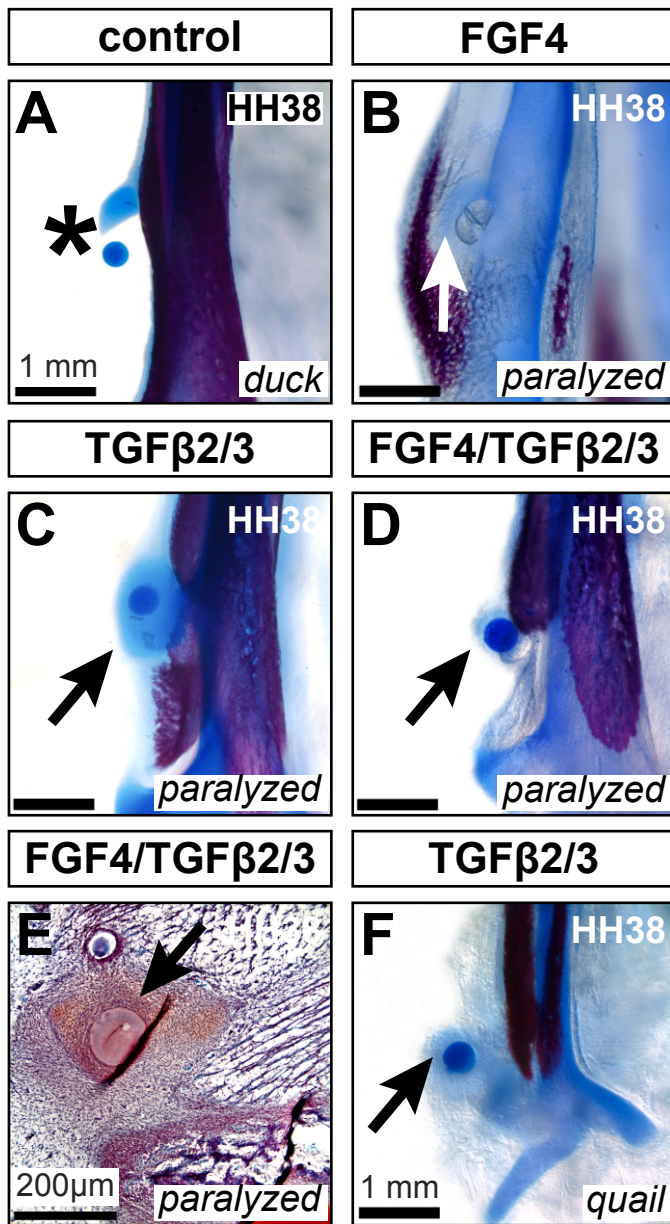
rescue of HH32 paralyzed duck

G

treated embryos (%)

100

50

0

FGF4   TGFβ2/3   FGF4/TGFβ

8   5   2

3   15   12

■ no cartilage   ■ cartilage induced
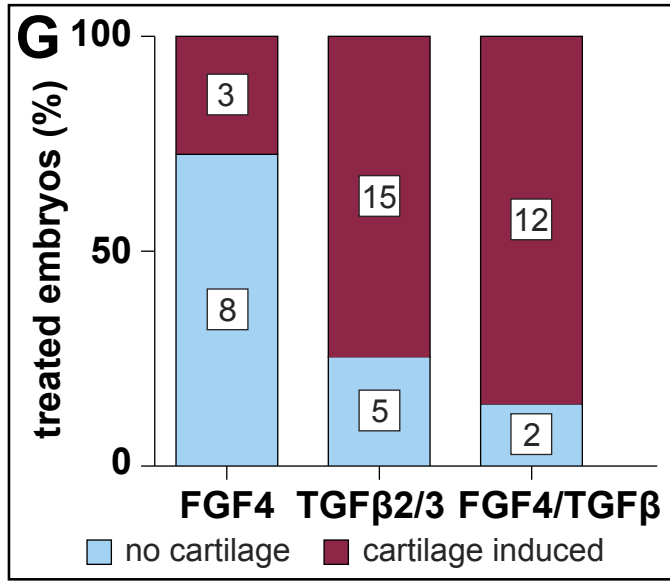
Figure 11. A model integrating form and function with FGF and TGFβ signaling. NCM mediated species-specific jaw geometry, (i.e., dorsal versus lateral mandibular adductor insertions) and functional loading by embryonic motility contribute to mechanical loading and tissue differentiation. The resultant mechanical stress leads to differential activation of FGF and TGFβ signaling and regulates the presence or absence of secondary cartilage on the coronoid process. We found three overlapping patterns of gene expression. One set of genes is altered by growth (blue boxes), another set is altered by load (red boxes), and a third set is altered by both growth and load (orange boxes). We found a fourth group of genes in which expression remains unaltered both during growth and despite manipulating embryonic motility (white boxes). Some genes are found in more than one category, reflecting the complex integration of form and function during embryonic development.

A model for the relationship between form and function

differential forces from species-specific morphology regulate secondary cartilage on the coronoid process

neural crest

form

motility

function

mechanical load

spatiotemporal patterns of gene expression

☐ altered by growth   ☐ altered by load
☐ unaltered   ☐ altered by growth and load

FGF signaling

TGFβ signaling

ligands

Fgf2
Fgf4
Fgf8

Tgfß2
Tgfß3

receptors

Fgfr1
Fgfr2
Fgfr3

Tgfßr1
Tgfßr2
Tgfßr2

effectors

Pea3
Erm

Smad3
Smad7b
Pai1

tissue differentiation

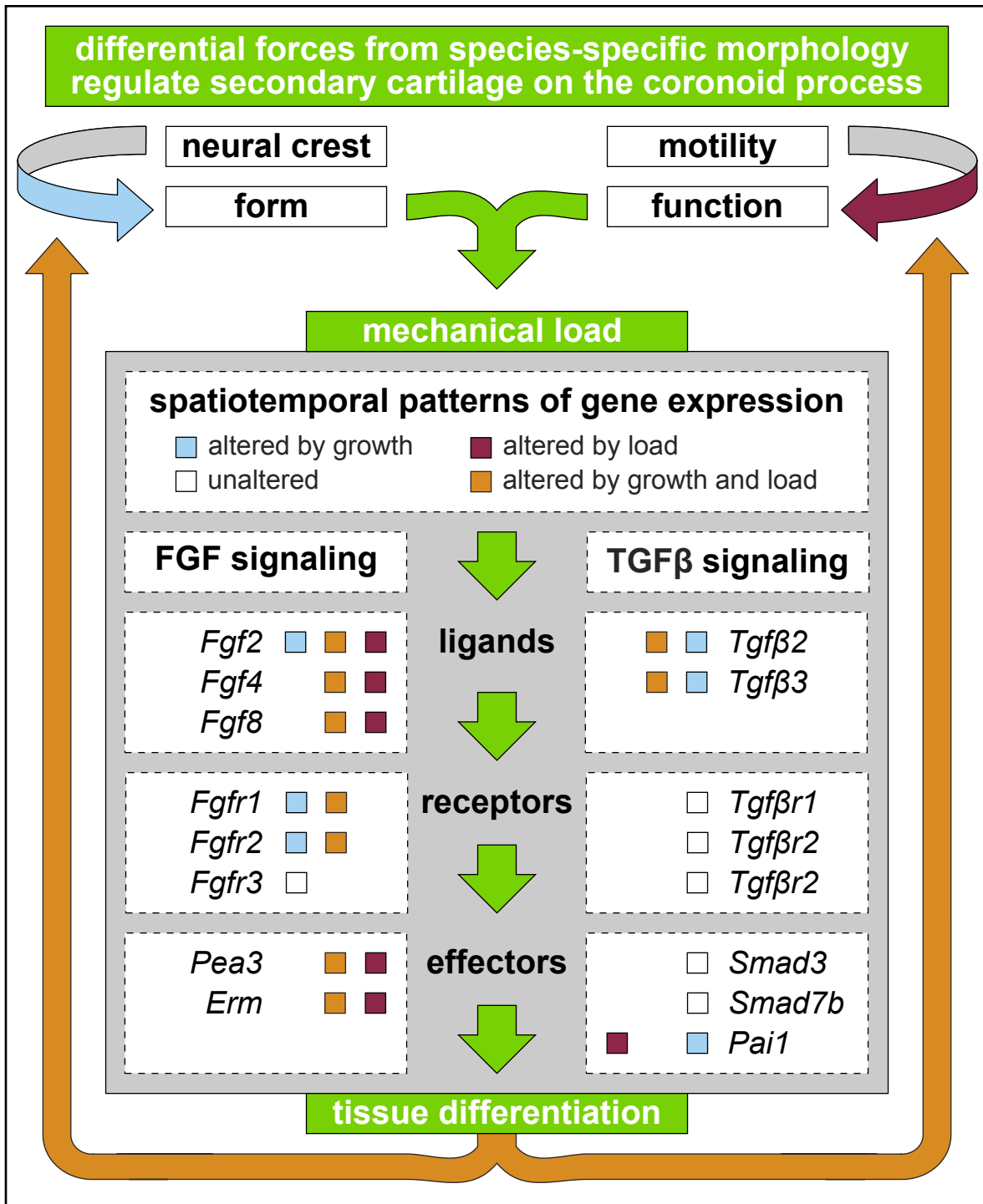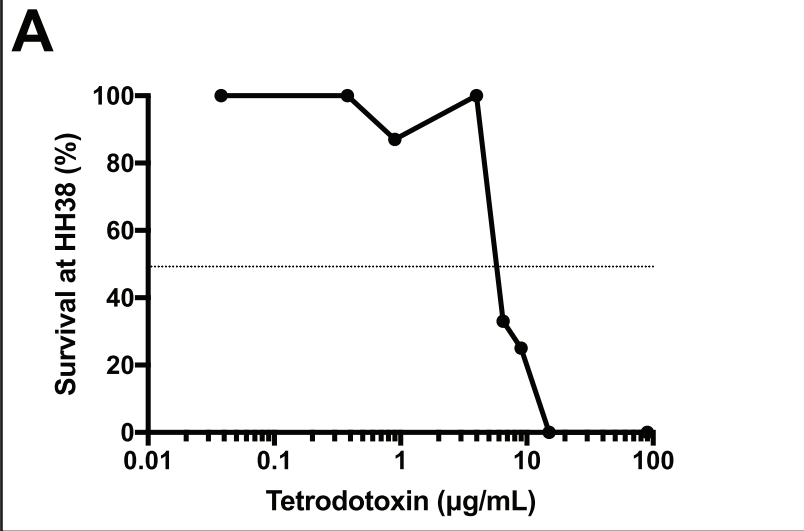**Figure 12. Effects of ion channel inhibition on embryonic survival and secondary chondrogenesis on the coronoid process.** (**A**) By HH38, embryonic survival is severely affected by voltage-gated sodium ion channel inhibition using tetrodotoxin. 50% survival occurs between doses of 4µg/mL and 6.5µg/mL. (**B,C,D,E**) Lateral and ventral views of a representative embryo upon collection and following clearing and staining show that gross anatomy and the size and shape of the coronoid process are unaffected by voltage-gated sodium channel inhibition (white arrows). (**F**) 4-AP blockade of voltage-gated potassium ion channels severely affects embryonic survival at HH38. 50% survival occurs between dosages of 1092µg/mL and 2000µg/mL. (**G,H,I,J**) Collection photos and clearing and staining reveal that neither the gross anatomy nor the secondary cartilage on the coronoid process are affected by voltage-gated potassium channel blockade (white arrows). (**K**) Nifedipine inhibition of L-type, voltage-gated calcium ion channels negatively affects survival by HH38. 50% survival is reached between 9.8µg/mL and 12µg/mL. (**L,M,N,O**) Upon collection, pools of blood are evident beneath the epithelium. Furthermore, the left eye appears to be stunted in growth. Clearing and staining reveals that secondary cartilage failed to form on the coronoid process (white asterisks).

Effect of Sodium Channel Blockade

A — Survival at HH38 (%) vs Tetrodotoxin (µg/mL)

Tetrodotoxin (9µg/mL)

B lateral — HH38 duck
C lateral — HH38 duck
D ventral
E ventral
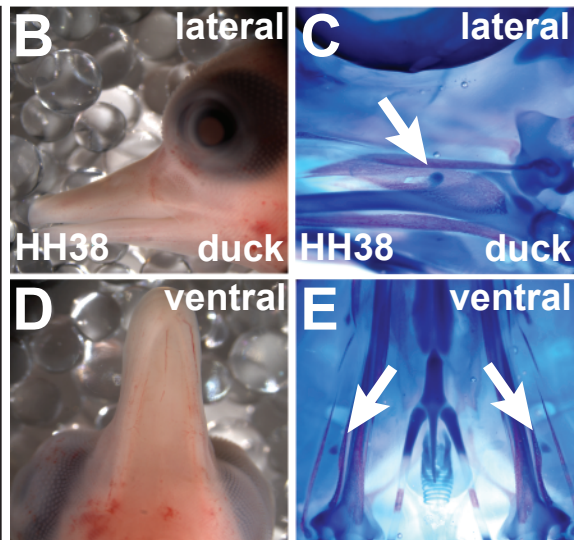
Effect of Potassium Channel Blockade

F — Survival at HH38 (%) vs 4-Aminopyridine (µg/mL)

4-AP (1092µg/mL)
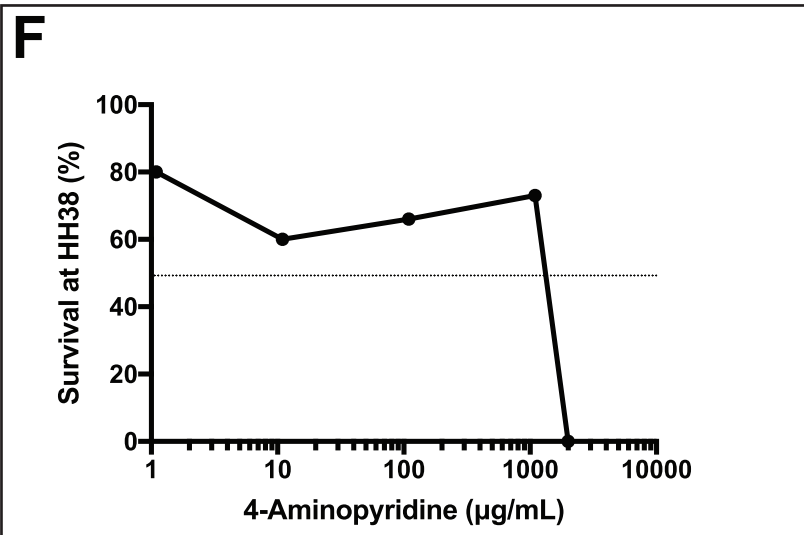
G lateral — HH38 duck
H lateral — HH38 duck
I ventral
J ventral
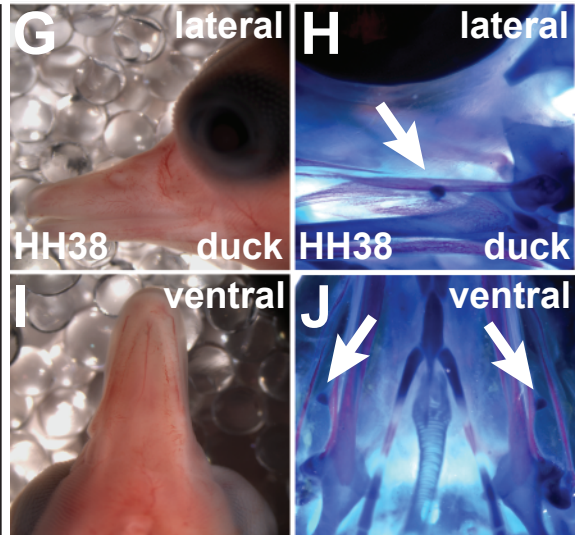
Effect of Calcium Channel Blockade

K — Survival at HH38 (%) vs Nifedipine (µg/mL)

Nifedipine (26µg/mL)
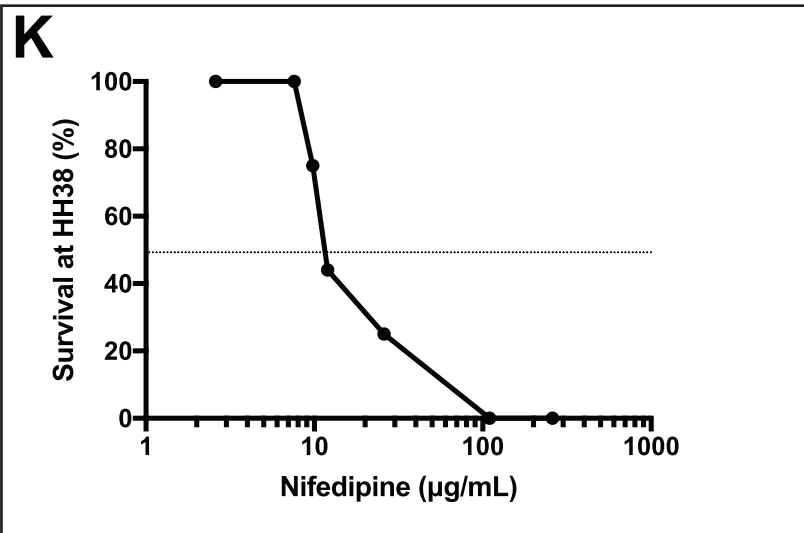
L lateral — HH38 duck
M lateral — HH38 duck
N ventral
O ventral
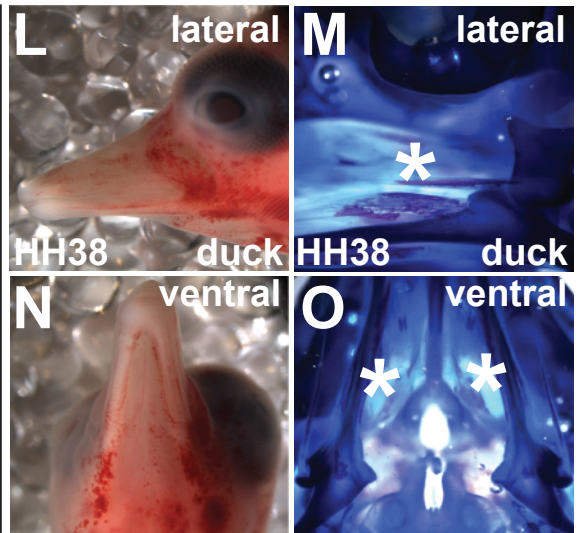
References

Abzhanov, A., Kuo, W.P., Hartmann, C., Grant, B.R., Grant, P.R., Tabin, C.J., 2006. The calmodulin pathway and evolution of elongated beak morphology in Darwin's finches. Nature 442, 563-567.

Abzhanov, A., Protas, M., Grant, B.R., Grant, P.R., Tabin, C.J., 2004. Bmp4 and morphological variation of beaks in Darwin's finches. Science 305, 1462-1465.

Abzhanov, A., Tabin, C.J., 2004. Shh and Fgf8 act synergistically to drive cartilage outgrowth during cranial development. Dev Biol 273, 134-148.

Ahlgren, S.C., Bronner-Fraser, M., 1999. Inhibition of sonic hedgehog signaling in vivo results in craniofacial neural crest cell death. Curr Biol 9, 1304-1314.

Ahlgren, S.C., Thakur, V., Bronner-Fraser, M., 2002. Sonic hedgehog rescues cranial neural crest from cell death induced by ethanol exposure. Proc Natl Acad Sci U S A 99, 10476-10481.

Alappat, S., Zhang, Z.Y., Chen, Y.P., 2003. Msx homeobox gene family and craniofacial development. Cell Res 13, 429-442.

Albrecht, U., Eichele, G., Helms, J.A., Lu, H.-C., 1997. Visualization of gene expression patterns by in situ hybridization. Molecular and cellular methods in developmental toxicology, 23-48.

Almubarak, S., Nethercott, H., Freeberg, M., Beaudon, C., Jha, A., Jackson, W., Marcucio, R., Miclau, T., Healy, K., Bahney, C., 2016. Tissue engineering strategies for promoting vascularized bone regeneration. Bone 83, 197-209.

Amin, S., Tucker, A.S., 2006. Joint formation in the middle ear: lessons from the mouse and guinea pig. Dev Dyn 235, 1326-1333.

Amorim, M.M., Borini, C.B., de Castro Lopes, S.L., de Oliveira Tosello, D., Berzin, F., Caria, P.H., 2010. Relationship between the angle of the coronoid process of the mandible and the electromyographic activity of the temporal muscle in skeletal Class I and III individuals. Journal of oral rehabilitation 37, 596-603.

Amorim, M.M., Borini, C.B., Lopes, S.L., Haiter-Neto, F., Berzin, F., Caria, P.H., 2008. Relationship between the inclination of the coronoid process of the mandible and the electromyographic activity of the temporal muscle in skeletal Class I and II individuals. Journal of oral science 50, 293-299.

Andres, G., 1949. Untersuchungen an Chimären von Triton und Bombinator. Genetica 24, 387-534.

Anthwal, N., Chai, Y., Tucker, A.S., 2008. The role of transforming growth factor-beta signalling in the patterning of the proximal processes of the murine dentary. Dev Dynam 237, 1604-1613.

Anthwal, N., Joshi, L., Tucker, A.S., 2013. Evolution of the mammalian middle ear and jaw: adaptations and novel structures. J Anat 222, 147-160.

Anthwal, N., Peters, H., Tucker, A.S., 2015. Species-specific modifications of mandible shape reveal independent mechanisms for growth and initiation of the coronoid. Evodevo 6.

Anthwal, N., Urban, D.J., Luo, Z.X., Sears, K.E., Tucker, A.S., 2017. Meckel's cartilage breakdown offers clues to mammalian middle ear evolution. Nat Ecol Evol 1, 93.

Apostolakos, J., Durant, T.J., Dwyer, C.R., Russell, R.P., Weinreb, J.H., Alaee, F., Beitzel, K., McCarthy, M.B., Cote, M.P., Mazzocca, A.D., 2014. The enthesis: a review of the tendon-to-bone insertion. Muscles, ligaments and tendons journal 4, 333-342.

Appel, T.A., 1987. The Cuvier-Geoffroy Debate: French Biology in the Decade before Darwin. Oxford University Press, Oxford.

Attanasio, C., Nord, A.S., Zhu, Y., Blow, M.J., Li, Z., Liberton, D.K., Morrison, H., Plajzer-Frick, I., Holt, A., Hosseini, R., Phouanenavong, S., Akiyama, J.A., Shoukry, M., Afzal, V., Rubin, E.M., FitzPatrick, D.R., Ren, B., Hallgrimsson, B., Pennacchio, L.A., Visel, A., 2013. Fine tuning of craniofacial morphology by distant-acting enhancers. Science 342, 1241006.

Baggiolini, A., Varum, S., Mateos, J.M., Bettosini, D., John, N., Bonalli, M., Ziegler, U., Dimou, L., Clevers, H., Furrer, R., Sommer, L., 2015. Premigratory and Migratory Neural Crest Cells Are Multipotent In Vivo. Cell Stem Cell 16, 314-322.

Bahney, C.S., Hu, D.P., Taylor, A.J., Ferro, F., Britz, H.M., Hallgrimsson, B., Johnstone, B., Miclau, T., Marcucio, R.S., 2014. Stem cell-derived endochondral cartilage stimulates bone healing by tissue transformation. J Bone Miner Res 29, 1269-1282.

Bailleul, A.M., Hall, B.K., Horner, J.R., 2012. First evidence of dinosaurian secondary cartilage in the post-hatching skull of Hypacrosaurus stebingeri (Dinosauria, Ornithischia). PLoS One 7, e36112.

Bailleul, A.M., Hall, B.K., Horner, J.R., 2013. Secondary cartilage revealed in a non-avian dinosaur embryo. PLoS One 8, e56937.

Baker, C.V., Bronner-Fraser, M., 1997. The origins of the neural crest. Part I: embryonic induction. Mechanisms of Development 69, 3-11.

Baroffio, A., Dupin, E., Le Douarin, N.M., 1988. Clone-forming ability and differentiation potential of migratory neural crest cells. Proc Natl Acad Sci U S A 85, 5325-5329.

Barrett-Jolley, R., Lewis, R., Fallman, R., Mobasheri, A., 2010. The emerging chondrocyte channelome. Front Physiol 1, 135.

Baumel, J.J., 1993. Handbook of avian anatomy : nomina anatomica avium. Nuttall Ornithological Club, 1993., Cambridge, Mass.

Benjamin, M., Ralphs, J.R., 1998. Fibrocartilage in tendons and ligaments--an adaptation to compressive load. J Anat 193 (Pt 4), 481-494.

Benkman, C.W., Lindholm, A.K., 1991. The Advantages and Evolution of a Morphological Novelty. Nature 349, 519-520.

Beresford, W.A., 1981. Chondroid bone, secondary cartilage, and metaplasia. Urban & Schwarzenberg, Baltimore, Md.

Beresford, W.A., 1993. Cranial skeletal tissues: diversity and evolutionary trends, in: Hanken, J., Hall, B.K. (Eds.), The Skull. University of Chicago Press, Chicago, pp. 69-130.

Bernstein, L., Fernandez, B., 1984. Bilateral hyperplasia of the coronoid process of the mandible. Report of a case. Archives of otolaryngology 110, 480-482.

Berthet, E., Chen, C., Butcher, K., Schneider, R.A., Alliston, T., Amirtharajah, M., 2013. Smad3 binds Scleraxis and Mohawk and regulates tendon matrix organization. J Orthop Res 31, 1475-1483.

Beverdam, A., Merlo, G.R., Paleari, L., Mantero, S., Genova, F., Barbieri, O., Janvier, P., Levi, G., 2002. Jaw transformation with gain of symmetry after Dlx5/Dlx6 inactivation: mirror of the past? Genesis 34, 221-227.

Blackiston, D.J., McLaughlin, K.A., Levin, M., 2009. Bioelectric controls of cell proliferation: ion channels, membrane voltage and the cell cycle. Cell Cycle 8, 3527-3536.

Blitz, E., Sharir, A., Akiyama, H., Zelzer, E., 2013. Tendon-bone attachment unit is formed modularly by a distinct pool of Scx- and Sox9-positive progenitors. Development 140, 2680-2690.

Blitz, E., Viukov, S., Sharir, A., Shwartz, Y., Galloway, J.L., Pryce, B.A., Johnson, R.L., Tabin, C.J., Schweitzer, R., Zelzer, E., 2009. Bone Ridge Patterning during Musculoskeletal Assembly Is Mediated through SCX Regulation of Bmp4 at the Tendon-Skeleton Junction. Developmental Cell 17, 861-873.

Bothe, I., Ahmed, M.U., Winterbottom, F.L., von Scheven, G., Dietrich, S., 2007. Extrinsic versus intrinsic cues in avian paraxial mesoderm patterning and differentiation. Dev Dyn 236, 2397-2409.

Boyd, T.G., Castelli, W.A., Huelke, D.F., 1967. Removal of the temporalis muscle from its origin: effects on the size and shape of the coronoid process. Journal of dental research 46, 997-1001.

Bradley, N.S., 1999. Transformations in embryonic motility in chick: Kinematic correlates of type I and II motility at E9 and E12. Journal of Neurophysiology 81, 1486-1494.

Brent, A.E., Braun, T., Tabin, C.J., 2005. Genetic analysis of interactions between the somitic muscle, cartilage and tendon cell lineages during mouse development. Development 132, 515-528.

Brent, A.E., Schweitzer, R., Tabin, C.J., 2003. A somitic compartment of tendon progenitors. Cell 113, 235-248.

Brito, J.M., Teillet, M.A., Le Douarin, N.M., 2006. An early role for sonic hedgehog from foregut endoderm in jaw development: ensuring neural crest cell survival. Proc Natl Acad Sci U S A 103, 11607-11612.

Bronner-Fraser, M., 1994. Neural crest cell formation and migration in the developing embryo. Faseb Journal 8, 699-706.

Bronner-Fraser, M., Fraser, S., 1989. Developmental potential of avian trunk neural crest cells in situ. Neuron 3, 755-766.

Bronner-Fraser, M., Fraser, S.E., 1988. Cell lineage analysis reveals multipotency of some avian neural crest cells. Nature 335, 161-164.

Brunt, L.H., Begg, K., Kague, E., Cross, S., Hammond, C.L., 2017. Wnt signalling controls the response to mechanical loading during zebrafish joint development. Development 144, 2798-2809.

Bunker, D.L., Ilie, V., Ilie, V., Nicklin, S., 2014. Tendon to bone healing and its implications for surgery. Muscles, ligaments and tendons journal 4, 343-350.

Buxton, P.G., Hall, B., Archer, C.W., Francis-West, P., 2003. Secondary chondrocyte-derived Ihh stimulates proliferation of periosteal cells during chick development. Development 130, 4729-4739.

Callahan, J.F., Burgess, J.L., Fornwald, J.A., Gaster, L.M., Harling, J.D., Harrington, F.P., Heer, J., Kwon, C., Lehr, R., Mathur, A., Olson, B.A., Weinstock, J., Laping, N.J., 2002. Identification of novel inhibitors of the transforming growth factor beta1 (TGF-beta1) type 1 receptor (ALK5). J Med Chem 45, 999-1001.

Campas, O., Mallarino, R., Herrel, A., Abzhanov, A., Brenner, M.P., 2010. Scaling and shear transformations capture beak shape variation in Darwin's finches. Proc Natl Acad Sci U S A 107, 3356-3360.

Carter, D.R., Beaupré, G.S., 2007. Skeletal Function and Form: Mechanobiology of Skeletal Development, Aging, and Regeneration. Cambridge University Press.

Cerny, R., Lwigale, P., Ericsson, R., Meulemans, D., Epperlein, H.H., Bronner-Fraser, M., 2004. Developmental origins and evolution of jaws: new interpretation of "maxillary" and "mandibular". Dev Biol 276, 225-236.

Chamberlain, F.W., 1943. Atlas of avian anatomy; osteology, arthrology, myology. Michigan State College, Agricultural Experiment Station, East Lansing, Mich.,.

Chambers, S.H., Bradley, N.S., Orosz, M.D., 1995. Kinematic Analysis of Wing and Leg Movements for Type-I Motility in E9 Chick-Embryos. Experimental Brain Research 103, 218-226.

Chong, H.J., Young, N.M., Hu, D., Jeong, J., McMahon, A.P., Hallgrimsson, B., Marcucio, R.S., 2012. Signaling by SHH rescues facial defects following blockade in the brain. Dev Dyn 241, 247-256.

Cordero, D.R., Schneider, R.A., Helms, J.A., 2002. Morphogenesis of the Face, in: Lin, K.Y., Ogle, R.C., Jane, J.A. (Eds.), Craniofacial Surgery: Science & Surgical Technique. W. B. Saunders Company, Philadelphia, pp. 75-83.

Coste, B., Mathur, J., Schmidt, M., Earley, T.J., Ranade, S., Petrus, M.J., Dubin, A.E., Patapoutian, A., 2010. Piezo1 and Piezo2 are essential components of distinct mechanically activated cation channels. Science 330, 55-60.

Couly, G., Creuzet, S., Bennaceur, S., Vincent, C., Le Douarin, N.M., 2002. Interactions between Hox-negative cephalic neural crest cells and the foregut endoderm in patterning the facial skeleton in the vertebrate head. Development 129, 1061-1073.

Couly, G.F., Coltey, P.M., Le Douarin, N.M., 1992. The developmental fate of the cephalic mesoderm in quail-chick chimeras. Development 114, 1-15.

Couly, G.F., Coltey, P.M., Le Douarin, N.M., 1993. The triple origin of skull in higher vertebrates: a study in quail-chick chimeras. Development 117, 409-429.

Creuzet, S., Schuler, B., Couly, G., Le Douarin, N.M., 2004. Reciprocal relationships between Fgf8 and neural crest cells in facial and forebrain development. Proc Natl Acad Sci U S A 101, 4843-4847.

Darwin, C.R., 1859. On the origin of species by means of natural selection, or the preservation of favoured races in the struggle for life. John Murray, London.

Dawson, M.M., Metzger, K.A., Baier, D.B., Brainerd, E.L., 2011. Kinematics of the quadrate bone during feeding in mallard ducks. Journal of Experimental Biology 214, 2036-2046.

De Beer, G., 1958. Embryos and ancestors, 3d ed. Clarendon Press, Oxford,.

de Beer, G.R., 1930. Embryology and Evolution. Clarendon Press, Oxford.

de Beer, G.R., 1937. The Development of the Vertebrate Skull. University of Chicago Press, Chicago.

del Rio, A., Perez-Jimenez, R., Liu, R.C., Roca-Cusachs, P., Fernandez, J.M., Sheetz, M.P., 2009. Stretching Single Talin Rod Molecules Activates Vinculin Binding. Science 323, 638-641.

Depew, M.J., Compagnucci, C., 2008. Tweaking the hinge and caps: testing a model of the organization of jaws. Journal of experimental zoology. Part B, Molecular and developmental evolution 310, 315-335.

Depew, M.J., Liu, J.K., Long, J.E., Presley, R., Meneses, J.J., Pedersen, R.A., Rubenstein, J.L., 1999. Dlx5 regulates regional development of the branchial arches and sensory capsules. Development 126, 3831-3846.

Depew, M.J., Lufkin, T., Rubenstein, J.L., 2002. Specification of jaw subdivisions by Dlx genes. Science 298, 381-385.

Depew, M.J., Simpson, C.A., Morasso, M., Rubenstein, J.L., 2005. Reassessing the Dlx code: the genetic regulation of branchial arch skeletal pattern and development. J Anat 207, 501-561.

Diogo, R., Kelly, R.G., Christiaen, L., Levine, M., Ziermann, J.M., Molnar, J.L., Noden, D.M., Tzahor, E., 2015. A new heart for a new head in vertebrate cardiopharyngeal evolution. Nature 520, 466-473.

Dupin, E., Calloni, G.W., Le Douarin, N.M., 2010. The cephalic neural crest of amniote vertebrates is composed of a large majority of precursors endowed with neural, melanocytic, chondrogenic and osteogenic potentialities. Cell Cycle 9, 238-249.

Dupont, S., Morsut, L., Aragona, M., Enzo, E., Giulitti, S., Cordenonsi, M., Zanconato, F., Le Digabel, J., Forcato, M., Bicciato, S., Elvassore, N., Piccolo, S., 2011. Role of YAP/TAZ in mechanotransduction. Nature 474, 179-U212.

Ealba, E.L., Jheon, A.H., Hall, J., Curantz, C., Butcher, K.D., Schneider, R.A., 2015. Neural crest-mediated bone resorption is a determinant of species-specific jaw length. Dev Biol 408, 151-163.

Ealba, E.L., Schneider, R.A., 2013. A simple PCR-based strategy for estimating species-specific contributions in chimeras and xenografts. Development 140, 3062-3068.

Eames, B.F., Allen, N., Young, J., Kaplan, A., Helms, J.A., Schneider, R.A., 2007. Skeletogenesis in the swell shark Cephaloscyllium ventriosum. J Anat 210, 542-554.

Eames, B.F., Schneider, R.A., 2005. Quail-duck chimeras reveal spatiotemporal plasticity in molecular and histogenic programs of cranial feather development. Development 132, 1499-1509.

Eames, B.F., Schneider, R.A., 2008. The genesis of cartilage size and shape during development and evolution. Development 135, 3947-3958.

Eames, B.F., Sharpe, P.T., Helms, J.A., 2004. Hierarchy revealed in the specification of three skeletal fates by Sox9 and Runx2. Dev Biol 274, 188-200.

Edom-Vovard, F., Bonnin, M., Duprez, D., 2001a. Fgf8 transcripts are located in tendons during embryonic chick limb development. Mech Dev 108, 203-206.

Edom-Vovard, F., Bonnin, M.A., Duprez, D., 2001b. Misexpression of Fgf-4 in the chick limb inhibits myogenesis by down-regulating Frek expression. Dev Biol 233, 56-71.

Edom-Vovard, F., Schuler, B., Bonnin, M.A., Teillet, M.A., Duprez, D., 2002. Fgf4 positively regulates scleraxis and tenascin expression in chick limb tendons. Dev Biol 247, 351-366.

Eichele, G., Tickle, C., Alberts, B.M., 1984. Microcontrolled release of biologically active compounds in chick embryos: beads of 200-microns diameter for the local release of retinoids. Analytical biochemistry 142, 542-555.

Eloy-Trinquet, S., Wang, H., Edom-Vovard, F., Duprez, D., 2009. Fgf signaling components are associated with muscles and tendons during limb development. Dev Dyn 238, 1195-1206.

Evans, D.J., Noden, D.M., 2006. Spatial relations between avian craniofacial neural crest and paraxial mesoderm cells. Dev Dyn 235, 1310-1325.

Fang, J., Hall, B.K., 1997. Chondrogenic cell differentiation from membrane bone periostea. Anat Embryol (Berl) 196, 349-362.

Fernandez Ferro, M., Fernandez Sanroman, J., Sandoval Gutierrez, J., Costas Lopez, A., Lopez de Sanchez, A., Etayo Perez, A., 2008. Treatment of bilateral hyperplasia of the coronoid process of the mandible. Presentation of a case and review of the literature. Medicina oral, patologia oral y cirugia bucal 13, E595-598.

Fish, J.L., Schneider, R.A., 2014a. Assessing species-specific contributions to craniofacial development using quail-duck chimeras. J Vis Exp.

Fish, J.L., Schneider, R.A., 2014b. Chapter 6 - Neural Crest-Mediated Tissue Interactions During Craniofacial Development: The Origins of Species-Specific Pattern, in: Trainor, P.A. (Ed.), Neural Crest Cells. Academic Press, Boston, pp. 101-124.

Fish, J.L., Sklar, R.S., Woronowicz, K.C., Schneider, R.A., 2014. Multiple developmental mechanisms regulate species-specific jaw size. Development 141, 674-684.

Fish, J.L., Villmoare, B., Koebernick, K., Compagnucci, C., Britanova, O., Tarabykin, V., Depew, M.J., 2011. Satb2, modularity, and the evolvability of the vertebrate jaw. Evolution & Development 13, 549-564.

Fitzgerald, T.C., 1969. The coturnix quail; anatomy and histology, [1st ed. Iowa State University Press, Ames,.

Galatz, L.M., Ball, C.M., Teefey, S.A., Middleton, W.D., Yamaguchi, K., 2004. The outcome and repair integrity of completely arthroscopically repaired large and massive rotator cuff tears. J Bone Joint Surg Am 86-A, 219-224.

Gammill, L.S., Gonzalez, C., Bronner-Fraser, M., 2007. Neuropilin 2/semaphorin 3F signaling is essential for cranial neural crest migration and trigeminal ganglion condensation. Dev Neurobiol 67, 47-56.

Gans, C., Northcutt, R.G., 1983. Neural Crest and the Origin of Vertebrates: A New Head. Science 220, 268-274.

Garstang, W., 1922. The Theory of Recapitulation: A Critical Re-statement of the Biogenetic Law. Journal of the Linnean Society of London, Zoology 35, 81-101.

Gatti, P.L., Salvi, C., Zampardi, C., 1985. Physiopathology of the masticatory system with particular reference to the apophyseal coronoid relation, temporal muscle, and intercuspidization. Parodontologia e stomatologia 24, 111-114.

Gaupp, E., 1913. Die Reichertsche Theorie (Hammer-, Amboss- und Kieferfrage). Archiv für Anatomie und Entwicklungsgeschichte 1912, 1-416.

Giori, N.J., Beaupre, G.S., Carter, D.R., 1993. Cellular-Shape and Pressure May Mediate Mechanical Control of Tissue Composition in Tendons. Journal of Orthopaedic Research 11, 581-591.

Golding, J.P., Trainor, P., Krumlauf, R., Gassmann, M., 2000. Defects in pathfinding by cranial neural crest cells in mice lacking the neuregulin receptor ErbB4. Nat Cell Biol 2, 103-109.

Goodrich, E.S., 1930. Studies on the Structure and Development of Vertebrates. University of Chicago Press, Chicago.

Gould, S.J., 1977. Ontogeny and phylogeny. Belknap Press of Harvard University Press, Cambridge, Mass.

Grenier, J., Teillet, M.A., Grifone, R., Kelly, R.G., Duprez, D., 2009. Relationship between neural crest cells and cranial mesoderm during head muscle development. PLoS One 4, e4381.

Griffin, J.N., Compagnucci, C., Hu, D., Fish, J., Klein, O., Marcucio, R., Depew, M.J., 2013. Fgf8 dosage determines midfacial integration and polarity within the nasal and optic capsules. Developmental Biology 374, 185-197.

Haeckel, E., 1891. Anthropogenie; oder, Entwickelungsgeschichte des menschen. Keimes- und stammesgeschichte, 4. umgearb. und verm. aufl. ... ed. W. Engelmann, Leipzig,.

Hall, B.K., 1967. The formation of adventitious cartilage by membrane bones under the influence of mechanical stimulation applied in vitro. Life Sciences 6, 663-667.

Hall, B.K., 1968. In Vitro Studies on Mechanical Evocation of Adventitious Cartilage in Chick. Journal of Experimental Zoology 168, 283-&.

Hall, B.K., 1972. Immobilization and Cartilage Transformation into Bone in Embryonic Chick. Anat Rec 173, 391-&.

Hall, B.K., 1979. Selective proliferation and accumulation of chondroprogenitor cells as the mode of action of biomechanical factors during secondary chondrogenesis. Teratology 20, 81-91.

Hall, B.K., 1981. The induction of neural crest-derived cartilage and bone by embryonic epithelia: an analysis of the mode of action of an epithelial-mesenchymal interaction. J Embryol Exp Morphol 64, 305-320.

Hall, B.K., 1983. Cartilage. Academic Press, New York.

Hall, B.K., 1986. The Role of Movement and Tissue Interactions in the Development and Growth of Bone and Secondary Cartilage in the Clavicle of the Embryonic Chick. J Embryol Exp Morph 93, 133-152.

Hall, B.K., 1999. Balfour, garstang and De Beer: The first century of evolutionary embryology. American Zoologist 39, 107a-107a.

Hall, B.K., 2005. Bones and cartilage : developmental and evolutionary skeletal biology. Elsevier Academic Press, San Diego, Calif.

Hall, B.K., Herring, S.W., 1990. Paralysis and Growth of the Musculoskeletal System in the Embryonic Chick. J Morphol 206, 45-56.

Hall, B.K., Miyake, T., 1992. The membranous skeleton: the role of cell condensations in vertebrate skeletogenesis. Anatomy and embryology 186, 107-124.

Hall, J., Jheon, A.H., Ealba, E.L., Eames, B.F., Butcher, K.D., Mak, S.S., Ladher, R., Alliston, T., Schneider, R.A., 2014. Evolution of a developmental mechanism: Species-specific regulation of the cell cycle and the timing of events during craniofacial osteogenesis. Dev Biol 385, 380-395.

Hamburger, V., 1965. Motility of Chick Embryos in Absence of Sensory Input. American Zoologist 5, 633-&.

Hamburger, V., Balaban, M., 1963. Observations and experiments on spontaneous rhythmical behavior in the chick embryo. Dev Biol 6, 533-545.

Hamburger, V., Balaban, M., Oppenheim, R., Wenger, E., 1965. Periodic motility of normal and spinal chick embryos between 8 and 17 days of incubation. J Exp Zool 159, 1-13.

Hamburger, V., Oppenheim, R., 1967. Prehatching Motility and Hatching Behavior in Chick. Journal of Experimental Zoology 166, 171-&.

Hamburger, V., Wenger, E., Oppenhei.R, 1966. Motility in Chick Embryo in Absence of Sensory Input. Journal of Experimental Zoology 162, 133-&.

Hamill, O.P., McBride, D.W., 1996. The pharmacology of mechanogated membrane ion channels. Pharmacological Reviews 48, 231-252.

Hammond, C.L., Simbi, B.H., Stickland, N.C., 2007. In ovo temperature manipulation influences embryonic motility and growth of limb tissues in the chick (Gallus gallus). Journal of Experimental Biology 210, 2667-2675.

Han, S.K., Wouters, W., Clark, A., Herzog, W., 2012. Mechanically induced calcium signaling in chondrocytes in situ. J Orthop Res 30, 475-481.

Hanken, J., Hall, B.K., 1993. The Skull, Volume 3: Functional and Evolutionary Mechanisms. University of Chicago Press.

Hashimoto, Y., Yoshida, G., Toyoda, H., Takaoka, K., 2007. Generation of tendon-to-bone interface "enthesis" with use of recombinant BMP-2 in a rabbit model. J Orthop Res 25, 1415-1424.

Havis, E., Bonnin, M.A., Esteves de Lima, J., Charvet, B., Milet, C., Duprez, D., 2016. TGFbeta and FGF promote tendon progenitor fate and act downstream of muscle contraction to regulate tendon differentiation during chick limb development. Development 143, 3839-3851.

Havis, E., Bonnin, M.A., Olivera-Martinez, I., Nazaret, N., Ruggiu, M., Weibel, J., Durand, C., Guerquin, M.J., Bonod-Bidaud, C., Ruggiero, F., Schweitzer, R., Duprez, D., 2014. Transcriptomic analysis of mouse limb tendon cells during development. Development 141, 3683-3696.

Hayamizu, T.F., Sessions, S.K., Wanek, N., Bryant, S.V., 1991. Effects of localized application of transforming growth factor beta 1 on developing chick limbs. Dev Biol 145, 164-173.

Helms, J.A., Schneider, R.A., 2003. Cranial skeletal biology. Nature 423, 326-331.

Hems, T., Tillmann, B., 2000. Tendon entheses of the human masticatory muscles. Anatomy and embryology 202, 201-208.

Henion, P.D., Weston, J.A., 1997. Timing and pattern of cell fate restrictions in the neural crest lineage. Development 124, 4351-4359.

Hernandez-Alfaro, F., Escuder, O., Marco, V., 2000. Joint formation between an osteochondroma of the coronoid process and the zygomatic arch (Jacob disease): report of case and review of literature. Journal of oral and maxillofacial surgery : official journal of the American Association of Oral and Maxillofacial Surgeons 58, 227-232.

Herring, S.W., 1993. Functional Morphology of Mammalian Mastication. American Zoologist 33, 289-299.

His, W., 1874. Unsere Körperform und das physiologische Problem ihrer Enstehung: Briefe an einen Befreundeten Naturforscher. FCW Vogel.

Horowitz, S.L., Shapiro, H.H., 1951. Modifications of mandibular architecture following removal of temporalis muscle in the rat. Journal of dental research 30, 276-280.

Hörstadius, S., 1950. The neural crest; its properties and derivatives in the light of experimental research. Oxford University Press, London, New York,.

Hosseini, A., Hogg, D.A., 1991. The Effects of Paralysis on Skeletal Development in the Chick-Embryo .1. General Effects. Journal of Anatomy 177, 159-168.

Hu, D., Marcucio, R.S., 2009. A SHH-responsive signaling center in the forebrain regulates craniofacial morphogenesis via the facial ectoderm. Development 136, 107-116.

Hu, D., Marcucio, R.S., 2012. Neural crest cells pattern the surface cephalic ectoderm during FEZ formation. Dev Dynam 241, 732-740.

Hu, D., Marcucio, R.S., Helms, J.A., 2003. A zone of frontonasal ectoderm regulates patterning and growth in the face. Development 130, 1749-1758.

Hu, D., Young, N.M., Li, X., Xu, Y., Hallgrimsson, B., Marcucio, R.S., 2015. A dynamic Shh expression pattern, regulated by SHH and BMP signaling, coordinates fusion of primordia in the amniote face. Development 142, 567-574.

Huang, A.H., Riordan, T.J., Wang, L., Eyal, S., Zelzer, E., Brigande, J.V., Schweitzer, R., 2013a. Repositioning forelimb superficialis muscles: tendon attachment and muscle activity enable active relocation of functional myofibers. Dev Cell 26, 544-551.

Huang, B., Takahashi, K., Sakata-Goto, T., Kiso, H., Togo, Y., Saito, K., Tsukamoto, H., Sugai, M., Akira, S., Shimizu, A., Bessho, K., 2013b. Phenotypes of CCAAT/enhancer-binding protein beta deficiency: hyperdontia and elongated coronoid process. Oral diseases 19, 144-150.

Hunt, P., Gulisano, M., Cook, M., Sham, M.H., Faiella, A., Wilkinson, D., Boncinelli, E., Krumlauf, R., 1991. A distinct Hox code for the branchial region of the vertebrate head. Nature 353, 861-864.

Inman, G.J., Nicolas, F.J., Callahan, J.F., Harling, J.D., Gaster, L.M., Reith, A.D., Laping, N.J., Hill, C.S., 2002. SB-431542 is a potent and specific inhibitor of transforming growth factor-beta superfamily type I activin receptor-like kinase (ALK) receptors ALK4, ALK5, and ALK7. Mol Pharmacol 62, 65-74.

Isberg, A., Eliasson, S., 1990. A cephalometric analysis of patients with coronoid process enlargement and locking. American journal of orthodontics and dentofacial orthopedics : official publication of the American Association of Orthodontists, its constituent societies, and the American Board of Orthodontics 97, 35-40.

Jeong, J., Li, X., McEvilly, R.J., Rosenfeld, M.G., Lufkin, T., Rubenstein, J.L., 2008. Dlx genes pattern mammalian jaw primordium by regulating both lower jaw-specific and upper jaw-specific genetic programs. Development 135, 2905-2916.

Jerome, L.A., Papaioannou, V.E., 2001. DiGeorge syndrome phenotype in mice mutant for the T-box gene, Tbx1. Nat Genet 27, 286-291.

Jheon, A.H., Schneider, R.A., 2009. The cells that fill the bill: neural crest and the evolution of craniofacial development. Journal of dental research 88, 12-21.

Jiang, X., Iseki, S., Maxson, R.E., Sucov, H.M., Morriss-Kay, G.M., 2002. Tissue origins and interactions in the mammalian skull vault. Dev Biol 241, 106-116.

Jing, Y., Zhou, X., Han, X., Jing, J., von der Mark, K., Wang, J., de Crombrugghe, B., Hinton, R.J., Feng, J.Q., 2015. Chondrocytes Directly Transform into Bone Cells in Mandibular Condyle Growth. Journal of dental research 94, 1668-1675.

Jollie, M.T., 1957. The Head Skeleton of the Chicken and Remarks on the Anatomy of this Region in Other Birds. J Morphol 100, 389-436.

Jones, N.C., Lynn, M.L., Gaudenz, K., Sakai, D., Aoto, K., Rey, J.P., Glynn, E.F., Ellington, L., Du, C., Dixon, J., Dixon, M.J., Trainor, P.A., 2008. Prevention of the neurocristopathy Treacher Collins syndrome through inhibition of p53 function. Nat Med 14, 125-133.

Kahn, J., Shwartz, Y., Blitz, E., Krief, S., Sharir, A., Breitel, D.A., Rattenbach, R., Relaix, F., Maire, P., Rountree, R.B., Kingsley, D.M., Zelzer, E., 2009. Muscle contraction is necessary to maintain joint progenitor cell fate. Dev Cell 16, 734-743.

Kantomaa, T., Rönning, O., 1997. Growth Mechanisms of the Mandible, in: Dixon, A.D., Hoyte, D.A.N., Rönning, O. (Eds.), Fundamentals of craniofacial growth. CRC Press, Boca Raton, pp. 189-204.

Kardon, G., 1998. Muscle and tendon morphogenesis in the avian hind limb. Development 125, 4019-4032.

Kardon, G., Harfe, B.D., Tabin, C.J., 2003. A Tcf4-positive mesodermal population provides a prepattern for vertebrate limb muscle patterning. Dev Cell 5, 937-944.

Kawarada, Y., Inoue, Y., Kawasaki, F., Fukuura, K., Sato, K., Tanaka, T., Itoh, Y., Hayashi, H., 2016. TGF-beta induces p53/Smads complex formation in the PAI-1 promoter to activate transcription. Sci Rep-Uk 6.

Kissel, P., André, J.M., Jacquier, A., 1981. The neurocristopathies. Masson Pub., New York.

Kleinnulend, J., Roelofsen, J., Sterck, J.G.H., Semeins, C.M., Burger, E.H., 1995. Mechanical Loading Stimulates the Release of Transforming Growth-Factor-Beta Activity by Cultured Mouse Calvariae and Periosteal Cells. J Cell Physiol 163, 115-119.

Koo, B.S., Song, Y., Lee, S., Sung, Y.K., Sung, I.H., Jun, J.B., 2017. Prevalence and distribution of sesamoid bones and accessory ossicles of the foot as determined by digital tomosynthesis. Clin Anat.

Krispin, S., Nitzan, E., Kassem, Y., Kalcheim, C., 2010. Evidence for a dynamic spatiotemporal fate map and early fate restrictions of premigratory avian neural crest. Development 137, 585-595.

Kulesa, P., Ellies, D.L., Trainor, P.A., 2004. Comparative analysis of neural crest cell death, migration, and function during vertebrate embryogenesis. Dev Dyn 229, 14-29.

Kuo, C.K., Tuan, R.S., 2008. Mechanoactive Tenogenic Differentiation of Human Mesenchymal Stem Cells. Tissue Eng Pt A 14, 1615-1627.

Kuraku, S., Takio, Y., Sugahara, F., Takechi, M., Kuratani, S., 2010. Evolution of oropharyngeal patterning mechanisms involving Dlx and endothelins in vertebrates. Dev Biol 341, 315-323.

Kuratani, S., Adachi, N., Wada, N., Oisi, Y., Sugahara, F., 2013. Developmental and evolutionary significance of the mandibular arch and prechordal/premandibular cranium in vertebrates: revising the heterotopy scenario of gnathostome jaw evolution. J Anat 222, 41-55.

Lamb, K.J., Lewthwaite, J.C., Lin, J.P., Simon, D., Kavanagh, E., Wheeler-Jones, C.P.D., Pitsillides, A.A., 2003. Diverse range of fixed positional deformities and bone growth restraint provoked by flaccid paralysis in embryonic chicks. Int J Exp Pathol 84, 191-199.

Lamichhaney, S., Berglund, J., Almen, M.S., Maqbool, K., Grabherr, M., Martinez-Barrio, A., Promerova, M., Rubin, C.J., Wang, C., Zamani, N., Grant, B.R., Grant, P.R., Webster, M.T., Andersson, L., 2015. Evolution of Darwin's finches and their beaks revealed by genome sequencing. Nature 518, 371-375.

Landmesser, L., Morris, D.G., 1975. The development of functional innervation in the hind limb of the chick embryo. J Physiol 249, 301-326.

Le Lièvre, C.S., 1978. Participation of neural crest-derived cells in the genesis of the skull in birds. J Embryol Exp Morph 47, 17-37.

Le Lievre, C.S., Le Douarin, N.M., 1975. Mesenchymal derivatives of the neural crest: analysis of chimaeric quail and chick embryos. J Embryol Exp Morphol 34, 125-154.

Lee, M.S.Y., Bell, G.L., Caldwell, M.W., 1999. The origin of snake feeding. Nature 400, 655-659.

Lee, S.H., Fu, K.K., Hui, J.N., Richman, J.M., 2001. Noggin and retinoic acid transform the identity of avian facial prominences. Nature 414, 909-912.

Lee, W., Leddy, H.A., Chen, Y., Lee, S.H., Zelenski, N.A., McNulty, A.L., Wu, J., Beicker, K.N., Coles, J., Zauscher, S., Grandl, J., Sachs, F., Guilak, F., Liedtke, W.B., 2014. Synergy between Piezo1 and Piezo2 channels confers high-strain mechanosensitivity to articular cartilage. Proc Natl Acad Sci U S A 111, E5114-5122.

LeResche, L., 1997. Epidemiology of temporomandibular disorders: implications for the investigation of etiologic factors. Critical reviews in oral biology and medicine : an official publication of the American Association of Oral Biologists 8, 291-305.

Lescroart, F., Hamou, W., Francou, A., Theveniau-Ruissy, M., Kelly, R.G., Buckingham, M., 2015. Clonal analysis reveals a common origin between nonsomite-derived neck muscles and heart myocardium. P Natl Acad Sci USA 112, 1446-1451.

Li, K.W., Lindsey, D.P., Wagner, D.R., Giori, N.J., Schurman, D.J., Goodman, S.B., Smith, R.L., Carter, D.R., Beaupre, G.S., 2006. Gene regulation ex vivo within a wrap-around tendon. Tissue Eng 12, 2611-2618.

Linde-Medina, M., Hallgrimsson, B., Marcucio, R., 2016. Beyond cell proliferation in avian facial morphogenesis. Dev Dyn 245, 190-196.

Liu, F., Steinkeler, A., 2013. Epidemiology, diagnosis, and treatment of temporomandibular disorders. Dental clinics of North America 57, 465-479.

Liu, J.K., Ghattas, I., Liu, S., Chen, S., Rubenstein, J.L., 1997. Dlx genes encode DNA-binding proteins that are expressed in an overlapping and sequential pattern during basal ganglia differentiation. Dev Dynam 210, 498-512.

Livak, K.J., Schmittgen, T.D., 2001. Analysis of relative gene expression data using real-time quantitative PCR and the 2(-Delta Delta C(T)) Method. Methods 25, 402-408.

Lu, H.H., Thomopoulos, S., 2013. Functional Attachment of Soft Tissues to Bone: Development, Healing, and Tissue Engineering. Annu Rev Biomed Eng 15, 201-226.

Lucas, A.M., Stettenheim, P.R., 1972. Avian Anatomy: Integument. United States Department of Agriculture, Washington, D.C.

Luo, R., Gao, J., Wehrle-Haller, B., Henion, P.D., 2003. Molecular identification of distinct neurogenic and melanogenic neural crest sublineages. Development 130, 321-330.

Maeda, T., Sakabe, T., Sunaga, A., Sakai, K., Rivera, A.L., Keene, D.R., Sasaki, T., Stavnezer, E., Iannotti, J., Schweitzer, R., Ilic, D., Baskaran, H., Sakai, T., 2011. Conversion of Mechanical Force into TGF-beta-Mediated Biochemical Signals. Curr Biol 21, 933-941.

Maier, W., 1989. *Ala temporalis* and alisphenoid in therian mammals, in: Splechtna, H., Hilgers, H. (Eds.), Trends in Vertebrate Morphology: Proceedings of the 2nd International Symposium on Vertebrate Morphology (1986). Gustav Fischer Verlag, Vienna, pp. 396-400.

Mallarino, R., Grant, P.R., Grant, B.R., Herrel, A., Kuo, W.P., Abzhanov, A., 2011. Two developmental modules establish 3D beak-shape variation in Darwin's finches. Proc Natl Acad Sci U S A 108, 4057-4062.

Mammoto, T., Ingber, D.E., 2010. Mechanical control of tissue and organ development. Development 137, 1407-1420.

Mancilla, E.E., Galindo, M., Fertilio, B., Herrera, M., Salas, K., Gatica, H., Goecke, A., 2007. L-type calcium channels in growth plate chondrocytes participate in endochondral ossification. J Cell Biochem 101, 389-398.

Mathew, S.J., Hansen, J.M., Merrell, A.J., Murphy, M.M., Lawson, J.A., Hutcheson, D.A., Hansen, M.S., Angus-Hill, M., Kardon, G., 2011. Connective tissue fibroblasts and Tcf4 regulate myogenesis. Development 138, 371-384.

Matthews, B.D., Overby, D.R., Mannix, R., Ingber, D.E., 2006. Cellular adaptation to mechanical stress: role of integrins, Rho, cytoskeletal tension and mechanosensitive ion channels. J Cell Sci 119, 508-518.

Matyas, J.R., Anton, M.G., Shrive, N.G., Frank, C.B., 1995. Stress Governs Tissue Phenotype at the Femoral Insertion of the Rabbit Mcl. J Biomech 28, 147-157.

McBeath, R., Pirone, D.M., Nelson, C.M., Bhadriraju, K., Chen, C.S., 2004. Cell shape, cytoskeletal tension, and RhoA regulate stem cell lineage commitment. Developmental Cell 6, 483-495.

McBratney-Owen, B., Iseki, S., Bamforth, S.D., Olsen, B.R., Morriss-Kay, G.M., 2008. Development and tissue origins of the mammalian cranial base. Dev Biol 322, 121-132.

McLennan, R., Schumacher, L.J., Morrison, J.A., Teddy, J.M., Ridenour, D.A., Box, A.C., Semerad, C.L., Li, H., McDowell, W., Kay, D., Maini, P.K., Baker, R.E., Kulesa, P.M., 2015a. Neural crest migration is driven by a few trailblazer cells with a unique molecular signature narrowly confined to the invasive front. Development 142, 2014-2025.

McLennan, R., Schumacher, L.J., Morrison, J.A., Teddy, J.M., Ridenour, D.A., Box, A.C., Semerad, C.L., Li, H., McDowell, W., Kay, D., Maini, P.K., Baker, R.E., Kulesa, P.M., 2015b. VEGF signals induce trailblazer cell identity that drives neural crest migration. Dev Biol 407, 12-25.

McLeod, W.M., 1964. Avian anatomy. Burgess Pub. Co., Minneapolis,.

Merida-Velasco, J.R., Rodriguez-Vazquez, J.F., De la Cuadra Blanco, C., Campos-Lopez, R., Sanchez, M., Merida-Velasco, J.A., 2009. Development of the mandibular condylar cartilage in human specimens of 10-15 weeks' gestation. J Anat 214, 56-64.

Merida-Velasco, J.R., Rodriguez-Vazquez, J.F., Merida-Velasco, J.A., Sanchez-Montesinos, I., Espin-Ferra, J., Jimenez-Collado, J., 1999. Development of the human temporomandibular joint. The Anatomical record 255, 20-33.

Merrill, A.E., Eames, B.F., Weston, S.J., Heath, T., Schneider, R.A., 2008. Mesenchyme-dependent BMP signaling directs the timing of mandibular osteogenesis. Development 135, 1223-1234.

Minoux, M., Rijli, F.M., 2010. Molecular mechanisms of cranial neural crest cell migration and patterning in craniofacial development. Development 137, 2605-2621.

Mitsiadis, T.A., Caton, J., Cobourne, M., 2006. Waking-up the sleeping beauty: recovery of the ancestral bird odontogenic program. J Exp Zoolog B Mol Dev Evol 306, 227-233.

Mitsiadis, T.A., Cheraud, Y., Sharpe, P., Fontaine-Perus, J., 2003. Development of teeth in chick embryos after mouse neural crest transplantations. Proc Natl Acad Sci U S A 100, 6541-6545.

Miyashita, T., 2016. Fishing for jaws in early vertebrate evolution: a new hypothesis of mandibular confinement. Biol Rev 91, 611-657.

Mobasheri, A., Lewis, R., Maxwell, J.E., Hill, C., Womack, M., Barrett-Jolley, R., 2010. Characterization of a stretch-activated potassium channel in chondrocytes. J Cell Physiol 223, 511-518.

Moore, W.J., 1973. An experimental study of the functional components of growth in the rat mandible. Acta anatomica 85, 378-385.

Moore, W.J., 1981. The Mammalian Skull. Cambridge University Press, Cambridge.

Mootoosamy, R.C., Dietrich, S., 2002. Distinct regulatory cascades for head and trunk myogenesis. Development 129, 573-583.

Morriss-Kay, G.M., 2001. Derivation of the mammalian skull vault. J Anat 199, 143-151.

Moss, M.L., Meehan, M.A., 1970. Functional cranial analysis of the coronoid process in the rat. Acta anatomica 77, 11-24.

Mouw, J.K., Imler, S.M., Levenston, M.E., 2007. Ion-channel regulation of chondrocyte matrix synthesis in 3D culture under static and dynamic compression. Biomech Model Mechan 6, 33-41.

Muller, G.B., 2003. Embryonic motility: environmental influences and evolutionary innovation. Evolution & Development 5, 56-60.

Murakami, S., Kan, M., McKeehan, W.L., de Crombrugghe, B., 2000. Up-regulation of the chondrogenic Sox9 gene by fibroblast growth factors is mediated by the mitogen-activated protein kinase pathway. P Natl Acad Sci USA 97, 1113-1118.

Muramatsu, S., Wakabayashi, M., Ohno, T., Amano, K., Ooishi, R., Sugahara, T., Shiojiri, S., Tashiro, K., Suzuki, Y., Nishimura, R., Kuhara, S., Sugano, S., Yoneda, T., Matsuda, A., 2007. Functional gene screening system identified TRPV4 as a regulator of chondrogenic differentiation. J Biol Chem 282, 32158-32167.

Murchison, N.D., Price, B.A., Conner, D.A., Keene, D.R., Olson, E.N., Tabin, C.J., Schweitzer, R., 2007. Regulation of tendon differentiation by scleraxis

distinguishes force-transmitting tendons from muscle-anchoring tendons. Development 134, 2697-2708.

Murray, P., 1963. Adventitious (Secondary) cartilage in the chick, and the development of certain bones and articulation in the chick skull. Australian Journal of Zoology 11, 368-430.

Murray, P., Smiles, M., 1965. Factors in the evocation of adventitious (secondary) cartilage in the chick embryo. Australian Journal of Zoology 13, 351-382.

Murray, P.D.F., Drachman, D.B., 1969. Role of Movement in Development of Joints and Related Structures - Head and Neck in Chick Embryo. J Embryol Exp Morph 22, 349-&.

Murray, P.D.F., Hall, B.K., 1966. Adventitious Cartilages in Embryonic and Post-Hatching Chick and Effect of Paralysis on Its Development. Journal of Anatomy 100, 937-&.

Naderi, J., Bernreuther, C., Grabinski, N., Putman, C.T., Henkel, B., Bell, G., Glatzel, M., Sultan, K.R., 2009. Plasminogen activator inhibitor type 1 up-regulation is associated with skeletal muscle atrophy and associated fibrosis. Am J Pathol 175, 763-771.

Nakase, J., Kitaoka, K., Matsumoto, K., Tomita, K., 2010. Facilitated tendon-bone healing by local delivery of recombinant hepatocyte growth factor in rabbits. Arthroscopy : the journal of arthroscopic & related surgery : official publication of the Arthroscopy Association of North America and the International Arthroscopy Association 26, 84-90.

Naples, V.L., 1999. Morphology, evolution and function of feeding in the giant anteater (Myrmecophaga tridactyla). J Zool 249, 19-41.

Nesti, L.J., Caterson, E.J., Li, W.J., Chang, R., McCann, T.D., Hoek, J.B., Tuan, R.S., 2007. TGF-beta1 calcium signaling in osteoblasts. J Cell Biochem 101, 348-359.

Nesti, L.J., Caterson, E.J., Wang, M., Chang, R., Chapovsky, F., Hoek, J.B., Tuan, R.S., 2002. TGF-beta1 calcium signaling increases alpha5 integrin expression in osteoblasts. J Orthop Res 20, 1042-1049.

Nguyen, J., Tang, S.Y., Nguyen, D., Alliston, T., 2013. Load Regulates Bone Formation and Sclerostin Expression through a TGF beta-Dependent Mechanism. Plos One 8.

Niswander, L., Tickle, C., Vogel, A., Booth, I., Martin, G.R., 1993. FGF-4 replaces the apical ectodermal ridge and directs outgrowth and patterning of the limb. Cell 75, 579-587.

Noden, D., Schneider, R.A., 2006. Neural Crest Cells and the Community of Plan for Craniofacial Development: Historical Debates and Current Perspectives, in: Saint-Jeannet, J.-P. (Ed.), Neural crest induction and differentiation. Landes Bioscience, Georgetown, Tex., pp. 1-23.

Noden, D.M., 1978. The control of avian cephalic neural crest cytodifferentiation. I. Skeletal and connective tissues. Developmental Biology 67, 296-312.

Noden, D.M., 1983a. The embryonic origins of avian cephalic and cervical muscles and associated connective tissues. The American journal of anatomy 168, 257-276.

Noden, D.M., 1983b. The Role of the Neural Crest in Patterning of Avian Cranial Skeletal, Connective, and Muscle Tissues. Developmental Biology 96, 144-165.

Noden, D.M., 1988. Interactions and fates of avian craniofacial mesenchyme. Development 103, 121-140.

Noden, D.M., 1991. Vertebrate Craniofacial Development: The Relation between Ontogenetic Process and Morphological Outcome. Brain, Behavior, and Evolution 38, 190-225.

Noden, D.M., Francis-West, P., 2006. The differentiation and morphogenesis of craniofacial muscles. Dev Dyn 235, 1194-1218.

Noden, D.M., Marcucio, R., Borycki, A.G., Emerson, C.P., Jr., 1999. Differentiation of avian craniofacial muscles: I. Patterns of early regulatory gene expression and myosin heavy chain synthesis. Dev Dyn 216, 96-112.

Noden, D.M., Trainor, P.A., 2005. Relations and interactions between cranial mesoderm and neural crest populations. J Anat 207, 575-601.

Northcutt, R.G., 2005. The new head hypothesis revisited. Journal of Experimental Zoology Part B: Molecular and Developmental Evolution 304B, 274-297.

Northcutt, R.G., Gans, C., 1983. The Genesis of Neural Crest and Epidermal Placodes. Quarterly Review of Biology 58, 1-27.

O'Conor, C.J., Leddy, H.A., Benefield, H.C., Liedtke, W.B., Guilak, F., 2014. TRPV4-mediated mechanotransduction regulates the metabolic response of chondrocytes to dynamic loading. Proc Natl Acad Sci U S A 111, 1316-1321.

Oka, K., Oka, S., Hosokawa, R., Bringas, P., Brockhoff, H.C., Nonaka, K., Chai, Y., 2008. TGF-beta mediated Dlx5 signaling plays a crucial role in osteo-chondroprogenitor cell lineage determination during mandible development. Developmental Biology 321, 303-309.

Oka, K., Oka, S., Sasaki, T., Ito, Y., Bringas, P., Nonaka, K., Chai, Y., 2007. The role of TGF-beta signaling in regulating chondrogenesis and osteogenesis during mandibular development. Developmental Biology 303, 391-404.

Olesnicky Killian, E.C., Birkholz, D.A., Artinger, K.B., 2009. A role for chemokine signaling in neural crest cell migration and craniofacial development. Dev Biol 333, 161-172.

Olsson, L., Falck, P., Lopez, K., Cobb, J., Hanken, J., 2001. Cranial neural crest cells contribute to connective tissue in cranial muscles in the anuran amphibian, Bombina orientalis. Dev Biol 237, 354-367.

Oppenheim, R.W., 1966. Amniotic Contraction and Embryonic Motility in Chick Embryo. Science 152, 528-&.

Oppenheim, R.W., 1968. Light Responsivity in Chick and Duck Embryos Just Prior to Hatching. Animal Behaviour 16, 276-&.

Oppenheim, R.W., 1970. Some Aspects of Embryonic Behaviour in Duck (Anas-Platyrhynchos). Animal Behaviour 18, 335-&.

Ornitz, D.M., Marie, P.J., 2015. Fibroblast growth factor signaling in skeletal development and disease. Genes Dev 29, 1463-1486.

Osborne, A.C., Lamb, K.J., Lewthwaite, J.C., Dowthwaite, G.P., Pitsillides, A.A., 2002. Short-term rigid and flaccid paralyses diminish growth of embryonic chick limbs and abrogate joint cavity formation but differentially preserve pre-cavitated joints. Journal of musculoskeletal & neuronal interactions 2, 448-456.

Owen, R., 1843. Lectures on the Comparative Anatomy and Physiology of the Invertebrate Animals: Delivered at the Royal College of Surgeons. Longman, Brown, Green, and Longmans, London.

Owen, R., 1848. On the Archetype and Homologies of the Vertebrate Skeleton. John Van Voorst, Paternoster Row, London.

Park, J., Gebhardt, M., Golovchenko, S., Perez-Branguli, F., Hattori, T., Hartmann, C., Zhou, X., deCrombrugghe, B., Stock, M., Schneider, H., von der Mark, K., 2015. Dual pathways to endochondral osteoblasts: a novel chondrocyte-derived osteoprogenitor cell identified in hypertrophic cartilage. Biol Open 4, 608-621.

Parsons, T.E., Schmidt, E.J., Boughner, J.C., Jamniczky, H.A., Marcucio, R.S., Hallgrimsson, B., 2011. Epigenetic Integration of the Developing Brain and Face. Dev Dynam 240, 2233-2244.

Patterson, C., 1977. Cartilage bones, dermal bones, and membrane bones, or the exoskeleton versus the endoskeleton, in: Andrews, S., Miles, R., Walker, A. (Eds.), Problems in Vertebrate Evolution. Academic Press, London, pp. 77-121.

Persson, M., 1983. The Role of Movements in the Development of Sutural and Diarthrodial Joints Tested by Long-Term Paralysis of Chick-Embryos. Journal of Anatomy 137, 591-599.

Pitsillides, A.A., 2006. Early effects of embryonic movement: 'a shot out of the dark'. Journal of Anatomy 208, 417-431.

Poiraudeau, S., Lieberherr, M., Kergosie, N., Corvol, M.T., 1997. Different mechanisms are involved in intracellular calcium increase by insulin-like growth factors 1 and 2 in articular chondrocytes: voltage-gated calcium channels, and/or phospholipase C coupled to a pertussis-sensitive G-protein. J Cell Biochem 64, 414-422.

Pollard, A.S., McGonnell, I.M., Pitsillides, A.A., 2014. Mechanoadaptation of developing limbs: shaking a leg. Journal of Anatomy 224, 615-623.

Presley, R., 1981. Alisphenoid equivalents in placentals, marsupials, monotremes and fossils. Nature 294, 668-670.

Presley, R., Steel, F.L.D., 1976. On the homology of the alisphenoid. Journal of Anatomy 121, 441-459.

Presnell, J.K., Schreibman, M.P., 1997. Humason's Animal Tissue Techniques. Johns Hopkins University Press.

Pruitt, B.L., Dunn, A.R., Weis, W.I., Nelson, W.J., 2014. Mechano-Transduction: From Molecules to Tissues. Plos Biol 12.

Pryce, B.A., Watson, S.S., Murchison, N.D., Staverosky, J.A., Duker, N., Schweitzer, R., 2009. Recruitment and maintenance of tendon progenitors by TGF beta signaling are essential for tendon formation. Development 136, 1351-1361.

Qiu, M., Bulfone, A., Ghattas, I., Meneses, J.J., Christensen, L., Sharpe, P.T., Presley, R., Pedersen, R.A., Rubenstein, J.L., 1997. Role of the Dlx homeobox genes in proximodistal patterning of the branchial arches: mutations of Dlx-1, Dlx-2, and Dlx-1 and -2 alter morphogenesis of proximal skeletal and soft tissue structures derived from the first and second arches. Developmental Biology 185, 165-184.

Qiu, M., Bulfone, A., Martinez, S., Meneses, J.J., Shimamura, K., Pedersen, R.A., Rubenstein, J.L., 1995. Null mutation of *Dlx-2* results in abnormal morphogenesis of proximal first and second branchial arch derivatives and abnormal differentiation in the forebrain. Genes & Development 9, 2523-2538.

Quinn, T.P., Schlueter, M., Soifer, S.J., Gutierrez, J.A., 2002. Mechanotransduction in the lung - Cyclic mechanical stretch induces VEGF and FGF-2 expression in pulmonary vascular smooth muscle cells. Am J Physiol-Lung C 282, L897-L903.

Radlanski, R.J., Renz, H., Lajvardi, S., Schneider, R.A., 2004. Bone remodeling during prenatal morphogenesis of the human mental foramen. Eur J Oral Sci 112, 301-310.

Raizman, I., De Croos, J.N., Pilliar, R., Kandel, R.A., 2010. Calcium regulates cyclic compression-induced early changes in chondrocytes during in vitro cartilage tissue formation. Cell calcium 48, 232-242.

Ramage, L., Nuki, G., Salter, D.M., 2009. Signalling cascades in mechanotransduction: cell-matrix interactions and mechanical loading. Scandinavian Journal of Medicine & Science in Sports 19, 457-469.

Richman, J.M., Lee, S.H., 2003. About face: signals and genes controlling jaw patterning and identity in vertebrates. Bioessays 25, 554-568.

Rinon, A., Lazar, S., Marshall, H., Buchmann-Moller, S., Neufeld, A., Elhanany-Tamir, H., Taketo, M.M., Sommer, L., Krumlauf, R., Tzahor, E., 2007. Cranial neural crest cells regulate head muscle patterning and differentiation during vertebrate embryogenesis. Development 134, 3065-3075.

Roach, H.I., 1992. Transdifferentiation of Hypertrophic Chondrocytes into Cells Capable of Producing a Mineralized Bone-Matrix. Bone Miner 19, 1-20.

Roach, H.I., 1997. New aspects of endochondral ossification in the chick: Chondrocyte apoptosis, bone formation by former chondrocytes, and acid phosphatase activity in the endochondral bone matrix. J Bone Miner Res 12, 795-805.

Robbins, J.R., Evanko, S.P., Vogel, K.G., 1997. Mechanical loading and TGF-beta regulate proteoglycan synthesis in tendon. Arch Biochem Biophys 342, 203-211.

Roberts, S.R., Knight, M.M., Lee, D.A., Bader, D.L., 2001. Mechanical compression influences intracellular Ca(2+) signaling in chondrocytes seeded in agarose constructs. J Appl Physiol 90, 1385-1391.

Robling, A.G., Kang, K.S., Bullock, W.A., Foster, W.H., Murugesh, D., Loots, G.G., Genetos, D.C., 2016. Sost, independent of the non-coding enhancer ECR5, is required for bone mechanoadaptation. Bone 92, 180-188.

Robling, A.G., Niziolek, P.J., Baldridge, L.A., Condon, K.W., Allen, M.R., Alam, I., Mantila, S.M., Gluhak-Heinrich, J., Bellido, T.M., Harris, S.E., Turner, C.H., 2008. Mechanical stimulation of bone in vivo reduces osteocyte expression of Sost/sclerostin. J Biol Chem 283, 5866-5875.

Roddy, K.A., Prendergast, P.J., Murphy, P., 2011. Mechanical Influences on Morphogenesis of the Knee Joint Revealed through Morphological, Molecular and Computational Analysis of Immobilised Embryos. Plos One 6.

Rolfe, R.A., Nowlan, N.C., Kenny, E.M., Cormican, P., Morris, D.W., Prendergast, P.J., Kelly, D., Murphy, P., 2014. Identification of mechanosensitive genes during skeletal development: alteration of genes associated with cytoskeletal rearrangement and cell signalling pathways. BMC Genomics 15, 48.

Romer, A.S., 1956. Osteology of the Reptiles. University of Chicago Press, Chicago.

Rot-Nikcevic, I., Downing, K.J., Hall, B.K., Kablar, B., 2007. Development of the mouse mandibles and clavicles in the absence of skeletal myogenesis. Histology and histopathology 22, 51-60.

Roycroft, A., Mayor, R., 2016. Molecular basis of contact inhibition of locomotion. Cell Mol Life Sci 73, 1119-1130.

Rundle, C.H., Chen, S.T., Coen, M.J., Wergedal, J.E., Stiffel, V., Lau, K.H., 2014. Direct lentiviral-cyclooxygenase 2 application to the tendon-bone interface promotes osteointegration and enhances return of the pull-out tensile strength of the tendon graft in a rat model of biceps tenodesis. PLoS One 9, e98004.

Russell, E.S., 1916. Form and Function: A Contribution to the History of Animal Morphology. John Murray Publishers Ltd., London.

Ryu, Y.U., Bradley, N.S., 2009. Precocious Locomotor Behavior Begins in the Egg: Development of Leg Muscle Patterns for Stepping in the Chick. Plos One 4.

Sadaghiani, B., Thiebaud, C.H., 1987. Neural crest development in the Xenopus laevis embryo, studied by interspecific transplantation and scanning electron microscopy. Dev Biol 124, 91-110.

Saint-Jeannet, J.-P., 2006. Neural crest induction and differentiation. Springer Science+Business Media ;
Landes Bioscience/Eurekah.com, New York, N.Y.
Georgetown, Tex.

Sambasivan, R., Gayraud-Morel, B., Dumas, G., Cimper, C., Paisant, S., Kelly, R.G., Tajbakhsh, S., 2009. Distinct regulatory cascades govern extraocular and pharyngeal arch muscle progenitor cell fates. Dev Cell 16, 810-821.

Sambasivan, R., Kuratani, S., Tajbakhsh, S., 2011. An eye on the head: the development and evolution of craniofacial muscles. Development 138, 2401-2415.

Sanchez-Villagra, M.R., Geiger, M., Schneider, R.A., 2016. The taming of the neural crest: a developmental perspective on the origins of morphological covariation in domesticated mammals. R Soc Open Sci 3, 160107.

Sánchez-Villagra, M.R., Smith, K.K., 1997. Diversity and Evolution of the Marsupial Mandibular Angular Process. Journal of Mammalian Evolution 4, 119-144.

Sanford, L.P., Ormsby, I., GittenbergerdeGroot, A.C., Sariola, H., Friedman, R., Boivin, G.P., Cardell, E.L., Doetschman, T., 1997. TGF beta 2 knockout mice have multiple developmental defects that are nonoverlapping with other TGF beta knockout phenotypes. Development 124, 2659-2670.

Sasaki, K., Kuroda, R., Ishida, K., Kubo, S., Matsumoto, T., Mifune, Y., Kinoshita, K., Tei, K., Akisue, T., Tabata, Y., Kurosaka, M., 2008. Enhancement of tendon-bone osteointegration of anterior cruciate ligament graft using granulocyte colony-stimulating factor. The American journal of sports medicine 36, 1519-1527.

Sato, T., Kurihara, Y., Asai, R., Kawamura, Y., Tonami, K., Uchijima, Y., Heude, E., Ekker, M., Levi, G., Kurihara, H., 2008. An endothelin-1 switch specifies maxillomandibular identity. Proc Natl Acad Sci U S A 105, 18806-18811.

Scammell, B.E., Roach, H.I., 1996. A new role for the chondrocyte in fracture repair: Endochondral ossification includes direct bone formation by former chondrocytes. J Bone Miner Res 11, 737-745.

Schneider, R.A., 1999. Neural crest can form cartilages normally derived from mesoderm during development of the avian head skeleton. Developmental Biology 208, 441-455.

Schneider, R.A., 2005. Developmental mechanisms facilitating the evolution of bills and quills. J Anat 207, 563-573.

Schneider, R.A., 2007. How to tweak a beak: molecular techniques for studying the evolution of size and shape in Darwin's finches and other birds. Bioessays 29, 1-6.

Schneider, R.A., 2015. Regulation of Jaw Length During Development, Disease, and Evolution. Curr Top Dev Biol 115, 271-298.

Schneider, R.A., Helms, J.A., 2003. The cellular and molecular origins of beak morphology. Science 299, 565-568.

Schneider, R.A., Hu, D., Helms, J.A., 1999. From head to toe: conservation of molecular signals regulating limb and craniofacial morphogenesis. Cell Tissue Res 296, 103-109.

Schneider, R.A., Hu, D., Rubenstein, J.L., Maden, M., Helms, J.A., 2001. Local retinoid signaling coordinates forebrain and facial morphogenesis by maintaining FGF8 and SHH. Development 128, 2755-2767.

Schnell, N.K., Johnson, G.D., 2017. Evolution of a Functional Head Joint in Deep-Sea Fishes (Stomiidae). PLoS One 12, e0170224.

Schoenebeck, J.J., Hutchinson, S.A., Byers, A., Beale, H.C., Carrington, B., Faden, D.L., Rimbault, M., Decker, B., Kidd, J.M., Sood, R., Boyko, A.R., Fondon, J.W.,

3rd, Wayne, R.K., Bustamante, C.D., Ciruna, B., Ostrander, E.A., 2012. Variation of BMP3 contributes to dog breed skull diversity. PLoS Genet 8, e1002849.

Schoenebeck, J.J., Ostrander, E.A., 2013. The genetics of canine skull shape variation. Genetics 193, 317-325.

Schultze, H., 1993. Patterns of Diversity in the Skulls of Jawed Fishes, in: Hanken, J., Hall, B.K. (Eds.), The Skull. University of Chicago Press, Chicago, pp. 189-254.

Schwartz, A., Thomopoulos, S., 2015. Tissue Engineering the Tendon Enthesis: Lessons from Development. Tissue Eng Pt A 21, S34-S34.

Schwartz, A.G., Pasteris, J.D., Genin, G.M., Daulton, T.L., Thomopoulos, S., 2012. Mineral distributions at the developing tendon enthesis. PLoS One 7, e48630.

Schweitzer, R., Chyung, J.H., Murtaugh, L.C., Brent, A.E., Rosen, V., Olson, E.N., Lassar, A., Tabin, C.J., 2001. Analysis of the tendon cell fate using Scleraxis, a specific marker for tendons and ligaments. Development 128, 3855-3866.

Schweitzer, R., Zelzer, E., Volk, T., 2010. Connecting muscles to tendons: tendons and musculoskeletal development in flies and vertebrates (vol 137, pg 2807, 2010). Development 137, Ee47-Ee47.

Selleck, M.A., Bronner-Fraser, M., 1996. The genesis of avian neural crest cells: a classic embryonic induction. Proceedings of the National Academy of Sciences of the United States of America 93, 9352-9357.

Selleck, M.A.J., Bronner-Fraser, M., 1995. Origins of the avian neural crest: The role of neural plate-epidermal interactions. Development 121, 525-538.

Shakibaei, M., Mobasheri, A., 2003. Beta1-integrins co-localize with Na, K-ATPase, epithelial sodium channels (ENaC) and voltage activated calcium channels (VACC) in mechanoreceptor complexes of mouse limb-bud chondrocytes. Histology and histopathology 18, 343-351.

Sharir, A., Stern, T., Rot, C., Shahar, R., Zelzer, E., 2011. Muscle force regulates bone shaping for optimal load-bearing capacity during embryogenesis. Development 138, 3247-3259.

Sheehan-Rooney, K., Swartz, M.E., Lovely, C.B., Dixon, M.J., Eberhart, J.K., 2013. Bmp and Shh signaling mediate the expression of satb2 in the pharyngeal arches. PLoS One 8, e59533.

Shellard, A., Mayor, R., 2016. Chemotaxis during neural crest migration. Semin Cell Dev Biol 55, 111-118.

Shi, M., Zhu, J., Wang, R., Chen, X., Mi, L., Walz, T., Springer, T.A., 2011. Latent TGF-beta structure and activation. Nature 474, 343-349.

Shibata, S., Sakamoto, Y., Baba, O., Qin, C., Murakami, G., Cho, B.H., 2013. An immunohistochemical study of matrix proteins in the craniofacial cartilage in midterm human fetuses. European journal of histochemistry : EJH 57, e39.

Shibata, S., Suda, N., Fukada, K., Ohyama, K., Yamashita, Y., Hammond, V.E., 2003. Mandibular coronoid process in parathyroid hormone-related protein-deficient mice shows ectopic cartilage formation accompanied by abnormal bone modeling. Anatomy and embryology 207, 35-44.

Shigetani, Y., Nobusada, Y., Kuratani, S., 2000. Ectodermally derived FGF8 defines the maxillomandibular region in the early chick embryo: Epithelial-mesenchymal interactions in the specification of the craniofacial ectomesenchyme. Developmental Biology 228, 73-85.

Shigetani, Y., Sugahara, F., Kawakami, Y., Murakami, Y., Hirano, S., Kuratani, S., 2002. Heterotopic shift of epithelial-mesenchymal interactions in vertebrate jaw evolution. Science 296, 1316-1319.

Shih, H.P., Gross, M.K., Kioussi, C., 2007. Cranial muscle defects of Pitx2 mutants result from specification defects in the first branchial arch. Proc Natl Acad Sci U S A 104, 5907-5912.

Shkoukani, M.A., Chen, M., Vong, A., 2013. Cleft lip - a comprehensive review. Front Pediatr 1, 53.

Shufeldt, R.W., 1909. Osteology of birds. University of the State of New York, Albany,.

Shwartz, Y., Blitz, E., Zelzer, E., 2013. One load to rule them all: mechanical control of the musculoskeletal system in development and aging. Differentiation 86, 104-111.

Shwartz, Y., Farkas, Z., Stern, T., Aszodi, A., Zelzer, E., 2012. Muscle contraction controls skeletal morphogenesis through regulation of chondrocyte convergent extension. Dev Biol 370, 154-163.

Sieber-Blum, M., 1989. Commitment of neural crest cells to the sensory neuron lineage. Science 243, 1608-1611.

Slijper, E.J., 1942. Biologic‐anatomical investigations on the bipedal gait and upright posture in mammals, with special reference to a little goat, born without forelegs. I. Proceedings of the Koninklijke Nederlandsche Akademie van Wetenschappen 45, 288-295.

Smith, K.K., 1993. The Form of the Feeding Apparatus in Terrestrial Vertebrates: Studies of Adaptation and Constraint, in: Hanken, J., Hall, B.K. (Eds.), The Skull. University of Chicago Press, Chicago, pp. 150-196.

Smith, K.K., Schneider, R.A., 1998. Have gene knockouts caused evolutionary reversals in the mammalian first arch? Bioessays 20, 245-255.

Smith, L., Xia, Y.N., Galatz, L.M., Genin, G.M., Thomopoulos, S., 2012. Tissue-Engineering Strategies for the Tendon/Ligament-to-Bone Insertion. Connect Tissue Res 53, 95-105.

Smith, T.G., Sweetman, D., Patterson, M., Keyse, S.M., Munsterberg, A., 2005. Feedback interactions between MKP3 and ERK MAP kinase control scleraxis expression and the specification of rib progenitors in the developing chick somite. Development 132, 1305-1314.

Snippert, H.J., van der Flier, L.G., Sato, T., van Es, J.H., van den Born, M., Kroon-Veenboer, C., Barker, N., Klein, A.M., van Rheenen, J., Simons, B.D., Clevers, H., 2010. Intestinal crypt homeostasis results from neutral competition between symmetrically dividing Lgr5 stem cells. Cell 143, 134-144.

Solem, R.C., Eames, B.F., Tokita, M., Schneider, R.A., 2011. Mesenchymal and mechanical mechanisms of secondary cartilage induction. Developmental Biology 356, 28-39.

Song, Y., Hui, J.N., Fu, K.K., Richman, J.M., 2004. Control of retinoic acid synthesis and FGF expression in the nasal pit is required to pattern the craniofacial skeleton. Dev Biol 276, 313-329.

Soni, N.N., Malloy, R.B., 1974. Effect of removal of the temporal muscle on the coronoid process in guinea pigs: quantitative triple fluorochrome study. Journal of dental research 53, 474-480.

Spyropoulos, M.N., 1977. The morphogenetic relationship of the temporal muscle to the coronoid process in human embryos and fetuses. The American journal of anatomy 150, 395-409.

Stemple, D.L., Anderson, D.J., 1992. Isolation of a stem cell for neurons and glia from the mammalian neural crest. Cell 71, 973-985.

Stutzmann, J., Petrovic, A., 1975. Nature and evolutive aptitudes of cells of the mitotic compartment of the secondary cartilages of the mandible and maxilla of the young rat. Experience with cytotypic culture and homotransplantation. Bulletin de l'Association des anatomistes 59, 523-534.

Subramanian, A., Schilling, T.F., 2015. Tendon development and musculoskeletal assembly: emerging roles for the extracellular matrix. Development 142, 4191-4204.

Sugimoto, T., Yoshino, M., Nagao, M., Ishii, S., Yabu, H., 1996. Voltage-gated ionic channels in cultured rabbit articular chondrocytes. Comp Biochem Physiol C Pharmacol Toxicol Endocrinol 115, 223-232.

Sugimoto, Y., Takimoto, A., Akiyama, H., Kist, R., Scherer, G., Nakamura, T., Hiraki, Y., Shukunami, C., 2013. Scx+/Sox9+ progenitors contribute to the establishment of the junction between cartilage and tendon/ligament. Development 140, 2280-2288.

Sun, L., Tran, N., Liang, C., Tang, F., Rice, A., Schreck, R., Waltz, K., Shawver, L.K., McMahon, G., Tang, C., 1999. Design, synthesis, and evaluations of substituted 3-[(3- or 4-carboxyethylpyrrol-2-yl)methylidenyl]indolin-2-ones as inhibitors of VEGF, FGF, and PDGF receptor tyrosine kinases. J Med Chem 42, 5120-5130.

Sun, L., Tran, N., Tang, F., App, H., Hirth, P., McMahon, G., Tang, C., 1998. Synthesis and biological evaluations of 3-substituted indolin-2-ones: a novel class of tyrosine kinase inhibitors that exhibit selectivity toward particular receptor tyrosine kinases. J Med Chem 41, 2588-2603.

Szabo-Rogers, H.L., Smithers, L.E., Yakob, W., Liu, K.J., 2010. New directions in craniofacial morphogenesis. Dev Biol 341, 84-94.

Tajbakhsh, S., Rocancourt, D., Cossu, G., Buckingham, M., 1997. Redefining the genetic hierarchies controlling skeletal myogenesis: Pax-3 and Myf-5 act upstream of MyoD. Cell 89, 127-138.

Talbot, J.C., Johnson, S.L., Kimmel, C.B., 2010. hand2 and Dlx genes specify dorsal, intermediate and ventral domains within zebrafish pharyngeal arches. Development 137, 2507-2517.

Tanck, E., Blankevoort, L., Haaijman, A., Burger, E.H., Huiskes, R., 2000. Influence of muscular activity on local mineralization patterns in metatarsals of the embryonic mouse. J Orthop Res 18, 613-619.

Theveneau, E., Mayor, R., 2012. Neural crest delamination and migration: from epithelium-to-mesenchyme transition to collective cell migration. Dev Biol 366, 34-54.

Thomopoulos, S., Genin, G.M., Galatz, L.M., 2010. The development and morphogenesis of the tendon-to-bone insertion - what development can teach us about healing. Journal of musculoskeletal & neuronal interactions 10, 35-45.

Thomopoulos, S., Kim, H.M., Rothermich, S.Y., Biederstadt, C., Das, R., Galatz, L.M., 2007. Decreased muscle loading delays maturation of the tendon enthesis during postnatal development. Journal of Orthopaedic Research 25, 1154-1163.

Thompson, D.A.W., 1917. On growth and form. University press, Cambridge Eng.

Thorogood, P., 1983. Morphogenesis of Cartilage, in: Hall, B.K. (Ed.), Cartilage. Academic Press, Inc., pp. 223-253.

Tokita, M., 2003. The skull development of parrots with special reference to the emergence of a morphologically unique cranio-facial hinge. Zoolog Sci 20, 749-758.

Tokita, M., 2004. Morphogenesis of parrot jaw muscles: understanding the development of an evolutionary novelty. J Morphol 259, 69-81.

Tokita, M., Kiyoshi, T., Armstrong, K.N., 2007. Evolution of craniofacial novelty in parrots through developmental modularity and heterochrony. Evol Dev 9, 590-601.

Tokita, M., Nakayama, T., Schneider, R.A., Agata, K., 2013. Molecular and cellular changes associated with the evolution of novel jaw muscles in parrots. Proceedings. Biological sciences / The Royal Society 280, 20122319.

Tokita, M., Schneider, R.A., 2009. Developmental origins of species-specific muscle pattern. Dev Biol 331, 311-325.

Tosney, K.W., 1982. The segregation and early migration of cranial neural crest cells in the avian embryo. Developmental Biology 89, 13-24.

Trainor, P.A., Ariza-McNaughton, L., Krumlauf, R., 2002a. Role of the isthmus and FGFs in resolving the paradox of neural crest plasticity and prepatterning. Science 295, 1288-1291.

Trainor, P.A., Krumlauf, R., 2000. Patterning the cranial neural crest: hindbrain segmentation and Hox gene plasticity. Nat Rev Neurosci 1, 116-124.

Trainor, P.A., Krumlauf, R., 2001. Hox genes, neural crest cells and branchial arch patterning. Curr Opin Cell Biol 13, 698-705.

Trainor, P.A., Melton, K.R., Manzanares, M., 2003. Origins and plasticity of neural crest cells and their roles in jaw and craniofacial evolution. Int J Dev Biol 47, 541-553.

Trainor, P.A., Sobieszczuk, D., Wilkinson, D., Krumlauf, R., 2002b. Signalling between the hindbrain and paraxial tissues dictates neural crest migration pathways. Development 129, 433-442.

Trainor, P.A., Tam, P.P., 1995. Cranial paraxial mesoderm and neural crest cells of the mouse embryo: co-distribution in the craniofacial mesenchyme but distinct segregation in branchial arches. Development 121, 2569-2582.

Trainor, P.A., Tan, S.S., Tam, P.P.L., 1994. Cranial Paraxial Mesoderm - Regionalization of Cell Fate and Impact on Craniofacial Development in Mouse Embryos. Development 120, 2397-2408.

Tu, X.L., Rhee, Y., Condon, K.W., Bivi, N., Allen, M.R., Dwyer, D., Stolina, M., Turner, C.H., Robling, A.G., Plotkin, L.I., Bellido, T., 2012. Sost downregulation and local Wnt signaling are required for the osteogenic response to mechanical loading. Bone 50, 209-217.

Tucker, A.S., 2017. Major evolutionary transitions and innovations: the tympanic middle ear. Philos Trans R Soc Lond B Biol Sci 372.

Tucker, A.S., Lumsden, A., 2004. Neural crest cells provide species-specific patterning information in the developing branchial skeleton. Evol Dev 6, 32-40.

Tyler, M.S., Hall, B.K., 1977. Epithelial Influences on Skeletogenesis in Mandible of Embryonic Chick. Anat Rec 188, 229-239.

Tzahor, E., 2009. Heart and craniofacial muscle development: a new developmental theme of distinct myogenic fields. Dev Biol 327, 273-279.

Tzahor, E., Kempf, H., Mootoosamy, R.C., Poon, A.C., Abzhanov, A., Tabin, C.J., Dietrich, S., Lassar, A.B., 2003. Antagonists of Wnt and BMP signaling promote the formation of vertebrate head muscle. Genes Dev 17, 3087-3099.

Uchiyama, Y., Guttapalli, A., Gajghate, S., Mochida, J., Shapiro, I.M., Risbud, M.V., 2008. SMAD3 functions as a transcriptional repressor of acid-sensing ion channel 3 (ASIC3) in nucleus pulposus cells of the intervertebral disc. J Bone Miner Res 23, 1619-1628.

Van den Heuvel, W.F., 1992. Kinetics of the Skull in the Chicken (*Gallus Gallus Domesticus*). Netherlands Journal of Zoology 42, 561-582.

Varga, Z., Juhasz, T., Matta, C., Fodor, J., Katona, E., Bartok, A., Olah, T., Sebe, A., Csernoch, L., Panyi, G., Zakany, R., 2011. Switch of voltage-gated K+ channel expression in the plasma membrane of chondrogenic cells affects cytosolic Ca2+-oscillations and cartilage formation. PLoS One 6, e27957.

Vargervik, K., Miller, A.J., 1984. Neuromuscular patterns in hemifacial microsomia. Am J Orthod 86, 33-42.

Villanueva, J., Gonzalez, A., Cornejo, M., Nunez, C., Encina, S., 2006. Osteochondroma of the coronoid process. Medicina oral, patologia oral y cirugia bucal 11, E289-291.

Vincent, T., Hermansson, M., Bolton, M., Wait, R., Saklatvala, J., 2002. Basic FGF mediates an immediate response of articular cartilage to mechanical injury. P Natl Acad Sci USA 99, 8259-8264.

Vincent, T.L., McLean, C.J., Full, L.E., Peston, D., Saklatvala, J., 2007. FGF-2 is bound to perlecan in the pericellular matrix of articular cartilage, where it acts as a chondrocyte mechanotransducer. Osteoarthritis Cartilage 15, 752-763.

Vinkka, H., 1982. Secondary cartilages in the facial skeleton of the rat. Proceedings of the Finnish Dental Society. Suomen Hammaslaakariseuran toimituksia 78 Suppl 7, 1-137.

Wadhwa, S., Kapila, S., 2008. TMJ disorders: future innovations in diagnostics and therapeutics. Journal of dental education 72, 930-947.

Wagner, G., 1959. Untersuchungen an Bombinator-Triton-Chimaeren. Roux' Archiv für Entwicklungsmechanik der Organismen 151, 136-158.

Wang, C.J., Weng, L.H., Hsu, S.L., Sun, Y.C., Yang, Y.J., Chan, Y.S., Yang, Y.L., 2010. pCMV-BMP-2-transfected cell-mediated gene therapy in anterior cruciate ligament reconstruction in rabbits. Arthroscopy : the journal of arthroscopic & related surgery : official publication of the Arthroscopy Association of North America and the International Arthroscopy Association 26, 968-976.

Wang, N., Tytell, J.D., Ingber, D.E., 2009. Mechanotransduction at a distance: mechanically coupling the extracellular matrix with the nucleus. Nat Rev Mol Cell Bio 10, 75-82.

Washburn, S.L., 1947. The relation of the temporal muscle to the form of the skull. The Anatomical record 99, 239-248.

Wassersug, R.J., 1976. A procedure for differential staining of cartilage and bone in whole formalin-fixed vertebrates. Stain Technol 51, 131-134.

Wen, J., Tao, H., Lau, K., Liu, H., Simmons, C.A., Sun, Y., Hopyan, S., 2017. Cell and Tissue Scale Forces Coregulate Fgfr2-Dependent Tetrads and Rosettes in the Mouse Embryo. Biophys J 112, 2209-2218.

West-Eberhard, M.J., 2005. Developmental plasticity and the origin of species differences. P Natl Acad Sci USA 102, 6543-6549.

Wilkinson, D.G., Bhatt, S., Cook, M., Boncinelli, E., Krumlauf, R., 1989. Segmental expression of Hox-2 homoeobox-containing genes in the developing mouse hindbrain. Nature 341, 405-409.

Wipff, P.J., Rifkin, D.B., Meister, J.J., Hinz, B., 2007. Myofibroblast contraction activates latent TGF-beta1 from the extracellular matrix. J Cell Biol 179, 1311-1323.

Wu, K.C., Streicher, J., Lee, M.L., Hall, B.K., Muller, G.B., 2001. Role of motility in embryonic development I: Embryo movements and amnion contractions in the chick and the influence of illumination. Journal of Experimental Zoology 291, 186-194.

Wu, P., Jiang, T.X., Shen, J.Y., Widelitz, R.B., Chuong, C.M., 2006. Morphoregulation of avian beaks: comparative mapping of growth zone activities and morphological evolution. Dev Dyn 235, 1400-1412.

Wu, P., Jiang, T.X., Suksaweang, S., Widelitz, R.B., Chuong, C.M., 2004. Molecular shaping of the beak. Science 305, 1465-1466.

Wu, Q.Q., Chen, Q., 2000. Mechanoregulation of chondrocyte proliferation, maturation, and hypertrophy: Ion-channel dependent transduction of matrix deformation signals. Exp Cell Res 256, 383-391.

Yang, G., Zhu, L., Hou, N., Lan, Y., Wu, X.M., Zhou, B., Teng, Y., Yang, X., 2014a. Osteogenic fate of hypertrophic chondrocytes. Cell Res 24, 1266-1269.

Yang, L., Tsang, K.Y., Tang, H.C., Chan, D., Cheah, K.S.E., 2014b. Hypertrophic chondrocytes can become osteoblasts and osteocytes in endochondral bone formation. P Natl Acad Sci USA 111, 12097-12102.

Yoshida, T., Vivatbutsiri, P., Morriss-Kay, G., Saga, Y., Iseki, S., 2008. Cell lineage in mammalian craniofacial mesenchyme. Mech Dev 125, 797-808.

Young, N.M., Chong, H.J., Hu, D., Hallgrimsson, B., Marcucio, R.S., 2010. Quantitative analyses link modulation of sonic hedgehog signaling to continuous variation in facial growth and shape. Development 137, 3405-3409.

Yu, H.H., Moens, C.B., 2005. Semaphorin signaling guides cranial neural crest cell migration in zebrafish. Dev Biol 280, 373-385.

Yuodelis, R.A., 1966. The morphogenesis of the human temporomandibular joint and its associated structures. Journal of dental research 45, 182-191.

Zelzer, E., Blitz, E., Killian, M.L., Thomopoulos, S., 2014. Tendon-to-bone attachment: from development to maturity. Birth defects research. Part C, Embryo today : reviews 102, 101-112.

Zhou, X., von der Mark, K., Henry, S., Norton, W., Adams, H., de Crombrugghe, B., 2014. Chondrocytes Transdifferentiate into Osteoblasts in Endochondral Bone during Development, Postnatal Growth and Fracture Healing in Mice. Plos Genet 10.

Zusi, R.L., 1993. Patterns of Diversity in the Avian Skull, in: Hanken, J., Hall, B.K. (Eds.), The Skull, First ed. University of Chicago Press, Chicago, pp. 391-437.

Zweers, G., 1974. Structure, movement, and myography of the feeding apparatus of the mallard (Anas platyrhynchos L.). A study in functional anatomy. Netherlands Journal of Zoology 24(4), 323-467.

Zweers, G.A., 1976. Bill Tip Organ and Mechanics of Feeding of Mallard. American Zoologist 16, 215-215.

Zweers, G.A., Gerritsen, A.F.C., Vankranenburg, P., 1976. Mechanics of Feeding of Mallard, Anasplatyrhynchos L - Structure, Cineradiography, Myography. Anat Rec 184, 571-571.

Zweers, G.A., Kunz, G., Mos, J., 1977. Functional anatomy of the feeding apparatus of the mallard (Anas platyrhynchos L.) structure, movement, electro-myography and electro-neurography. Anat Anz 142, 10-20.

Appendix I

Protocols

Kate's Laser Capture Microdissection Protocol

Laser capture microdissection is a powerful tool for isolating small populations of cells. With basic histology, you can excise samples enriched for your region or cell-type of interest. **Take all precautions to prepare RNase free samples, materials, and solutions.** Anything that comes into contact with the slide should be RNase free. Work quickly being mindful that RNA degrades rapidly.

Prepare Beforehand:

UV baked, poly L-lysine coated metal-framed slides
1- Remove hinges from a slide box to free the lid
2- Lay 8 metal framed slides horizontally in the slide box
3- UV bake (this produces microscopic cracks on the membrane and helps tissue adhere to the membrane)
4- Apply 3 to 4 drops of poly-L-lysine solution per slide (provides a positive charge to the slide and further promotes tissue adherence)
5- Store baked, poly-L-lysine treated slides in a closed slide box until use

---

Step 1 – Sample Collection

Be obsessively **RNase free!**
For best RNA quality, collect, embed, section, and microdissect on the same day.
Ice crystals destroy tissue so be mindful of time in sucrose and OCT.
Snap freeze blocks as quickly as possible to minimize ice crystal formation.

Collect
1- Prepare 5% sucrose solution in RNF CMF PBS and chill in ice bucket
2- Prepare 10%, and 15% sucrose solutions in RNF CMF PBS, rock at 4°C
3- Once sucrose solutions are chilled, collect samples into ice cold 5% sucrose
Sucrose Sink
During washes, prepare crushed/riced dry ice, liquid nitrogen, cart, and supplies
4- Rock samples in 5% sucrose at 4°C for 10-15 mins
5- Transfer samples to 10% sucrose
6- Continue to rock at 4°C 10-15 mins
7- Transfer samples to 15% sucrose
8- Continue to rock at 4°C 10-15 mins
Embed
9- Wash each sample in OCT embedding medium before embedding
(may use a drop of colored OCT to denote orientation of sample within the block)
10-Wrap block in aluminum foil and submerge in liquid nitrogen until bubbling stops

Step 2 – Assemble cart to wheel to the Fisher Lab

- 7 baked Copland Jars covered with foil squares
- Hinged slide box
- 50mL conical of filter sterilized 0.1% Toluidine Blue solution
- AB Arcturus Pico Pure extraction buffer
- Gloves
- Optically clear 8 strip PCR tubes and caps
- Timer
- Marker
- Pen
- Notepad
- Kimwipes
- 200uL pipette and tips
- hat and lab coat
- 1 bottle of RNF CMF PBS
- USB drive

Prepare ice buckets

- Fill rectangular ice bucket with 6 Copland Jars and pack the bucket full of ice (the 7th Copland Jar is for Toluidine Blue which stains poorly when cooled)
- Fill a second rectangular bucket with crushed or riced dry ice
  (crush dry ice pellets in a rubberized bucket using a hammer if riced dry ice is unavailable)

Prepare six solutions on ice

Pour 50mL each into Copland Jars and label with lab tape
- RNF CMF PBS
- RNF CMF PBS
- 75% EtOH
- 95% EtOH
- 100% EtOH
- 100% EtOH

Step 3 – Section on cryostat

Be mindful of keeping blocks and slides cold during throughout cryostat sectioning.
May need to experiment with ambient cryostat temperature and block temperature.
I used ambient temperature around -9°C and block temperature about -12°C.
Isolate the tissue of interest in as few sections as possible. I used 20-30µm sections.
Label metal framed slides with a marker.

1- Line slide box with riced dry ice to keep slides cold
2- Collect tissue on frosted test slides until the region of interest is reached
3- Collect as many sections per metal-framed slide as possible
4- As sections are collected, keep slides in dry ice filled slide box and cover each slide with a layer of dry ice as you work through each block.

Step 4 – Prepare the LCM microscope

Wear a hat or tie hair back to prevent strands from contaminating LCM samples. Plus, you won't be temped to make your gloves dirty by wiping hair from your eyes.
Laser settings vary depending on section thickness and tissue properties.
Use lowest laser power possible to preserve RNA and to minimize static cling.
Laser is ionizing so static cling is a problem. Humid air (like a foggy day) mitigates this somewhat, as does brushing the stage with an anti-static brush.
In addition to collecting your region of interest, collect regions with known gene expression as positive controls.

Prepare Microscope

1- Load 8 cap strip onto the stage (don't forget to tighten thumbscrews)
2- Fill each cap you plan to use with 50µL Pico Pure Extraction Buffer. These are collection wells.
3- Laser Settings:
     Power: 52
     Aperture: 6
     Speed: 11
     Specimen Balance: 18
4- Calibrate Touch Screen Stylus
5- Name each cap. Ex. Muscle, tendon, cartilage, bone.

Step 5 – Thaw Slides, Stain, Microdissect

Remember that RNA rapidly degrades so work efficiently to maximize quality and yield from each thawed slide.

Any quickly staining solution that doesn't harm RNA can be used. We use Toluidine Blue for this reason.

Only thaw **one slide** at a time.

Hold the edges of the metal frame in fingertips to thaw. CAREFUL! It's quite cold!

Once the ice crystals on the slide and membrane have thawed, start a **30-minute timer**

You have 30 minutes to complete the following

    Remove OCT
    1- RNF CMF PBS – 2 mins

    Stain
    2- Toluidine Blue (not on ice remember) – 3 mins
    3- RNF CMF PBS – 1 dip

    Dehydrate
    4- 75% EtOH – 30 secs
    5- 95% EtOH – 30 secs
    6- 100% EtOH – 30 secs
    7- 100% EtOH – 30 secs

    Air dry using nitrogen tank
    8- Dry using a light stream of nitrogen. Turn regulator to a low number like 2 or 3.

    Microdissect
    9- Samples that are collected into PicoPure Extraction Buffer filled caps are stable
    10- After excising the last sample, seal 8 strip caps with PCR tubes and begin
       Arcturus Pico Pure RNA extraction protocol

Solutions

5% sucrose
2.5g sucrose
bring volume to 50mL with RNF CMF PBS

10% sucrose
5g sucrose
bring volume to 50mL with RNF CMF PBS

15% sucrose
7.5g sucrose
bring volume to 50mL with RNF CMF PBS

1% Toluidine Blue (10x)
1g Toluidine Blue
100mL ddH$_2$0
sterile filter, cover with foil, store at room temperature

Product Numbers

- Arcturus PEN membrane metal-framed slides
  Applied Biosystems, Foster City, CA, LCM0521

- Poly-L-Lysine
  Sigma-Aldrich, St. Louis, MO, P8920-100ML

- O.C.T. medium
  Tissue-Tek O.C.T. compound, Sakura Finetek USA Inc., Torrance, CA, 4583

- Shandon Cryochrome O.C.T. medium
  Thermo Fisher Scientific, Waltham, MA, 9990422

- Arcturus PicoPure RNA Isolation Kit
  Applied Biosystems, Foster City, CA, 12204-01

- Optically clear 8-strips of 0.2mL PCR tubes and caps
  Sorenson BioScience, Murray, UT, 38790

Kate's Paraffin Section In Situ Protocol

Day 1 – All Steps RNase Free

From citrisolv to hybridization ~3.5 to 4 hours

Deparaffination and Rehydration
1. Citrisolv   2 x 5 mins
2. 100% EtOH   5 mins
3. 95% EtOH   5 mins
4. 70% EtOH   3 mins
5. ddH$_2$O   3 mins

Post-Fixation
6. 4% PFA   20 mins
7. PBT   2 x 5 mins

Digestion and Post-Fixation
8. Proteinase K*   10 mins
9. PBT   5 mins
10. 4% PFA   15 mins
11. ddH$_2$O   quick rinse

Acetylation
12. Acetylation*   10 mins
13. PBT   5 mins

Hybridization
14. Pre-Hybridization at 65°C   1-4 hours
15. Hybridize Probes at 65°C   O/N

---

*Solutions Made Fresh

Proteinase K
- 75mLPBT
- 37.5µL Proteinase K (if using 20mg/ml stock)

Acetic Anhydride Solution
- 90mL ddH$_2$O
- 10mL 10x TEA, pH 8.0
- 250 µL acetic anhydride (stored in acids cabinet under fume hood)

Day 1 – Notes

- All materials and solutions used on Day 1 need to be **RNase free**

- Pre-warm hyb chamber prior to incubating slides
- Keep humidity chamber wrapped with plastic wrap to minimize evaporation of hyb chamber buffer, hyb, and probes

- These are post-fixes, no need for fresh PFA, may use and re-use up to 1 month
- Make up acetylation at least 10 mins before you plan to use it, solution should sit on a stir plate until acetic anhydride beads disappear (~10 mins)

- Some pap pens melt in the 65°C oven and ruin the in situs, test any new brand of pap pen before use, draw a ring on a blank slide and fill the ring with hyb, check after a few mins, if the hyb leaked all over the slides get a new pap pen

- Avoid pre-hyb incubations over 1 hour, even with a plastic wrapped chamber, hyb solution evaporates
- Pre-warm hyb solution and probes before applying to slides
- Add 3 to 4 drops of hyb or probe per ringed section
- After applying probe to slide, cover with a strip of parafilm to prevent evaporation overnight

- To save time on Day 2, make up and pre-heat all SSC solutions overnight so they're ready when you are

Day 2 – No longer RNase free

From first SSC wash to antibody ~3.5 to 4 hours

Make up at least 450mL 2x SSC by diluting 20x SSC pH7 stock in ddH$_2$O
- Set aside 225ml at RT
- Pre-heat 150mL at 65°C
- Pre-heat 75ml at 37°C

Make up at least 225mL 0.2x SSC by diluting 20x SSC pH7 stock in ddH$_2$O
- Set aside 75mL at RT
- Pre-heat 150mL at 65°C

2x SSC Washes
1. 2x SSC at 65°C   15 mins
2. 2x SSC at RT   5 mins
3. RNase A in 2x SSC* at 37°C   30-45 mins
4. 2x SSC at RT   2 x 5 mins

0.2x SSC Washes
5. 0.2x SSC at 65°C   2 x 30 mins
6. 0.2x SSC at RT   2 mins
7. PBT at RT   2 x 20 mins

Block and Antibody Incubation
8. Block in 10% heat-shocked sheep serum in PBT   30 mins – 1 hour at RT
9. Incubate 1:2000 AP-α-Dig abody in 10% HSSS   O/N at 4°C or 1hr at RT

---

*Solutions Made Fresh

RNase A in 2x SSC
- 75ml 2x SSC
- 37.5µL RNase A (if using 20mg/ml stock)

Day 2 – Notes

- Once probes are hybridized, there is not need for any solutions or materials to be maintained RNase free

- Re-circle slides with pap pen before blocking
- During blocking and antibody steps, incubate slides in a humidity chamber (line a slide box with paper towels and moisten towels with PBS)
- If using old AP-α-Dig, dilute 1:1000 in block

Day 3

From washes to color reaction ~1.5 to 2 hours

Washes
  1. PBT at RT   3 x 20 - 30 mins
  2. Alkaline Phosphatase Buffer*   5 mins
  3. levamisole in Alk Phos Buffer*   5 mins

Color Reaction
  4. Develop at 4°C in the dark*   30 mins
     Check color
     Continue to monitor color reaction at 4°C or at RT, may take up to 1 week
     Change color reaction every day or two

Dehydrate and Coverslip
  5. PBT at RT   2 x 10 mins
  6. 4% PFA   15 mins
  7. ddH$_2$O   dip 3x
  8. 30% EtOH   5 mins
  9. 50% EtOH   5 mins
  10. 70% EtOH   5 mins
  11. 95% EtOH   2 x 5 mins
  12. 100% EtOH   2 x 5 mins
  13. Citrisolv   3 x 5 mins
  14. mount with CoverSafe

---

*Solutions made fresh

Alkaline Phosphatase Buffer
  • 25mL 2M Tris pH 9.5
  • 12.5mL 2M MgCl$_2$
  • 10mL 5M NaCl
  • 500ul 100% Tween-20
  • Bring volume to 500mL using ddH$_2$O, filter sterilize

Color reaction
  • 1µL 1000x levamisole/mL Alk Phos Buffer
  • 1µL NBT/mL Alk Phos Buffer
  • 3.5µL BCIP/mL Alk Phos Buffer

Day 3 – Notes

- Make up Alkaline Phosphatase Buffer Fresh (up to 1 month works fine)

- levamisole inhibits endogenous alkaline phosphatase activity (bones express alk phos)

- Develop color reaction in the dark
- May need to develop color reaction multiple days, up to one week

- Attempt to keep slides in the dark as much as possible while dehydrating and coverslipping

Solutions List

Make all solutions **RNase free**
Use baked glassware, MiliQ ddH$_2$O, and autoclave before use

PBT
- 1mL Tween-20
- 1L RNase free, calcium and magnesium free PBS

1M (10x) Triethanolamine, pH 8.0
- 66.5mL Triethanolamine
- 20mL concentrated HCl
- add 400mL ddH$_2$O
- adjust pH using HCl or NaOH
- Bring volume to 500ml using ddH$_2$O

20x SSC, pH 7.0
- 175.3g NaCl
- 88.2g Sodium Citrate
- add 800mL ddH$_2$O
- adjust pH using HCl
- Bring volume to 1L using ddH$_2$O

Humidity Chamber Buffer
- 500mL formamide
- 250mL 20x SSC, pH 7.0
- Bring volume to 1L using ddH$_2$O

0.5M EDTA pH 8.0
- 186.1g EDTA
- add 800ml ddH$_2$O
- Adjust pH using NaOH, this will bring EDTA into solution
- Bring volume to 1L ddH$_2$O

10% CHAPS
- 1g CHAPS
- bring volume to 10mL using ddH$_2$O

Hybridization Solution
- 25mL Formamide
- 3.25mL 20x SSC, pH 7.0
- 0.5mL 0.5M EDTA, pH 8.0
- 50µL 50mg/mL yeast t-RNA
- 100µL Tween-20
- 2.5mL 10% CHAPS in ddH_2O
- 100µL 50mg/mL heparin
- Bring volume to 50ml using ddH_2O

1000x levamisole
- 250mg levamisole
- 500µL ddH_2O

Kate's Protocol for Surgical Implantation of Chromatography Beads into Late-Stage Embryos

This protocol outlines the process of delivering small molecules, ligands, or anything else that can be bound to a chromatography bead by surgical implantation into a highly-motile, late-stage, avian embryo.

Delivering small molecule inhibitors
Prepare 50ul aliquots of reconstituted small-molecule inhibitors, store at -20°C

AG1-X2 - Bio-Rad, Foster City, CA, 140-1231
converted to formate-bound form, strong anionic charge
50-100 mesh, 180-500μm (I selected 250-350μm diameter beads)
These beads tend to sink. They will also chip if pinched too tightly by forceps.
- **SB431542** – 100mM in DMSO
  TGFβ signaling inhibitor
  Santa Cruz Biotechnology, Santa Cruz, CA, sc-204265
- **SU5402** – 10mM in DMSO
  FGF signaling inhibitor
  Sigma Aldrich, St. Louis, MO

SM-2 - Bio-Rad, Foster City, CA, 152-8920
nonpolar
300-1,180μm
- **XAV-939** 100mM in DMSO
  Wnt signaling inhibitor
- **LDN-193189** 50mM in DMSO
  BMP signaling inhibitor

AG1-X2 Bead Conversion
These beads come in a chloride bound form. To maximize affinity for positively charged molecules, AG1-X2 beads must be converted to the formate bound form.
1- Run 3 bead volumes of 0.5-1.0M formic acid over beads
2- Wash with ddH_2O until pH5.0 (may test pH with litmus paper)
3- Store beads in ddH_2O in a conical tube (I stored mine like this for years)
OPTIONAL
4- Transfer beads to large petri dish to dry
5- Incubate in 37°C incubator overnight – do not over dry, bead performance suffers (I never dried my beads)
6- Store at room temperature in a microfuge tube wrapped with parafilm

Delivering proteins
Protein solutions can be freeze thawed (2µL aliquots would not store well)

Affigel Blue Gel – Bio-Rad, Foster City, CA, 153-7301
nonpolar
50-100 mesh, 150-300µm (I selected 250-300µm diameter beads)
These beads are quite soft and tend to adhere to forceps tips if squeezed too tightly.
- **TGFβ2** – 80µg/mL 4mM HCl in 0.1% filter sterilized BSA in 1x PBS
  R&D Systems, Minneapolis, MN, 302-B2-002
- **TGFβ3** – 80µg/mL 4mM HCl in 0.1% filter sterilized BSA in 1x PBS
  R&D Systems, Minneapolis, MN, 243-B3-002

Heparin-Acrylic – Sigma-Aldrich, St. Louis MO, H-5263, discontinued
For delivery of heparin binding molecules
Large range in bead size (I selected 250-350µm diameter beads)
These beads crumble if gripped too tightly. They also tend fall out of shallow incisions.
- **FGF4** – 1mg/mL 0.1% filter sterilized BSA in 1x PBS
  R&D Systems, 235-F4-025

Preparing the embryos
Window eggs early before vitelline vessels adhere to the egg shell

> **For duck, remove 1-1.5mL albumin** to drop the level low enough that you can orient the egg and gain access to the jaw when it's time to do surgery, but also these embryos will need enough albumin to keep from dehydrating when you collect after bead implantation

> **For quail, remove 0.5-1mL albumin**, this is the same principal as in duck, remove enough albumin that the egg can be windowed wide enough for bead implantation and the egg can be tilted to gain a good surgical angle, but also the quail are very quick to dry out so leave as much albumin in the egg as possible

---

Tools

- ≥200µL microfuge tube
- 200µL or 1000µL pipette and tips
- Fast Green
- PBS
- Kimwipes
- watch glass and petri dish or Parafilm
- 20µL pipette and tips
- Scissors and 2 pairs of forceps (1 blunt, 1 sharp)
- Thin cellophane tape

Step 1 – Allow eggs to cool down

If the embryos are not going to be paralyzed, move 1 or 2 trays of eggs into a humidified, room temperature incubator. As you complete surgeries, maintain about two trays of eggs in the room temperature incubator at a time.

Step 2 – Binding small molecules to beads

1- Isolate ≥30 beads by 200µL or 1000µL pipette depending on bead diameter

2- Remove excess fluid from beads and suspend in 50µL carrier in a microfuge tube
   Optional: add 2-3µL Fast Green to carrier to increase visibility of lightly-colored beads (AG1-X2 or Heparin-Acrylic for example) during surgery

3- Allow beads to soak for 15-30 mins

4- As beads soak in carrier, line a petri dish with PBS moistened Kimwipes

5- Clean and dry a watch glass of the appropriate size

6- Place watch glass inside of petri dish and cover with the lid

7- Thaw an aliquot of reconstituted small molecule or the vial of protein

8- Pipette 10-20 beads into the center of the watch glass, remove excess fluid

9- Pipette 20µL of inhibitor or 2µL of protein onto beads

10- Place lid on petri dish and allow beads to soak 30 mins before the first surgery

Step 3 – Implanting beads

1- Position egg in a putty filled ashtray.

2- Widen the window until you have just enough room to maneuver forceps inside the egg. You do not want to tip the egg over or to chip pieces of eggshell with the forceps because the window is too small.

   Try to **center the head within the opening** as you widen the window.

3- At this point, it is easy to determine under the microscope whether the embryo appears normal and healthy. If it does, then proceed.

4- Visualize the region of the vitelline that would be best for accessing the mandible.

   Remember this spot, you will retrieve a bead and place it on top of the vitelline membrane adjacent to this region.

5- Set the egg aside. **Use the blunt forceps** under the microscope to select a bead from the humidified petri dish. Set the bead on top of the vitelline membrane.

6- If a second bead is desired, select it and place it on top of the vitelline membrane next to the first bead.

7- Now visualize the egg under the microscope at low magnification.

8- Transfer the blunt forceps to your nondominant hand. Grasp the fine forceps in your dominant hand. Use the forceps to grasp the vitelline membrane and carefully tease apart.

   Avoid vessels where possible. Blood in the albumin makes visualizing the mandible and implanting the bead quite difficult.

   The amnion continues to contract whether or not the embryo is paralyzed. With this in mind, **make an opening in the vitelline as if you were attempting to operate on the forelimb area**.

   When possible, I try to avoid all the vessels by tearing an opening in the non-vascularized margin of the membrane. The embryo is typically positioned with its back to this region.

9- Grasp the chorion and amnion and tear these membranes open as well

10- Use the blunt forceps to pull on the amnion, the innermost membrane, to position the jaw so it points at a shallow angle away from you and into the egg. This angle makes for the easiest bead placement.

11- Continue gripping the membrane to maintain the position of the head and use the sharp forceps to make an incision pointing towards the region where the coronoid process is expected to form.

   In duck this region is lateral and easy to access.

   In quail and chick, the bead should be placed **superior to the mandible and deep to the quadratojugal**.

12- Still gripping the membrane with you nondominant hand, locate the first bead floating on the vitelline and gently pinch it between the tips of the sharp forceps using light pressure.

13- Insert the bead into the incision. The incision typically leaks blood which makes it an easy landmark to spot. If desired, insert second bead into the same incision.

14- Use both pairs of forceps to remove and bits of egg shell that fell into the egg

15- Do your best to put the membranes back where they came from, especially if you applied quite a bit of tension to get the jaw accessible.

16- Seal the window carefully with cellophane tape. Dehydration is easily prevented by creating a tight seal.

17- Place egg into the original, warm incubator.

Tips for implanting chromatography beads

Surface markers for targeting the coronoid process
In my experience, the coronoid process can be accurately targeted by implanting beads relative to surface markers.

- **Normal embryos lay on their left side**, exposing the right side of the mandible, I tend to avoid operating on embryos with the right side exposed as this indicates abnormal development.

- Imagine a line originating from the most inferior point of the eye and intersecting the mandible perpendicular to its proximodistal axis. The intersection of this line with the mandible is the **approximate point where the secondary cartilage will form**. Any bead distal to the imaginary intersection of the line with the mandible will not be near enough to the coronoid process.

- If the position relative to the eye is difficult to judge, I use the oral commissure and the external auditory meatus as additional landmarks. Imagine a point halfway between these two landmarks. The bead should be placed along the more proximal half. In other words, **the bead should be closer to the external auditory meatus than to the oral commissure**.

Recovering beads
Sometimes, the beads will sink into the albumin where it become out of reach or float out of sight between the vitelline membrane and the eggshell.

- If you need to take a rest or if you need to expand the incision, you can let the bead settle into the external auditory meatus rather than lifting it out of the albumin and returning it to the surface of the vitelline.

- If the bead slips from the forceps or rolls off the vitellin and begins to sink into the albumin, you can use the forceps in your nondominant hand to press the membranes downward and create an upsurge that usually carries the bead back to rest on the surface of the vitelline.

- If you notice the bead float between the vitelline and the eggshell, it is sometimes possible to get the bead to return by pressing down on the vitelline membrane near where the bead disappeared, creating an upswell fo fluid from around the margin of the egg.

Improving Survival
These are some strategies for increasing the rate of survival.

- **Check the incubators for dead eggs the following day.**

- **Move the eggs to clean trays the following day** also**.**

- **Do not let the eggs dry out.** Make sure the incubators are always maintained at about 70% humidity.

- Strive to make the operations as quick as possible. **Try for 3 minutes or less** from removing tape from the window to taping the window back up.

- If a vessel gets nicked, **use either pair of forceps to clamp the vessel shut** for a few seconds. This technique stems bleeding from any but the largest vessels.

- **If the yolk leaks, the embryo will not survive**. Move on to a new embryo.

- **Clean forceps every few surgeries** with ethanol or bleach. This keeps the eggs from getting contaminated with filth and it cleans any dried albumin or membrane from the tips of the forceps. This will keeping them nice and sharp. Dry the forceps before handling any beads or putting them into the egg, of course.

- **Take notes on each surgery**. I typically record the time that I first place trays into the humid, room temperature incubator, the time that I began soaking beads in the inhibitor or the protein. And then I number every egg with a ebad implanted and record the time the surgery began, the time the surgery ended, and any notes on other events. Did the vessels bleed? Did lots of eggshell fall into the egg? Was the embryo especially active or inactive? How confident do I feel about the position of the implanted bead? Were there any especially difficult attributes of the surgery?

Kate's Protocol for Endoscopic Recording of *in ovo* Embryonic Movements

This technique enables recording of localized *in ovo* embryonic motility while maintaining physiological incubation conditions.

List of Tools
1088 HD High Definition Camera (Stryker, Kalamazoo, MI)
4mm, 30° arthroscope (Stryker, Kalamazoo, MI)
Universal dual-quartz halogen fiber-optic light source (CUDA Surgical, Jacksonville, FL)
Two-prong clamp (Fisher Scientific, Hampton, NH)
Lattice rod clamp (Fisher Scientific, Hampton, NH)
36 inch lattice rod (Fisher Scientific, Hampton, NH)
23 inch vertical support stand (Fisher Scientific, Hampton, NH)

Step 1 – Assemble camera support stand

The camera needs to be held steady in order to confidently identify embryonic motility. The whole assembly also needs to be a little bit adjustable as each embryo is positioned differently inside the egg. A vertical stand supporting a lattice rod, in a set-up that resembles a chemistry lab, meets these demands.

1- Position vertical support stand next to an empty, humidified, 37.5°C incubation chamber.
2- Affix lattice rod perpendicular to the vertical support stand using a lattice clamp.
3- Attach the camera to the horizontal lattice rod using a two-prong clamp.
4- Assemble the arthroscope onto the camera.
5- Thread fiber-optic light source onto the arthroscopy attachment.
6- Turn on camera, light source, and launch iGrabber program

Step 2 – Position egg

The egg should have a window large enough that the 4mm arthroscope can easily fit inside the egg.

1- Position egg beneath the opening in the lid of the incubator.
2- Adjust height of the lattice rod so the arthroscope just touches the albumin.
3- Use the iGrabber live image to locate the mandible. Take advantage of the 30° bevel to view the jaw in profile. This perspective helps when quantifying motility because is shows the widest possible angle of jaw opening.
4- Allow embryo to acclimate to light for 15 mins.
5- Record motility.

Step 3 – Quantify motility periods
1- It may help to define activity periods as Hamburger and Balaban did (1963).
2- Using their definition, an activity period is the time from the onset of mandible motility until 5 seconds after the motility ends. If mandible movements are separated by fewer than 5 seconds, they are considered part of the same activity period. If the mandible is motionless for more than 5 seconds, the activity period ends. Using these parameters, the shortest activity period is 5 seconds long.
3- Calculate mean percent motility for each species by stage.
4- Calculate 95% confidence intervals.
5- Calculate standard deviation.
6- Perform unpaired, two tailed t-tests at each developmental stage.

Hamburger, V. and Balaban, M., 1963. Observations and experiments on spontaneous rhythmical behavior in the chick embryo. *Developmental biology*, 7, pp.533-545.

Kate's Protocol for Creating 3D Reconstructions from Trichrome Stained Sections

This technique allows 3D reconstruction of soft tissues that are otherwise difficult or impossible to visualize with microCT. This protocol outlines the process for sectioning, imaging, alignment, segmentation, and exporting different file types.

Sectioning and imaging

1. Take a block and make crazy 8 sections (groups of 8 slides, each with 4 tissue sections on it)

2. Select a set of slides such that every eighth slide has 4 sections, none missing

3. Do Milligan's Trichrome Stain on this set

4. Image on the brightfield scope, carefully align each image so that it corresponds as closely as possible with the previously captured image.
- Images captured using SPOT are immediately available to view in adobe photoshop. This makes it convenient to compare pairs of sections. Section 1A and section 1B for example.

Tips
- Use 2.5X objective when reconstructing quail and duck mandibles
- When capturing an image in SPOT for reconstruction, it's best to capture 8 bit images or smaller. Click Preferences > Image Acquisition > Captured Image Bits per > 8 (this corresponds to a 12.5MB image)
- Do not capture images for z-stack from one edge to the other. Don't begin with slide 1 for example. This is especially helpful if your regions of interest are not in the first sections collected. Start in the middle of the z-stack and work your way to one end. For example, start in the middle and move deep. Then return to the slide where you started capturing images and move superficial. This helps ensure that the regions of interest will remain within the field of view as you create your z-stack.

Tutorials of Interest

Getting Started – the basics of Amira
Reading Images – how to read images
Visualizing 3D Images – slices, isosurfaces, volume rendering
Image Segmentation – segmentation of 3D image data
Surface Reconstruction – surface reconstruction from 3D images
Grid Generation – creating a tetrahedral grid from a triangular surface
Alignment of 2D physical cross sections – how to reconstruct a 3D model
Import Files

1. Import the TIFFs into Amira
   • Open data > (command) select all files of interest > load

2. Image Read Parameters-
   • Set: channel conversion: luminance (Amira requires black and white images for creating 3D reconstructions of stacked images. An RBGA color field cannot be segmented. Before opening the segmentation editor, the images must be converted to luminance data.)
   • Specify the dimensions of the bounding box
   • For images captured at 2.5X use these dimensions:
     > X-axis = 3600
     > Y-axis = 3600
     > Z-axis varies with each reconstruction. Z depends on the number of sections per reconstruction

       o X- & Y- dimensions have been quantified using a scale bar and measuring the length of that scale bar at 2.5X using WinSurf

Ex.   20 images gives 19 gaps at 80um each.
       19gaps * 80um/gap = 1520um z stack
       Dimensions of the images captured using 2.5x objective
           X=3600 (constant)
           Y=3600 (constant)
           Z=1520

3. You now have a green data module in the pool with the suffix ".am" (amira mesh binary). Attach an Orthoslice module to the green data module. The Orthoslice module allows visualization of each image in the stack.

Align Sections

1. Right click the green ".am" data module, from the dropdown menu: compute > align slices
   • In the properties pane > select edit

The screen will display a pair of adjacent sections superimposed on each other. Clicking and dragging will move the upper image.

   Hot Keys
   • click and drag – translate upper image
   • command + click and drag – rotate upper image
   • 1 – view only top slice
   • 2 – view only bottom slice
   • Use move slice slider (at bottom of image) to progress through images

2. When alignment is complete:
   - Properties > select close (this will save work)

3. In the properties pane, Action: Resample > a new green module will appear with suffix ".align.am."

Leave all steps in the pool if you wish to save the entire workflow. Alternatively, delete the first green module, leaving only the ".align.am" file in the pool if you want to make the pool simpler to look at.

4. Save your work!
   - To save an entire network: File > Save Network As > select the suffix ".hx" (amira script).
   - To save an individual data module, click on the module then: File > Save Data As

Tips
- pick a landmark that appears throughout the entire z-stack and use this as a reference when aligning
- Don't be afraid to press the question mark button in the properties box to learn more about any module.

Segmentation Editor

1. Right click green module of the grayscale data > labeling > label field

2. Edit "Image Data" from drop-down menu, must select: ".align.am" file type
   - If you choose to improve the alignment after you begin segmentation, you can transfer your segmentation work to the updated alignment file. Just change the file in the "Image Data" drop down menu to the resampled alignment data module. The regions you have already encircled will appear, but may need to be clicked and dragged to correct their position in the new ".align.am" file.
"Label Data" from drop-down menu, select: "new"
   - You may keep the same set of label data and apply it to a re-aligned file.

3. Rename or create new "Materials:"
Don't use the default fields named "Exterior" or "Inside."
Example labels: surangular, adductor, etc.

4. Change the color of each material now. Click on the colored square to the left of each material. A "Color Dialog" box will appear. I have a standard palette of colors that I use for each tissue.

Here are the Hue, Saturation, and Vibrancy setting I use:
- Bone is red (H:1.000, S:1.000, V:1.000)
- Cartilage is blue (H:0.622, S:1.000, V:1.000)
- Muscle is purple (H:0.818, S:1.000, V:0.629)

5. Zoom in on image using magnifying glass in middle panel, "zoom and data window."

6. Select brush tool from bottom panel, adjust size as necessary
  - black mouse icon allows encircled regions to be clicked and dragged
  - lasso tool auto traces regions of the map, check "auto trace" box, click as many times as necessary to encircle the region of interest
  - magic wand??

7. Click and drag brush over region of interest to highlight it in red

8. Click "+" button on the "selection" panel on the left side of screen

9. Repeat for each image in the stack

   Hot Keys
   - f- fill in the center of the highlighted region
   - ctrl- hold while brushing to erase
   - "+" - add region to the selected material
   - "-" - subtract region from the selected material
   - d - change pattern of segmented regions, outlined, cross-hatched, filled in, etc.
   - "command +" - increase the size of the highlighted region before adding to the selected material
   - "command -" - decrease the size of the highlighted regions before adding to the selected material

10. Return to the data pool by clicking the icon with green, orange, and red colored modules. This button in located at the top left corner of the Amira window.

Tips
- Open images using Preview or some other program to compare the grayscale Amira image to the original color image.
- Completely fill in the region of interest.
- When highlighting a new tissue, don't forget to select the name of the new material in the "Materials" menu.
- Choose the colors of each material now or it will be a pain to change the colors once the surface is generated.

Interpolate

1. Select green "labels.am" module > Compute > Interpolate Labels. In the properties pane, Interpolation: cubic > Apply.

Generate Surface View and Files for FEA

1. From the new, green "labels.intpol.am" data module > Compute > SurfaceGen, in the properties pane, press the green "Apply" button.

2. From the new green ".surf" surface data module > Display > SurfaceView

3. To simplify the reconstructed surface, click on the green .surf module. Click on the icon with black and white triangles in the properties window.
        Surface: tells the number of faces, edges, points, etc.
        Simplify: input the desired number of faces
        Action: simplify now

Tips

- Play with the SurfaceView Draw Style Settings
- Draw Style: Shaded or Lines look great for visualizing the 3D reconstruction
- Draw Style: More Options drop down menu, try either triangle normals (very geometric looking, can see the triangulation easliy), vertex normals, (smooths the surface except for contact regions between materials), direct normals (smooths surface including contact regions between materials)

4. Save the simplified surface as a mesh for finite element analysis by clicking on the green .surf module. file > save data as > from the drop down menu, select .dxf extension

Alternatively, you may choose to generate a line set. Though this is not desirable for FEA.
        Select green ".labels.intpol.am" data module > Compute > Compute Contours. In the properties pane, Orientation: z > Apply.

        Select green ".contours" data module, > Display > LineSetView.

        File: Save data as ".dxf"

5. Before capturing screen shots it may be desirable to add a scale bar.

        Right click > Create > Scale. The scale bar measures pixels by default.

Scaling to microns requires a bit of work.

Visualize the bounding box belonging to the aligned data module. It needs to be 3600um in the x-axis. Rotate the bounding box until the x-axis is parallel to the x-axis scale bar. Adjust the length of the scale bar and the position of the bounding box until it's x-axis and the scale are parallel and the exact same length. Check the box for fixed size. With the length of the scale bar constant, change the scale of the units until it reads 3600 units in length.

Now that the scale bar reads 3600 units and corresponds exactly with the x-dimension of the bounding box, uncheck the box for fixed size, and change the length of the scale bar until it is 500um long.

The scale bar should now read round numbers for length as zoom is changed.

> Example Settings:
> pos x - 0.5
> pos y - 0.5
> size x - 0.11804
> size y - 0.9
> frame - x-axis
> ticks - none
> sub ticks - none
> units - microns
> line width - 2
> options - fixed size - no
> x factor - 0.8314
> y factor - 1

Generate Separate Surfaces for Each Material

Should you choose to generate separate surfaces for individual materials, use the surface view module in the pool.

1. In the properties pane, Materials: select one of the materials you wish to exclude from the reconstruction. For example, Meckel's Cartilage. Buffer: Remove. Continue removing materials until only the desired materials remain. You can also add materials back to the reconstructed surface by pressing Buffer: Add.

2. In the properties pane, Draw Style: more options drop down menu, select Create Surface.

3. Visualize this new surface object. Attach a SurfaceView.

4. Make sure to add all the patches to the surface so there are no holes.

5. Save each new green surface data module as a DXF file.

Generate Movie

1. Right click > Create > CameraRotate. Select axis of rotation in the properties pane, Action: select from the drop down menu, most vertical, x-axis, y-axis, etc.

2. Rotate the surface to the desired orientation, then press Action: recompute from the properties pane.

3. Use the Time slider bar in the properties pane to preview the movie.

4. Create a DemoMaker module, right click, Create > Animation/Demo > DemoMaker.

5. Attach the green CameraRotate module to the blue DemoMaker module by clicking the white square on the left of the blue module, Data > select CameraRotate by connecting the connecting the dots.

6. Select DemoDirector from the large box below the pane displaying the reconstructions. DemoDirector is the icon directly next to the Console icon at the top of this pane.

7. Click New event… > select CameraRotate from the menu and time from the submenu. Press OK.

8. Adjust the length time for the rotation to take place.

9. Right click the blue DemoMaker module > MovieMaker.

10. In the properties pane of the red MovieMaker module, select the appropriate movie file format, File format > MPEG movie. Windows computers have the option to make an AVI movie.

11. Create an appropriate filename and location. In the properties pane, press Filename: browse.

12. Press the green Apply button in the bottom of the properties pane. MPEG files are viewable using Quicktime.

Troubleshooting

1. Surface and alignment don't match up?

   Check if one of the two modules has italicized name
   This means a transform is applied to one data set but not the other

   Ex. The visualization of the data has been transformed but the coordinates of the data object have not been

   Solution — Use the transform editor (the button with 7 green dots connected by black lines) to apply the same transform to both modules or remove the transform so neither are transformed

   Action: Copy. Then go to the data module you wish to transform, select the transform editor, then > Action: Paste. Now both modules carry the same transform. Removing transforms from both will also solve the problem.

2. Can't open the segmentation editor?

   Solution — The images must be converted from color to black and white luminance data.

3. Didn't convert to gray-scale when first importing images?

   Solution — Convert to luminance data.

   Convert color field to scalar field using "Cast Field." There should now be an "align to byte" file

4. You want to save properly?

   To save network, click in the pool to de-select any data modules.
   File > Save Network As > select Amira Script (.hx) from the "File type" drop down menu.

   > If you want to access the network as well as the data from another computer: File > Save Network > select Amira Script and data files (pack & go) (.hx) from the "File type" drop down menu.

   To save data, click on the desired green data module in the pool.
   File > Save Data As > choose desired location, name, and file type

5. Importing images to Amira and receive the error:
   ".... LOAD EXCEEDS THE OUT-OF-CORE THRESHOLD?"

Check image size. They're probably too large. You need to downsample.

Solution — Open image using Photoshop.
Press Command + Alt + I > change size to: 1200-1800 pixels. Save image.
Repeat on all images.

6. Oops! Segmented before alignment?

   Solution — Apply alignment to your label field.

   > Select the green label field data module (labels.am) > Compute
   > >AlignSlices. Attach input port to the aligned data by clicking the white
   > square on the AlignSlices module. Select "Reference" and click on the
   > aligned data module.

   In the properties pool, Action > Resample. This will generate an aligned label
   field in the Pool.

7. Taking too long to interpolate labels or generate a surface?

   Solution - You need to downsample.

   You may either downsample the data before you add the label fields, or you may
   downsample after you add the label fields.

   > Before Adding Label Fields Ex. After importing a stack of images, select
   > the green data module with the suffix ".am" > Compute > Resample.
   > Manually enter values for the number of voxels for each dimension: x, y,
   > and z. A good ballpark is half the default input resolution values in the
   > properties pane.
   >
   > Mode: Dimensions
   >
   > Resolution: x 2048 y 2048 z 35 >>> Enter values x 1024 y 1024 z 35 (note
   > that voxel size scales as you alter Resolution values.) > Apply.

   After Adding Label Fields Ex. Click on any green data module in the pool. Glance
   at the properties pane and you will see a summary of the number of voxels and
   the voxel size.

   > Info: 2048 x 2048 x 20 bytes
   >
   > Voxel Size: 0.8979336 x 0.8979336 x 40

   There is super high resolution in the x and y dimensions and there are 20
   sections.

To learn the dimensions of the bounding box, look in the properties pane and click the icon with the black square and the diagonal line through it. A window will open. In the resolution pane > Mode: bounding box.

Max Coord: 1800 1800 1360 for example.

This means the x, y, and z dimensions have all been halved. This had no effect on the burden for the computer. Keep this equation in mind:

bounding box dimension = (voxel size)(voxel number)

Shrinking the dimensions of the bounding box will not decrease voxel number. It will only contract the voxel size.

Try halving the amount of detail in the x and y dimensions while leaving the z-axis untouched.

Click on the "labels.am" data module. Compute > Resample. In the properties pane, Average: x2 y2 z1 > Apply.

This means that voxel number in the x and y axes will each be halved, while the z-axis will remain unchanged. Each voxel will increase accordingly in size, doubling in length in the x and y dimensions while the z dimension remains unchanged.

The properties pane in the resulting data module will read:

Info: 1024 x 1024 x 20 bytes

Voxel Size: 1.75867 x 1.75867 x 80

8. Hmm…I need to change the colors of my surfaces

You have two options.

Option one requires that you go to the segmentation editor and change the color of each separate segmentation. Then you will need to resample and go through all the motions to create a new surface with the desired colors.

Option two is quick and dirty, however, you're only editing the color of the surface. The segmentation will retain the original colors. If you go back to edit the segmentation and re-derive a surface, you will need to change the colors back again.

To start, select the green ".surf" module. In the properties pane, click on the parameter dialog icon (looks like a list). Select the drop down materials menu. For each material, there is a drop down menu containing "color." Select "color" and a colored rectangle will appear on the lower right of the parameter dialog box. Click on this to edit the colors as you wish.

9. Does the surface have strange looking white lines around the peripheral edges?

    Click on the "Surface View" module attached to your .surf surface module. Draw Style > more options > move the checkmark from "both faces" to "front face."

10. Gahh!! When I used the interpolation function, it created contact regions that I didn't draw in the segmentation editor!

    To remove the contact region, use the segmentation editor. Label Data: interpolation images. There will be several hundred slices depicting segmented regions on an all black background. Now manually edit the series of slices that have the false contact region.

    Instead of selecting the paintbrush from the lowest panel on the left, select the black pointing arrow icon. Check the box for "All slices."

    In the Selection window, select the option "All slices." The text and the square icons above it will all turn red. This is to indicate that any change you make will affect all sections with that material.

    Click inside the material you with to edit. The fill inside the material will turn from black to red.

    Next click on the "Shrink selection" icon on the upper right corner of the Selection panel. It looks like a blue blob with four arrows pointing at it. You will see the red fill decrease in size leaving a black border between it and the original segmentation.

    Click on the "Replace selected region" icon in the Selection panel. The image for the icon is two clockwise circling arrows.

    Now all slices with the selected material have been decreased in size. If there are any other contact regions that belong on this material, you will need to flip through each slice and redraw the contact regions.

    Return to the pool. Now you must resample the green interpolated data module and produce the surface from there. When resampling, be sure that no downsampling occurs. This means that in the Properties pane > Average: x, y, and z, should all be 1.

Notes
Amira License number: ASTND48406

Contact Info

Ken Moore – UCSF Amira Rep
ken.moore@fei.com

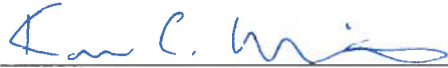Kathy Tinoco – Technical Support
kathy.tinoco@fei.com
858-539-6888

Include Amira License number in the subject line of any emails asking for technical support.
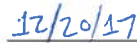
Publishing Agreement

It is the policy of the University to encourage the distribution of all theses, dissertations, and manuscripts. Copies of all UCSF theses, dissertations, and manuscripts will be routed to the library via the Graduate Division. The library will make all theses, dissertations, and manuscripts accessible to the public and will preserve these to the best of their abilities, in perpetuity.

Please sign the following statement:

I hereby grant permission to the Graduate Division of the University of California, San Francisco to release copies of my thesis, dissertation, or manuscript to the Campus Library to provide access and preservation, in whole or in part, in perpetuity.

_____   _12/20/17_____
Author Signature   Date

186